İZMİR KÂTİP ÇELEBİ ÜNİVERSİTESİ
2010
GRADUATE SCHOOL OF NATURAL AND APPLIED SCIENCES

3D Modelling Performance and Usage Area Analysis of Popular UAVs in the Surveying and Mapping Industry

Submitted to the Graduate School of Natural and Applied Sciences in partial fulfillment of the requirements for the degree of

Master of Science

in Geomatics Engineering

by

Metehan MARAL

ORCID 0000-0002-9434-8539

Thesis Advisor: Assist. Prof. Dr. Serkan KARAKIŞ

July 2023

This is to certify that we have read the thesis **3D Modelling Performance and Usage Area Analysis of Popular UAVs in the Surveying and Mapping Industry** submitted by **Metehan MARAL**, and it has been judged to be successful, in scope and in quality, at the defense exam and accepted by our jury as a MASTER'S THESIS.

APPROVED BY:

Advisor: **Assist. Prof. Dr. Serkan KARAKIŞ**
İzmir Kâtip Çelebi University

Committee Members:

Assist. Prof. Dr. Mehmet Güven KOÇAK
İzmir Kâtip Çelebi University

Assist. Prof. Dr. Kutan KORUYAN
Dokuz Eylül University

Date of Defense: July 14, 2023

Declaration of Authorship

I, **Metehan MARAL**, declare that this thesis titled **3D Modelling Performans and Usage Area Analysis of Popular UAVs in the Surveying and Mapping Industry** and the work presented in it are my own. I confirm that:

- This work was done wholly or mainly while in candidature for the Master's degree at this university.
- Where any part of this thesis has previously been submitted for a degree or any other qualification at this university or any other institution, this has been clearly stated.
- Where I have consulted the published work of others, this is always clearly attributed.
- Where I have quoted from the work of others, the source is always given. This thesis is entirely my own work, with the exception of such quotations.
- I have acknowledged all major sources of assistance.
- Where the thesis is based on work done by myself jointly with others, I have made clear exactly what was done by others and what I have contributed myself.

Date: 14.07.2023

3D Modelling Performance and Usage Area Analysis of Popular UAVs in the Surveying and Mapping Industry

Abstract

3D realistic models are used in many fields such as engineering, archaeology, and city planning. The most effective technique used to create these models is the photogrammetry technique. The hardware and software features of the unmanned aerial vehicles to be used to implement this technique are of great importance. Many different unmanned aerial vehicles can be used for photogrammetric studies in the surveying and mapping industry, and therefore users have difficulties choosing needed unmanned aerial vehicles for their studies. In this study, 3D modelling performance and usage areas of popular unmanned aerial vehicles used in the surveying and mapping industry were examined. For this, a business center building located in an area of approximately 10,771 m^2 in Dresden was chosen as the study area. To create the 3D model of the building, 5 ground control points and 1 check point were placed in the study area, and oblique rgb and thermal aerial photographs were taken with 7 different unmanned aerial vehicles. Using photogrammetry software, 3D textured rgb and thermal models were created with each unmanned aerial vehicle data. As a result of the analyses made by considering criteria such as positional accuracy, model quality, and cost, it has been recommended that the DJI Mavic 3E model unmanned aerial vehicle with 1.72 cm horizontal and 2.43 cm vertical root-mean-square error is the optimum model that can be used for 3D modelling purposes. In addition, DJI Matrice 30T is recommended for thermal applications, and the WingtraOne Gen II model is recommended for large-scale 3D city modelling projects.

Keywords*:* Photogrammetry, 3D Modelling, Unmanned Aerial Vehicles, oblique flight, aerial photographs

Harita Sektöründe Kullanılan Popüler İnsansız Hava Araçlarının 3D Modelleme Performans ve Kullanım Alanı Analizi

Öz

3D gerçekçi modeller mühendislik, arkeoloji, şehir planlama gibi birçok alanda kullanılmaktadır. Bu modelleri oluşturmak için kullanılan en etkili teknik fotogrametri tekniğidir. Bu tekniğin uygulanabilmesi için kullanılacak insansız hava araçlarının donanım ve yazılım özellikleri büyük önem taşımaktadır. Ölçme ve haritacılık endüstrisinde fotogrametrik çalışmalar için pek çok farklı insansız hava aracı kullanılabilmekte ve bu nedenle kullanıcılar, çalışmaları için ihtiyaç duydukları insansız hava araçlarını seçmekte zorluk çekmektedir. Bu çalışmada, ölçme ve haritacılık sektöründe kullanılan popüler insansız hava araçlarının 3 boyutlu modelleme performansları ve kullanım alanları incelenmiştir. Bunun için Dresden`de yaklaşık 10.771 m^2'lik bir alanda bulunan bir iş merkezi binası çalışma alanı olarak seçilmiştir. Bina modelini oluşturmak için çalışma alanına 5 adet yer kontrol noktası ve 1 adet kontrol noktası yerleştirilmiş ve 7 farklı insansız hava aracı ile eğik rgb ve termal hava fotoğrafları çekilmiştir. Fotogrametri yazılımı kullanılarak her bir insansız hava aracı verisi ile 3 boyutlu dokulu rgb ve termal modeller oluşturulmuştur. Konum doğruluğu, model kalitesi, maliyet gibi kriterler dikkate alınarak yapılan analizler sonucunda yatayda 1.72 cm ve düşeyde 2.43 cm karesel ortalama hata değerine sahip DJI Mavic 3E model insansız hava aracının 3D modelleme amaçları için kullanılabilecek optimum model olduğu sonucuna varılmıştır. Ayrıca termal uygulamalar için DJI Matrice 30T, büyük ölçekli 3 boyutlu şehir modelleme projeleri için ise WingtraOne Gen II modeli önerilmiştir.

Anahtar Kelimeler: Fotogrametri, 3D Modelleme, İnsansız Hava Araçları, eğik uçuş, hava fotoğrafları

The thesis is dedicated to my lovely family.

Acknowledgment

Firstly, I would like to express my gratitude to my supervisor Assist. Prof. Dr. Serkan Karakış for his support, suggestions and consultancy to me to write this thesis. Besides, I also thank you to the company “Airclip Service GmbH” and my team members there, especially Lucas Günther to support me to write this thesis both by their equipments and technical support.

Last but not least, my special gratitude and appreciation towards my family for their support and prayers for my success.

Table of Contents

List of Figures

List of Tables

List of Abbreviations

GNSS	Global Navigation Stallite Systems
GIS	Geographic Information System
SfM	Structure form Motion
MMV	Motion Multi View
DEM	Digital Elevation Model
UAV	Unmanned Aerial Vehicle
RTK	Real Time Kinematic
DSLR	Digital Single Lense Reflex
DTM	Digital Terrain Model
DIFFDTM	Differential Digital Elevation Model
EDM	Electronic Distance Measurement
MP	Manual Tape
WW1	World War 1
3D	3 Dimensional
WW2	World War 2
IMU	Inertial Measurement Unit
ER	Electromagnetic Radiation
POI	Point of Interest
FPS	Frame Per Second
CCD	Charge Coupled Device
CMOS	Complementary Metal Oxide Semiconductor
GCP	Ground Control Point
DTM	Digital Surface Model

MSL	Mean Sea Level
TIN	Triangulated Irregular Surface
USGS	United States Geological Survey
EXIF	Exchangeable Image File Format
NASA	National Aeronautics and Space Administration
ISPRS	International Society for Photogrammetry and Remote Sensing
ESRI	Environmental System Research Institute
PPK	Post Process Kinematic
LiPo	Lithium Polymer
LIDAR	Light Detection and Ranging
RC	Remote Controller
GSD	Ground Sampling Distance
DC	Direct Current
ESC	Electronic Speed Controller
RF	Radio Frequency
VTOL	Verical Take-off and Landing
VR	Virtual Reality
FPV	First Person View
CORS	Continiously Operated Referace System
SAPOS	Satellitenpositionierungsdienst Deutschen Landesvermessung
TUSAGA-Aktif	Türkiye Ulusal Sabit GNSS Ağı Aktif
RINEX	Receiver Independent Exchange Format
IO	Interior Orientation
EO	Exterior Orientation
RMSE	Root-Mean-Square-Error

List of Symbols

m	Meter
m^2	Square Meter
cm	Centimetre
MP	Megapixel
s	Second (Time)
nm	Nanometer
°	Degree (Angle)
'	Minute (Angle)
"	Second (Angle)
g	Gram
kg	Kilogram
°C	Celsius
min	Minute (Time)
px	Pixel
Hz	Hertz
GHz	Gigahertz
ppm	Parts Per Million

Chapter 1

Introduction

Photogrammetry, as a scientific discipline, has been evolving and expanding its application areas, especially in the engineering industry, by closely following technological advancements in the past decade. Its development gained momentum primarily for military reasons after World War I, and it has continued to evolve by incorporating advancements in imaging technologies over time. Sensor-carrying platforms, starting with kites and balloons, have evolved from manned aircraft to satellites and unmanned aerial vehicles, thereby rapidly expanding and continuing to expand their areas of use.[1]

Photogrammetry can be summarized as the measurement of surfaces or any desired object in a three-dimensional plane by using overlapping photographs. When considered, the close relationship between photogrammetric perspective and the mechanisms of human vision, perception, perspective, and depth detection becomes apparent. In fact, our brain processes the overlapped image from our relatively different eye positions, enabling us to perceive three-dimensionality, estimate distances, and have depth perception.[2] When closely examined, the process of processing overlapping images collected in the field through specific photogrammetry software is similar to obtaining a resulting product. In this analogy, the sensing system camera is replaced by the human eye, the data processing system and photogrammetry software represent our brain, and the resulting output represents three-dimensionality and depth perception.

Although some believe that the concept of perspective, which forms the basis of photogrammetry, dates back to the ancient Greeks, some of the most significant evidence in the scientific world comes from Leonardo da Vinci's works on perspective

in the 15th century. Later, thanks to scientists who strengthened the mathematical foundation of perspective and projection principles, we see the progress of photogrammetry in the scientific world. In addition, Joseph Nicéphore Niépce (1765-1833) contributed to the birth of photogrammetry by taking the first photograph in history with an 8-hour exposure.[3] The overlapping photographs developed in the early applications still form the fundamental building blocks of photogrammetry, including the concepts of relative and absolute image orientation that we use today. According to Konency [4], photogrammetry has followed four development cycles since 1850. These are plane table photogrammetry (1850-1900), analog photogrammetry (1900-1960), analytical photogrammetry (1960-present), and the ever-evolving digital photogrammetry that has reached its peak today.

The rapid advancements in computer hardware, data processing software, and unmanned aerial vehicle (UAV) technologies have accelerated the development and usage of photogrammetry in numerous fields today, reducing data processing times and eliminating certain requirements in data processing steps. Particularly, advancements in photography, Global Navigation Satellite Systems (GNSS) receivers, microprocessors, navigation, gimbals, and UAVs have brought revolutionary developments and changes to the techniques used. Carrier systems that began with kites, pigeons, and balloons evolved into manned aircraft and helicopters, and are now continuing their journey with fixed-wing and rotary-wing UAVs. The transition from manned aircraft and helicopters to UAVs has reduced costs in photogrammetric works, while the shift from analog to digital cameras has replaced specialized analog and analytical plotters in the data processing phase with high-performance computers, which are less laborious and time-consuming. As a result, the financial barriers to the use of photogrammetry, especially for small areas, have been eliminated.

In today's world, 3D models, which are the photogrammetric output, offer users exceptional awareness, ease of measurement, and a wide range of applications. The creation of three-dimensional models from aerial images obtained through unmanned aerial vehicles (UAVs) is an active area of research and application in digital photogrammetry and computer vision fields. [5] Especially in the mapping industry, the integration of 3D models with Geographic Information System (GIS) provides a new perspective and convenience in creating 3D city models. Users can now obtain

elevation and perspective information that is not available in 2D maps with ease through the GIS infrastructure. Additionally, 3D models are widely used in various fields such as communication, energy, transportation, marketing, tourism, gaming, automated unmanned vehicles, and more. The advancements in areas like artificial intelligence and machine learning also closely relate to 3D models. In fact, there are now artificial intelligences capable of automating the steps of 3D model production and generating 3D models by processing images from a database without requiring input data from the user.[6] In today's rapidly evolving computer science and digital photogrammetry, it is evident that the demand for 3D models will continue to increase, and their applications will further expand. With the advancements in technology, it is believed that the utilization of 3D models will continue to grow and find new applications in various fields.

1.1 Purpose of the Thesis

In this thesis, utilizing photogrammetry techniques commonly applied in the mapping and surveying industry, performance analyses were conducted on various popular unmanned aerial vehicles (UAVs) and cameras used in the field. The study incorporated digital cameras specifically produced for certain UAVs by technology companies such as DJI, as well as digital cameras manufactured by leading camera companies like Sony. Aerial photographs were obtained in the study through aerial photogrammetry techniques based on the shooting position of the image, and digital photogrammetry techniques were employed according to the camera selection.

In the study, various flights were conducted using popular UAVs from brands such as DJI and Wingtra in the industry. The captured images from these flights were processed using photogrammetric image processing software Agisoft Metashape Pro, employing Structure from Motion (SfM) and Motion Multi View (MMV) techniques. Orthomosaics, Digital Elevation Models (DEMs), and 3D Models, which are photogrammetric output products, were generated and presented in this study. Focusing specifically on 3D models, the performance of different popular UAVs and payload cameras in 3D model generation was examined. In addition to these analyses, the current usage areas of 3D models, ranging from GIS-supported 3D city models to

the gaming industry, were explored, along with potential future applications of 3D models.

Care was taken in the study to use scientifically accepted methods, reliable equipment, and appropriate image processing software. The presence of numerous different unmanned aerial vehicles and camera systems in today's industry creates uncertainty and indecision for individuals who need to choose the most suitable equipment and may lead to uncertainties regarding the output model products. The aim of this study, which primarily focuses on the fields of mapping and surveying, as well as UAVs and 3D models, is to provide readers engaged in these areas with information about the 3D model generation performance of popular UAVs in the industry. It also aims to alleviate their uncertainties and fill the gaps in knowledge when making decisions about optimal equipment selection.

1.2 Importance of the Study

In this study, various works were presented to provide users engaged in photogrammetric activities with information about the quality of output products they can obtain using unmanned aerial vehicles. It is an important study for users from various sectors, particularly in the mapping and surveying departments, who face uncertainties in selecting the optimal system comprising popular UAVs and mounted payload cameras. Acquiring and testing numerous UAVs and camera systems is not always feasible due to increasing costs. Additionally, some technology companies advertise technical specification on drones obtained under ideal conditions such as wind-free, precipitation-free, and maximum satellite geometry as part of their marketing strategy, which can mislead users according to the features they have seen on the specification list of drones. However, achieving these optimum conditions is not always possible. In this context, this study is crucial for readers to gain insights into the applications of 3D models and the 3D model generation performance of popular UAVs in the industry.

1.3 Literatur Review

Li and Nan [7] conducted a study on the simplification of 3D mesh models generated from either Lidar point clouds or photogrammetric methods. In their work, they applied mesh filtering, structure extraction, and mesh decimation steps in order. They mentioned that in projects involving large-scale 3D models, the face count imposes a heavy burden on the system in terms of capacity and memory usage. They also emphasized the need for low memory footprint and a fast interface in such projects, particularly in cases where texture information is not required (e.g., disaster simulation, communication protection analysis, etc.). They focused on model simplification in these scenarios. Through the algorithms they used, they were able to reduce the face count of the model while achieving smooth surfaces and sharp model corners. As a result, they achieved the necessary low memory footprint and fast computational capability required for large projects.

Matys et al.[8] conducted a study where they investigated the potential use of photogrammetry in meeting the digitalization and optimization needs of companies in the industry. They performed several tests to explore this possibility. The motivation behind their work was to provide a method that allows companies to test their planned changes in a digital environment before implementing them, thus fulfilling the need for a 3D model that enables such testing. This approach offers various benefits, including avoiding additional costs that may arise from discrepancies and the ability to anticipate and make updates beforehand. In their study, they selected a forklift as the object to be modeled in transportation vehicles and captured its photographs using a smartphone camera from at least three different heights in a circular manner. They utilized an open-source photogrammetric data processing software called "Meshroom" to create a 3D textured model. The authors were satisfied with the quality of the resulting model and concluded that photogrammetric 3D models can be used in industrial digitalization and optimization projects. They also highlighted the advantages in terms of production cost and time, emphasizing that it offers a favorable approach.

Gomez and Kennedy [9] conducted a study to calculate the 3D shape and volume of volcanic ash plumes. They performed unmanned aerial vehicle flights and data

acquisition at the Yasur Volcano vent on Tanna Island in the South Pacific Ocean using photogrammetric techniques. The aim of their work was to create a 3D model of the mushroom-shaped smoke structure in the volcano vent, including parameters such as ash height, volume, shape, and 2D plan form. Obtaining these data is crucial for understanding the eruption dynamics of volcanic vents and calculating and monitoring the emissions of gases released into the atmosphere. These emissions can have harmful effects on agriculture, aviation, and human health, so monitoring and taking preventive measures are of utmost importance. In their study, Gomez and Kennedy used a DJI Phantom 3 UAV to capture 146 aerial photographs in a circular orbit around the volcanic vent. They also employed a Trimble R8 RTK GNSS receiver for Ground Control Point (GCP) measurements and correction data transmission. Using the obtained 3D model and Digital Elevation Model (DEM), they calculated the volume of the volcanic ash plume to be 13,430 $m^3 \pm 512\ m^3$ and determined its height as 63m. Additionally, they reported an error of 4-8 m in the Z coordinate and sub-meter accuracy in the X and Y coordinates based on the closest GNSS measurement to the crater. They emphasized that the error values were influenced by the irregular distribution of ground control points due to the risk of eruptions and other hazardous conditions in the study area. This study is significant as it represents one of the first successful measurements of volcanic ash plumes in the literature.

Karakış et al. [10] conducted a study using a homemade octocopter unmanned aerial vehicle to highlight the capabilities of UAVs in area and volume calculation. They equipped the UAV with a 12 MP Canon Digital Single Lense Reflex (DSLR) camera as the payload and integrated an electronic timer for flight control, stability, and timed photography. They performed periodic stereographic aerial photography and GNSS measurements on a building under construction at Bülent Ecevit University, and then conducted photogrammetric evaluations to generate contour lines and a Digital Terrain Model (DTM). They presented a height-based Differential Digital Elevation Model (DIFFDTM) to visually express the difference between the final and initial data. They reported that the height difference reached up to -4.5 meters based on their findings. This study serves as an example highlighting the capabilities of UAVs in resolving the accuracy of 3D models and point clouds with low-altitude acquisition direction.

Jeong et al. [11] conducted a study to investigate the accuracy and usability of output products obtained through the photogrammetric processing of aerial photographs captured by unmanned aerial vehicles in measuring building dimensions such as columns and beams. They selected traditional timber buildings in Naju, South Korea, as their study area. Initially, they measured the building columns and beams using traditional Electronic Distance Measurement (EDM) and Manual Tape (MP) methods. Subsequently, they compared these measurements with the digital measurements obtained from the point cloud and 3D textured model generated through photogrammetry. They also compared the results by varying parameters such as the photo capture interval, gimbal pitch angle, flight speed, and altitude of the UAV measurements. According to their findings, they determined that there was a difference of 0.21% and 0.91% between the measurements obtained through traditional methods and photogrammetric UAV, respectively, indicating that photogrammetry was sufficiently accurate for these measurements. They also emphasized that the most accurate results were obtained with a photo capture interval of 2 seconds, a flight speed of 1 m/s, and a camera gimbal angle of 45°. This study serves as an example demonstrating the ease and necessity of using photogrammetry in the documentation, maintenance, and deformation measurements of cultural heritage sites, particularly in hazardous and challenging working environments.

Chapter 2

Photogrammetry

Photogrammetry is a scientific and artistic discipline that extracts metric information from images obtained from aerial or terrestrial platforms. The development of this field was influenced by various factors, such as Leonardo da Vinci's studies on perspective, Joseph Nicephore Niepce's (1765-1833) invention of the first photograph, the use of carrier platforms like kites and balloons, and the increased demand from the military during World War I (WW1). Nowadays, photogrammetry provides support to the field of computer science, particularly in computer vision, which has a much larger community.[12]

Photogrammetry is primarily used by geomatics experts in the fields of surveying and mapping. However, it also serves in various other domains such as 3D recording of archaeology, architecture, historical documentation, canopy documentation, and more. Additionally, it finds applications in non-topographic areas such as real estate advertising, industrial measurements, medical imaging, and forensic medicine.

The development and use of Unmanned Aerial Vehicles (UAVs), particularly accelerated during World War II (WW2), have surpassed other carrier platforms such as satellites and manned aircraft due to their lower cost and flexibility advantages. Stemming from military needs, photogrammetry has played a significant role in the development of unmanned aerial vehicles. In fact, during WW2, UAVs (e.g., V1 and V2 rockets) were utilized to carry explosive bombs. Another example is the "UAV Ryan 147" that the United States used during the Vietnam War to gather information from the battlefield. Even today, military-driven UAV development continues rapidly.[13] The benefits of this development in terms of photogrammetric perspective have been in the direction of advancing autonomous navigation systems, gimbals,

Inertial Measurement Units (IMU), and cameras. These systems, which were initially expensive, have been advancing and becoming more cost-effective over time, making photogrammetry usage even more effective. Currently, researchers are investing in on-board navigation systems capable of direct georeferencing. With this promising field, imagine a UAV system that can perform direct georeferencing using an on-board GNSS system, without the need for any post-processing after the flight, automatically processing the accurately coordinated photos in the cloud and delivering output products to us in a very short time, even before landing, through photogrammetry software. Considering the impressive growth rate and momentum of technology, it becomes apparent that such a system is not impossible.

2.1 Light, Colour and Photograph

Understanding the concepts of light, color, and photography is crucial for grasping the working principles of photogrammetry and establishing a solid foundation for its operation. The first of these terms is light. Many scientists (e.g., Isaac Newton, Thomas Young, James Clerk Maxwell, Albert Einstein, etc.) have conducted studies to comprehend the definition and characteristics of light. While historical definitions have varied over time, in modern times, light refers to the visual perception created by the visible wavelengths of the electromagnetic spectrum, which correspond to wavelengths ranging from 380nm to 780nm within the human retina. [14] **Figure 2.1.** illustrates the electramagnetic spectrum and the visible region.[15] This Electromagnetic Radiation (ER) encompasses both particle and wave characteristics, propagating in empty space with the electromagnetic and magnetic fields perpendicular to each other.

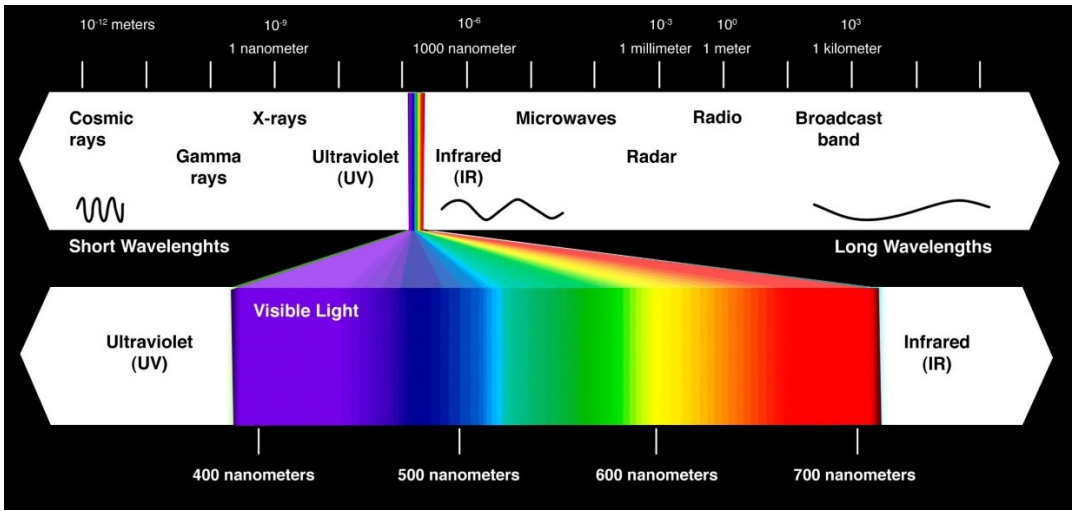

Figure 2.1: Electromagnetic spectrum and visible region

Electromagnetic radiation emitted from any source interacts with objects it encounters, undergoing absorption, scattering, reflection, or a combination of these behaviors, as well as being influenced to varying degrees by these interactions as it continues its path. The ER that interacts with objects and is reflected back, reaching our eyes, is perceived by the three different types of cone cells in our eyes (e.g., red, green, and blue), which then transmit the signals to the brain. The interpretation of these signals by the brain results in the perception of color. For example, the color red is perceived when green and blue radiation is absorbed by objects and red radiation is reflected, while white color is perceived when all colors are reflected, and black color is perceived when all colors are absorbed by objects, according to the brain's interpretation. The human eye contains approximately 6-7 million rod cells and 3 million cone cells, which are responsible for visual perception. The human eye has an approximate resolution of 576 MP, and its focal length, which can change with the contraction and relaxation of the eye lens, is typically around 17mm. [16] The number of Frames Per Second (FPS) that the human eye can perceive varies depending on factors such as ambient brightness, contrast, etc. However, if the human eye watches video footage below 60 FPS, it will be able to perceive stuttering and blurriness in the image. Therefore, for smooth video playback, a minimum FPS rate of 60 FPS is often recommended in many applications.

The term "photograph" is derived from the words "photon" (light) and "graph". It refers to the process of light or any form of electromagnetic radiation interacting with three-dimensional objects, being detected on a photosensitive surface, and then being

reduced to a two-dimensional plane to obtain an image output.[17] The photosensitive surface mentioned here refers to the rod and cone cells located in the retina of the human eye, while in cameras, it refers to the Charge Coupled Device (CCD) and Complementary Metal-Oxide-Semiconductor (CMOS) sensors.

2.2 Definition of Photogrammetry

Photogrammetry is the technique, science, and art of obtaining precise measurements and creating 3D models using 2D photographs or images without the need for physical contact with the object being measured. It typically focuses on the visible range of the electromagnetic spectrum (i.e., light) and utilizes specialized data processing software to establish geometric and spatial relationships between objects through sequential overlapping stereoscopic photographs. This enables us to obtain metric outputs such as orthomosaics, point clouds, and 3D models. Photogrammetry can be classified into terrestrial, close-range, and aerial photogrammetry based on the image capture position, and analog and digital photogrammetry based on the type of camera used. **Figure 2.2** shows the illustrations for the image capture both in aerial [18] and close range photorammetry.[19]

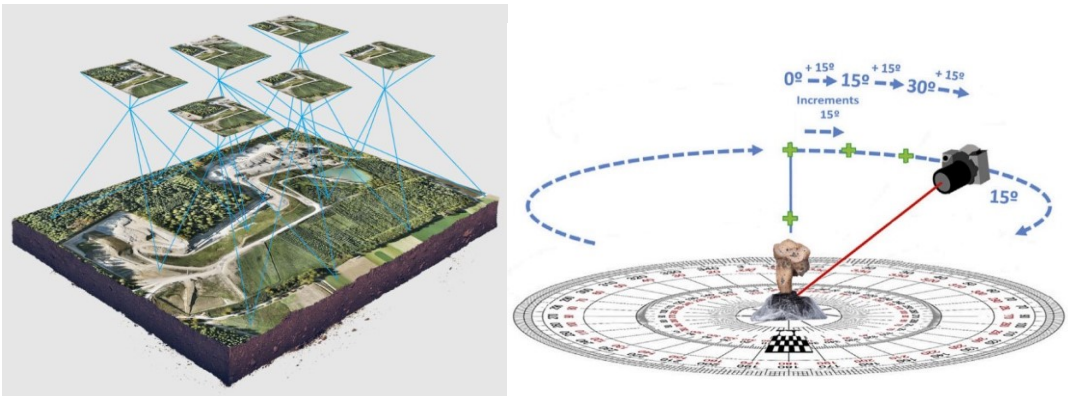

a) b)

Figure 2.2: a) Image capturing in aerial photogrammetry ; b)Image capturing in close range photogrammetry

Photogrammetry is a technique that is widely used in various fields such as surveying, archaeology, heritage documentation, GIS, and architecture, providing exceptional metric and visual presentation through output products. Recent advancements and cost

reductions in camera and unmanned aerial vehicle systems have improved the quality of output products, making this method more budget-friendly. As a result, it is widely used in both the industry and among researchers, and it frequently appears as a research topic due to its close relationship with computer science and computer vision.

The Structure from Motion (SfM) technique, developed in the 1990s and rooted in the computer vision community, has the capability to produce 3D models with a similar algorithm to photogrammetry. This technique, which can be considered as a subfield of photogrammetry, also reconstructs 3D scenes or objects using overlapping 2D images captured from different angles and viewpoints. Although the basic reconstruction methods are the same, there are some differences between the two techniques.

In the photogrammetry technique, image and image acquisition coordinates, or Ground Control Points (GCP), are required to generate 3D points. In cases where image acquisition coordinates are not available, camera positions are calculated using the resection method similar to traditional surveying techniques, and data processing continues. However, in SfM, this is not necessary because in the SfM method, the image geometry and camera positions are simultaneously computed during the reconstruction stage using the common points in the images and their geometric relationships. This is achieved by iteratively applying least squares minimization to the initially estimated coordinates, making adjustments to refine the results. [20] This method is inexpensive and ideal for low-budget projects because it does not rely on additional equipment such as a GNSS receiver, electromagnetic compass, or IMU. However, the generated model is in a relative image coordinate system and lacks scale and orientation. Therefore, in studies that require accurate position information, the conversion of SfM image-space coordinates to real object-based coordinates is necessary, which is achieved through the use of GCPs. Typically, high-contrast GCPs are placed on the object to enable this conversion. **Figure 2.3** represent the data acquisition method to capture multiple, overlapping photographs to extract features and perform 3D reconstruction. [20]

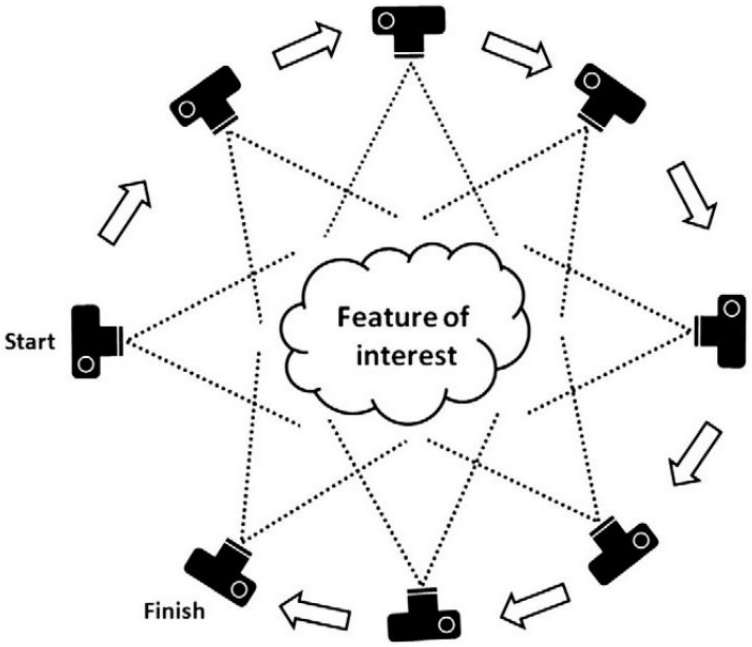

Figure 2.3: Data acquisition method to capture multiple, overlapping photographs for Structure from Motion (SfM) algorithm.

2.3 Outputs of Photogrammetry

After the photogrammetric data collection step, various data processing steps such as photo alignment, dense point cloud creation, and mesh building are performed using the necessary software tools. These steps result in photogrammetric output products such as point clouds, 3D meshes, orthomosaics, and digital elevation models.

2.3.1 Point Cloud

A point cloud is a collection of high-density 3D coordinates (X, Y, Z) generated on the surface of an object. These points can be colorized as true color or pseudocolored, depending on the acquisition method. Photogrammetry software tools can create both sparse and dense point clouds. The acquisition method relies on the use of certain software (e.g., Reality Capture, Pix4DMapper, Context Capture, Agisoft) and involves aerial triangulation and bundle block adjustment techniques. By identifying matching common points in the images and, if available, Ground Control Points (GCPs), these techniques ensure accurate positioning and 3D orientation of the photos. As a result, millions of coordinate points belonging to objects can be generated from the converted object-coordinate photos. The sparse point cloud is formed after the SfM steps, while

the dense point cloud is generated after the bundle block adjustment. Unlike aerial triangulation, bundle block adjustment calculates the position and orientation of the photos based on multiple images, providing denser and more accurate results. **Figure 2.4.** represent the sample point clouds; sparse point cloud created with SfM algorith on “A”, and dense point cloud created with bundle block adjustment on “B”. [21]

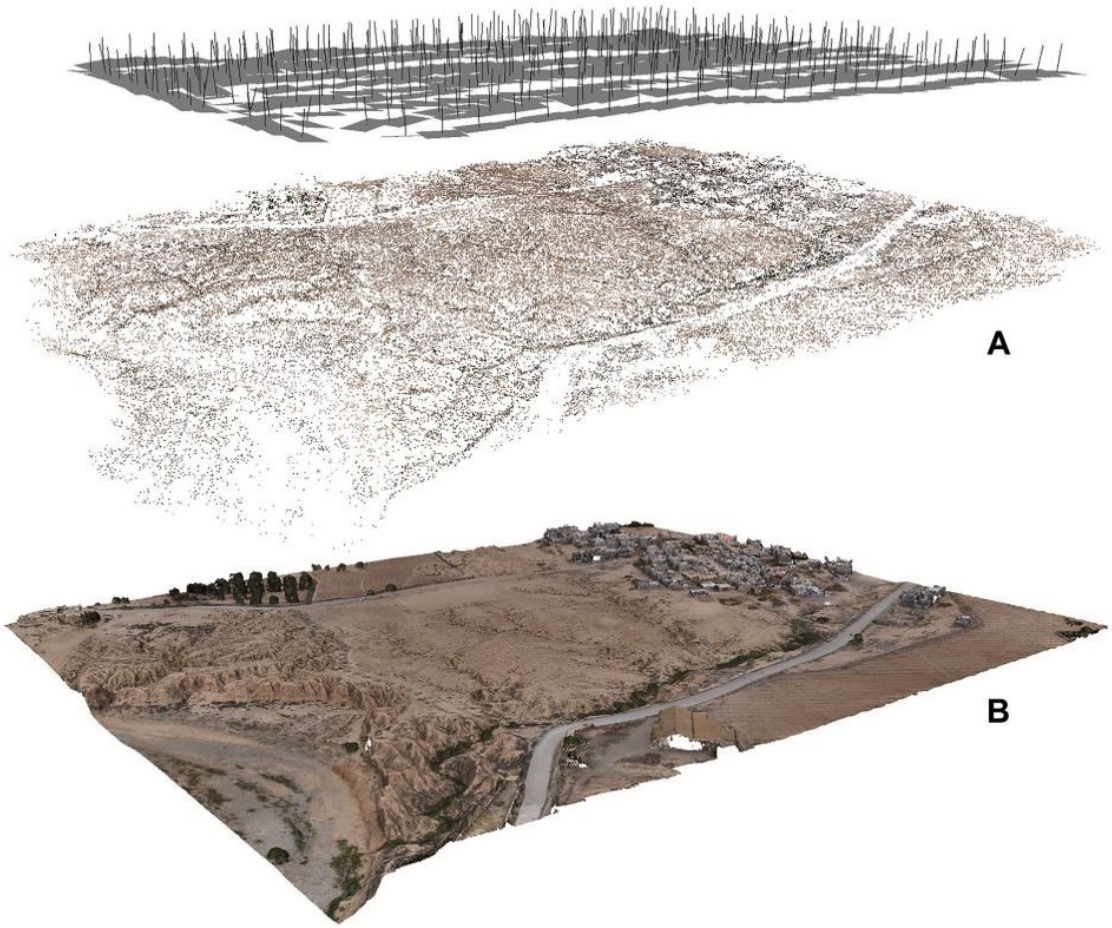

Figure 2.4: a) Sparse point cloud created with SfM algorithm ; b) dense point cloud created with bundle block adjustment

2.3.2 Orthomosaic

An orthomosaic refers to a scaled and georeferenced collection of aerial photographs that have been geometrically corrected. To achieve this, the overlapping aerial photos need to be corrected for camera tilt, lens distortions, and defects caused by the camera-object distance. Each of these geometrically corrected, distortion-free images is referred to as an "orthophoto" or "true-photo." The collection of orthophotos obtained by merging them together is called an orthomosaic. Orthomosaics are commonly used

in various fields such as GIS, surveying, land management, cadastre, and urban planning as a photogrammetric product. **Figure 2.5** presents an orhomosaic sample created from 452 aerial orthophotos.[22]

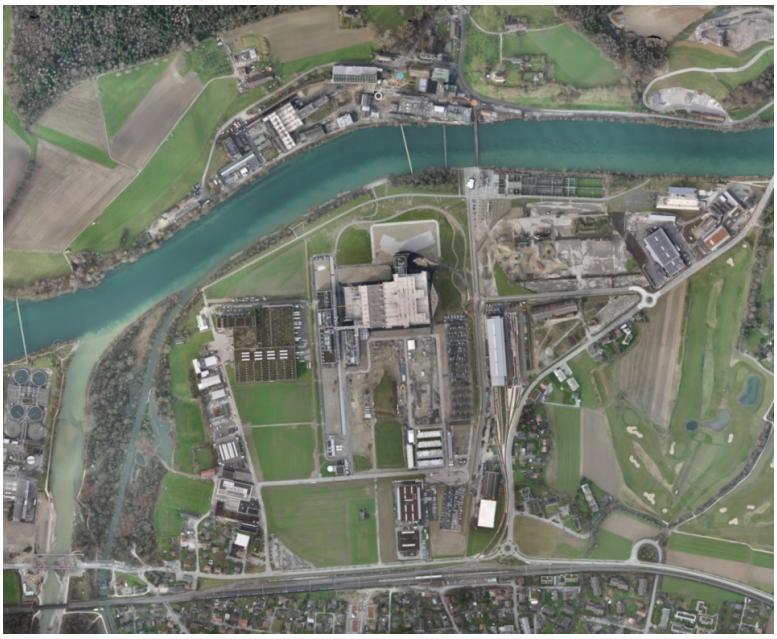

Figure 2.5: An orhomosaic sample created from 452 aerial orthophotos via WingtraOne fixed wing UAV

2.3.3 Digital Elevation Model

Digital Elevation Models (DEM) are digital representations of terrain topography, providing elevation values at equal intervals. They are created using techniques such as radar, remote sensing (e.g., LiDAR), or photogrammetry. Depending on the underlying data used in the creation process, if ground elevation values are employed, it is referred to as a Digital Terrain Model (DTM). On the other hand, if surface elevation values (i.e., including the height of objects on the terrain) are used, it is called a Digital Surface Model (DSM). The resolution of DEMs can vary depending on the source data. They find applications in various fields such as GIS, hydrology, 3D mapping, and urban modeling. **Figure 2.6** represent samples of DEM from a forestry area; a) DTM sampe and b) DSM sample.[23]

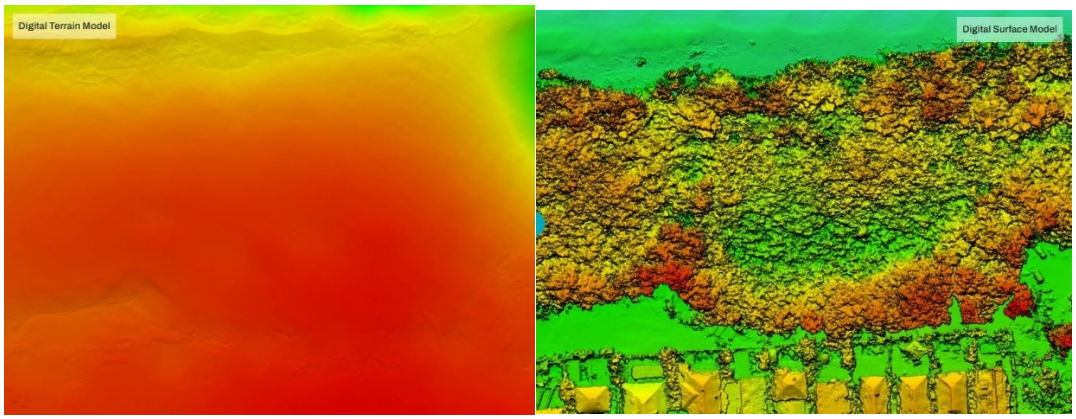

a) **b)**

Figure 2.6: Sample of DEMs from a forestry area; a) DTM sampe and b) DSM sample

2.3.4 3D Mesh

A 3D mesh is a digital representation of the earth's surface or three-dimensional objects, created by combining vertices, edges, and faces. It is formed through a process that involves capturing overlapping photographs of objects or the earth's surface from different angles and positions, followed by geometric correction and removal of lens distortions. These processed images result in the creation of 3D meshes. Realistic digital models, known as 3D textured meshes or models, are obtained by applying the texture structure derived from the photographs onto the surfaces of the 3D mesh. In order to create high-quality models where building facades are clearly visible, oblique flight planning is preferred over nadir flight planning. Oblique flight planning involves tilting the camera pitch angle from the horizon, resulting in better outcomes. Jeong et al. [11] conducted a study on traditional timber building modeling, and they determined that the highest quality 3D model was achieved using a 45-degree gimbal pitch angle, 2-second time interval shooting, and a flight speed of 1m/s. 3D models find applications in various fields such as virtual reality, product design, 3D urban planning, GIS, and heritage preservation, among others. **Figure 2.7** shows an 3D textured model of a building created from a circular oblique flight via DJI Mavic Mini 3 Pro UAV.

Figure 2.7: 3D textured model of a building created from a circular oblique flight via DJI Mavic Mini 3 Pro UAV.

2.3.5 Contour Map

A contour map is a type of map that is created by connecting points on the terrain surface that have the same elevation, forming lines and curves. These maps visually represent information about the structure, elevation, and slope orientation of the land, allowing the reader to identify various geographical features such as peaks and valleys. While contour maps are generally created with reference to Mean Sea Level (MSL), they can also be generated using any other reference surface. They are commonly used in topographic maps to provide elevation information and depict topographic features. This photogrammetric output is frequently employed in fields such as surveying, landslide monitoring, cadastre, cartography, and engineering. **Figure 2.8** represent a saple of contour map.[24]

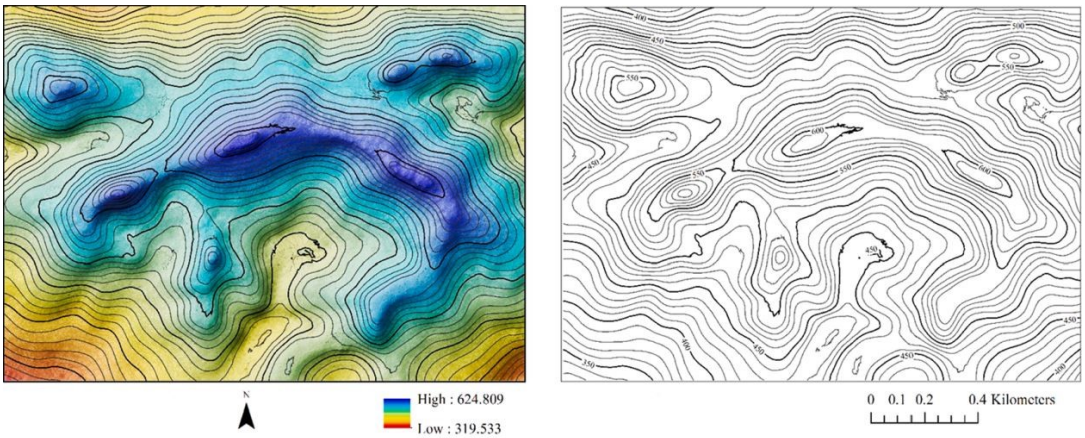

Figure 2.8: Contour map on the right, and contourlines on the interpolated surface with respec to heıght

2.3.6 Triangulated Irregular Surface

A Triangulated Irregular Network (TIN) is a type of 3D model that represents the terrain surface using triangular meshes. It consists of randomly distributed points that represent the terrain surface, which can be collected from sources such as lidar, photogrammetry, or traditional ground surveys. These points are then connected to form a set of triangles that vary in size and shape based on the structure of the terrain. The resulting 3D model, composed of interconnected irregular triangles, represents the terrain surface and is referred to as a TIN. TINs are used in applications such as terrain area and volume calculations, GIS, and spatial analysis. **Figure 2.9** shows the application of TIN over land-sea topography.[25]

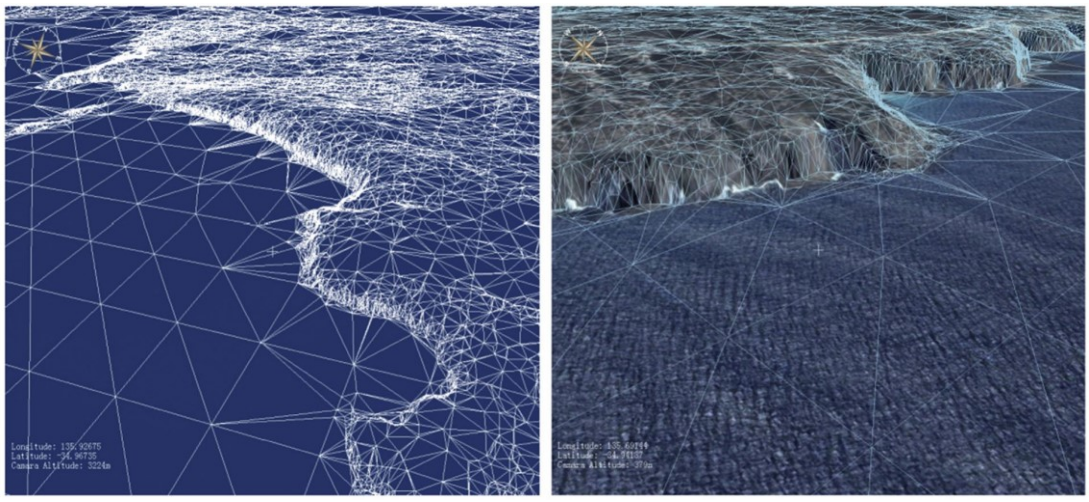

a) **b)**

Figure 2.9: The application of TIN over land-sea topography.(a) TIN wireframe. (b) TIN blebded with image data

2.4 Hisorical Development of Photogrammetry

In today's world, although photogrammetry is performed using high-quality digital cameras and their captured photographs, the foundations of this technique date back much earlier than the invention of the camera. The mathematical principles of photogrammetry are based on perspective and projective geometry, and its historical origins are rooted in these concepts. The famous artist and scientist Leonardo da Vinci stated the following in the year 1480:

> "*Perspective is nothing else than the seeing of an object behind a sheet of glass, smooth and quite transparent, on the surface of which all the things may be marked that are behind this glass. All things transmit their images to the eye by pyramidal lines, and these pyramids are cut by the said glass. The nearer to the eye these are intersected, the smaller the image of their cause will appear.*[26]"

In the following years, Leonardo da Vinci continued his contributions by conducting studies on perspective and central projections. Other scientists in the subsequent years further solidified the foundations of this technique through their work on mathematical projective geometry. Johan Heinrich Lambert, in 1759, developed the mathematical foundations of perspective by using space resection to determine the position of a point in a painting depicting space. The relationship between projective geometry and photogrammetry was first described in 1883 by R. Sturms and Guido Hauck. **Figure 2.10** illustrate the photogrammetric perspective by Hauck.[27]

The first photograph was obtained by Joseph Nicéphore Niépce (1765-1833) with an exposure time of 8 hours. In the 1840s, geodesist Dominique François Jean Arago advocated for the use of photogrammetry in front of the French Academy of Arts and Sciences.

Konecny [28] the development cycles of photogrammetry, starting from 1850, are divided into four cycles, each representing a 50-year time span. These cycles are: plane table photogrammetry, analog photogrammetry, analytical photogrammetry, and digital photogrammetry.

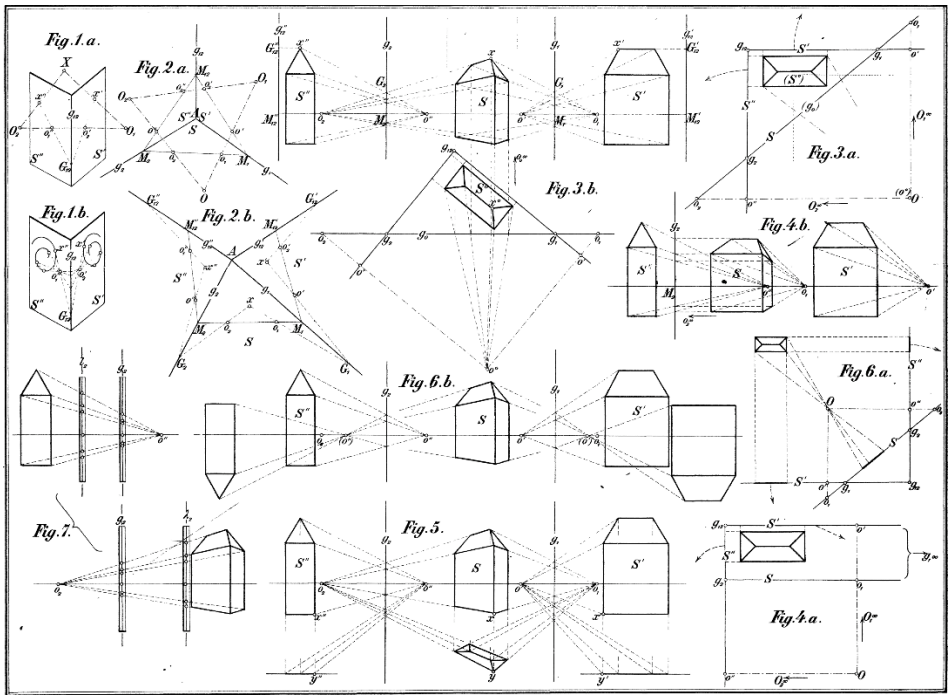

Figure 2.10: Photogrammetric perspective by Hauck.

2.4.1 Plane Table Photogrammetry (1850-1900)

Plane table photogrammetry has entered the stage as a continuation of traditional plane table surveying. This technique involves the use of traditional surveying methods such as resection and intersection. After capturing the photographs, the resection method is employed to calculate the positions where the photos were taken and marked on the plane table. Subsequently, the orientation of the photos is determined on the plane table, and the orientations towards other objects are identified to position them on the map base.

During this period, notable works include: Aimé Laussedat, known as the "Father of Photogrammetry," became the first person to use ground-based photographs for the production of topographic maps in 1849. He experimented with this technique, which he called "iconometry," using kites (1858) and balloons (1862). He even became the first person to capture aerial photographs using balloons. In 1867, at the Paris Exhibition, Laussedat showcased the first known phototheodolite and the photogrammetric techniques he used to produce the Paris plans. Nadar (Gaspard-Félix Tournachon) took the first aerial photograph captured from a height of 80 meters using a balloon in 1855. Emperor Napoleon had reconnaissance aerial photographs taken

before the Battle of Solferino in 1859. These examples highlight the pioneering efforts of Laussedat, Nadar, and others in the early development and application of aerial and ground-based photography for mapping and reconnaissance purposes.

Paulo Ignazio Pietro Porro (an Italian geodesist) invented the first tacheometer instrument in 1839. By 1858, a Frenchman named Chevallier developed the "photographic plane table. **Figure 2.11** show the photographic plane table developed by Chevallier.[3] James Fairman obtained a patent in the United States for "Apparatus for aerial photography," which involved timed photography using kites and balloons. Additionally, in 1893, he received a patent for the "Method of Photogrammetry," which pertained to the technique he used in capturing aerial photographs with balloons. In 1867, Dr. Albrecht Meydenbauer introduced the first wide-angle lens (105°) for mapping purposes and went on to design several cameras in the following years.

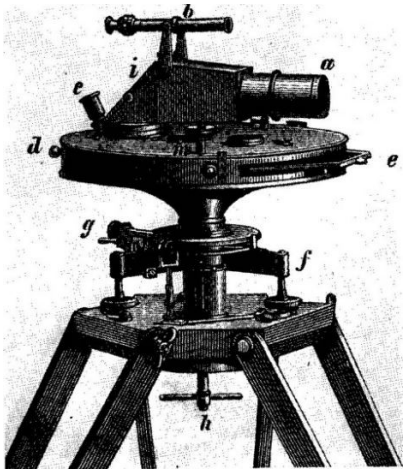

Figure 2.11: Photographic plane table developed by Chevallier.

2.4.2 Analog Photogrammetry (1900-1960)

With the advancement and popularity of stereoscopy and the development of the airplane by the Wright brothers in 1903, photogrammetry transitioned into its iconic phase known as analog photogrammetry. During this period, film cameras were commonly used for capturing photographs, and significant progress was made in the areas of resolution, distortion correction, and calibration. Here are some notable developments in the field of analog photogrammetry: Wilbur Wright took the first aerial photograph from an airplane in Italy in 1909, while Captain Cesare Tardivo

captured the first photograph for mapping purposes, specifically for a 1:4000 scale mosaic of Benghazi, Italy.

In 1896, Edouard Deville invented the first stereoscopic-plotting instrument called the "Stereo Planigraph." The United States Geological Survey (USGS) adopted photogrammetry for the production of topographic maps starting in 1904. They improved and updated cameras by incorporating level bubbles and internal scaling instruments. In 1903, Scheimpflug developed the radial triangulation technique, and due to his successful utilization of aerial photographs for practical mapping purposes, he was referred to as the "initiator of aerial photogrammetry."

In 1899, German Sebastian Finsterwalder published the principles of modern double-image photogrammetry, as well as relative and absolute orientation. In 1901, Dr. Carl Pulfrich introduced the first stereocomparator device, which included X and Y coordinate scales. This device is significant as it was the first photogrammetry instrument manufactured by the Zeiss brand.

Professor Reinhard Hugershoff is known for his significant contributions to surveying and mapping, particularly in the field of measurement instruments. In 1921, he invented the first analog plotter, which he named the Hugershoff Autocartograph. **Figure 2.12** illustrates Hugershoff's Autocartograph.[29] The plotter could be used for various purposes, including terrestrial, oblique, and vertical aerial photography. In 1926, Hugershoff introduced the "Aerocartograph," which provided users with the ability to perform analog aerotriangulation.

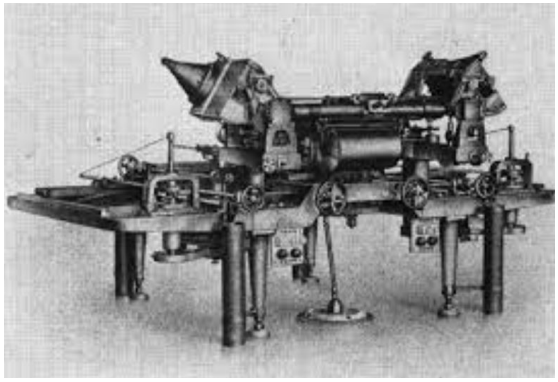

Figure 2.12: Hugershoff's Autocartograph.

In 1926, Heinrich Wild made some modifications to the instrument he had invented for terrestrial mapping and adapted it for aerial photography use, naming it

"Autograph." One of the most unique aerial cameras ever produced was the 9-lens aerial camera developed by Captain O.S. Reading for the U.S. Coast and Geodetic Survey. **Figure 2.13** shows the USC&GS 9-lens camera.[30]

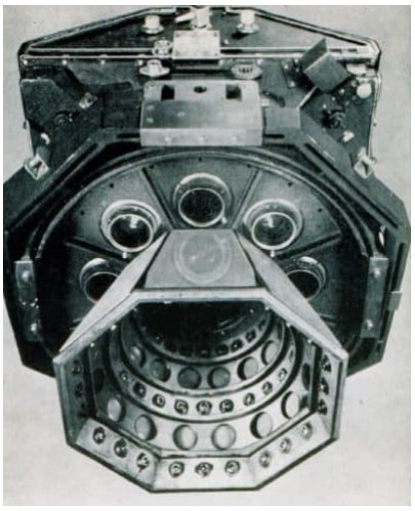

Figure 2.13: USC&GS 9-lens camera.

Ressel K. Bean earned the patent for "Ellipsoidal Reflector Projector for Stereo-Photogrammetric Map Plotting" in recognition of his significant contribution to photogrammetric instruments through the development of the ER-55 Plotter in 1956. **Figure 2.14** represent the ER-55 plotter which arranged for convergent photography.[31]

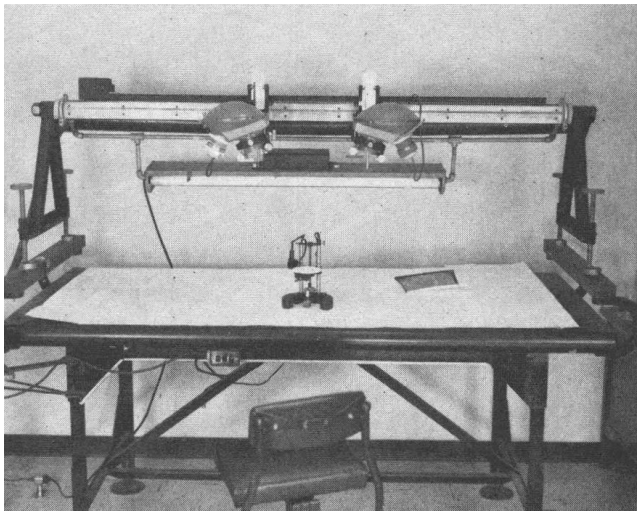

Figure 2.14: ER-55 plotter which arranged for convergent photography.

Wild Heerbrugg was founded in 1921, becoming a global leader in the field of surveying and mapping instruments. As a result of its merger with Kern in 1988, Leica was established in 1990.

2.4.3 Analytical Photogrammetry (1960 to present)

The significant scientific and technical advancements during the era of analog photogrammetry paved the way for the next phase known as analytical photogrammetry. The works of Finsterwalder, von Gruber, and Church were notable during this transition. The invention of the computer also played a crucial role in this transition. In the era of analytical photogrammetry, the following important developments took place: In 1947, Ralph O. Anderson developed a semi-analytical approach for performing analytical control. In his approach, the orientation of photographs was achieved semi-graphically, while the control extensions were calculated analytically.

In 1950, Everett Merritt published works that provided analytical solutions in the areas of interior and exterior orientation, relative and absolute orientation, space resection, and camera calibration. The independent inventions of the computer by Zure (Germany, 1941) and Aitken (U.S., 1943) brought significant advancements to photogrammetry.[4]

Duane Brown (August 1929-July 1994) is another important scientist who made significant contributions to analytical photogrammetry. While working on the RCA Missile test project in 1955, he developed new mathematical models in the areas of bundle adjustment and camera calibration. Brown also conducted research on improving the accuracy and reliability of photogrammetric adjustment and implementing self-calibration in large photogrammetric blocks. In his work with the modified ballistic camera in 1962, he achieved a scale of 1:50,000 and 2mm accuracy. Additionally, Brown assisted computer programmers in the development of software for bundle adjustment that could run on personal computers. This software, called STARS (Simultaneous Triangulation and Resection Software), was developed with his mathematical assistance. Brown successfully introduced the use of film instead of glass plates with his invention, the CRC-1 (Close-Range Camera 1). [3] This camera is also equipped with a continuously focusable lens. Additionally, Brown contributed to the development of monocomparators that offered fully automated measurements. He assisted in the development of the AutoSet-1 and later the AutoSet-2 monocomparators, which provided advanced measurement capabilities. **Figure 2.15**

shows the CRC-1 camera nd Autoset-2 as a components of the STARS system used in industrial photogrammetry.[32]

Figure 2.15: CRC-1 camera (left) nd Autoset-2 (right) as a components of the STARS system used in industrial photogrammetry.

Traditional aerial triangulation could be performed with well-metric cameras that had calibrated camera parameters. However, Houssam Mahmoud (Sam) Karara and Y.I. Abdel-Aziz conducted a series of studies that allowed photogrammetric work to be carried out with non-metric cameras. In 1971, they developed the Direct Linear Transformation (DLT) technique for this purpose. With DLT, they discovered a way to transform comparator measurements into object-space coordinates without the need for camera calibration data, comparator to photo coordinate conversion, or initial approximation of unknowns. This approach relied on polynomial equations and was derived from the affine coordinate transformation model.

2.4.2 Digital Photogrammetry (Present)

The biggest difference between digital photogrammetry and its previous generations is the use of digital photographs instead of analog, film-based photographs. This shift to digital photography is a result of advancements in imaging and computing industries. With this benefit, the need for processes such as film procurement, photochemical development for obtaining analog photographs, and steps like scanning for transitioning to the photogrammetric phase are eliminated. Furthermore, the current image Exchangeable Image File Format (EXIF) files allow embedding of crucial information such as the image capture date, camera model, resolution, focal length,

and precise geographic location of the photo capture. This enables the initiation of the processing workflow in photogrammetry software without the need for additional location files or documents containing precise photo capture coordinates.

Indeed, Gilbert Louis Hobrough was one of the important pioneers in the development of digital photogrammetry. With his extensive work in areas such as radar, three-dimensional machine vision, and barometric altimetry, he obtained patents in at least 47 fields. One of his significant contributions was the development of the electronic dodging printer. In 1961, he introduced his own image correlation concept, which played a role in the development of the Raytheon-Wild B8 Stereomat. **Figure 2.16** presents the Raytheon-Wild B8 Stereomat developed by Hobrough.[33] In 1967, Gilbert Louis Hobrough developed the Gestalt Photo Mapper (GPM), an automated orthophotographic device that utilized correlation in stereo images. The GPM consisted of a printer, scanner, computer, operator console, input/output devices, and correlator.

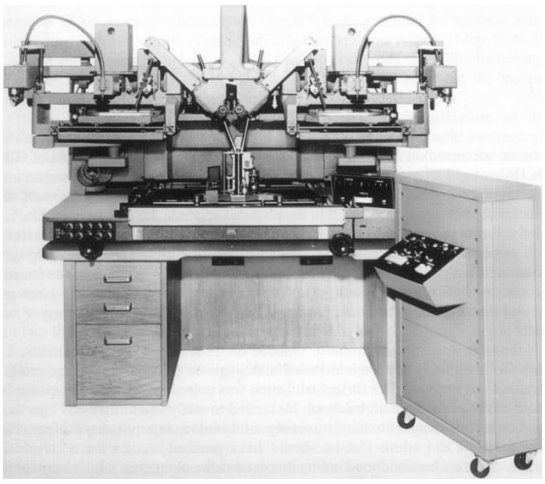

Figure 2.16: Raytheon-Wild B8 Stereomat.

The first artificial satellite was launched by the Soviet Union in 1957. It was followed by the launch of the first scientific observation satellite, Explorer 6, by the National Aeronautics and Space Administration (NASA) in 1959. This marked the addition of a new type of carrier platform to photogrammetric applications. [34]

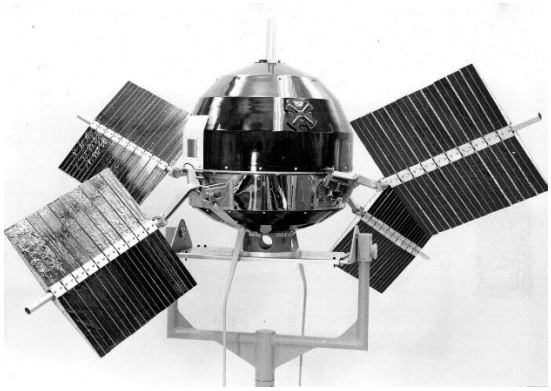

Figure 2.17: Explorer 6 observation satellite.

Uki Helava also played an important role in the development of digital photogrammetry. In 1986, he collaborated with General Dynamics to assist the Defense Mapping Agency in the development of photogrammetric workstations. Additionally, he established GDE System and formed a partnership with Leica Geosystems in 1997.

Lawrence Gilman Roberts presented his doctoral thesis titled "Machine perception of Three-Dimensional Solids" at the Massachusetts Institute of Technology (MIT) in 1963, where he examined the extraction of 3D information from 2D photographs. This study holds the distinction of being one of the first works to explore the relationship between computer vision technology and photogrammetry. [35] In 1990, during the International Society for Photogrammetry and Remote Sensing (ISPRS) symposium held in Zurich, emphasis was placed on the relationship between Close Range Photogrammetry and computer vision. [36]

In 1999, Environmental Systems Research Institute (ESRI) released ArcGIS, which is currently the most popular GIS software in the market. ESRI also introduced an open-source alternative to ArcGIS called Geographic Resources Analysis Support System (GRASS). Another open-source GIS software, QGIS, was released in 2009.

In 2008, Microsoft Live Labs released the Photosynth software, which combines computer vision and photogrammetry techniques to create high-resolution 3D point clouds and 3D models from 2D digital stitched photographs. Today, in the industry, various open-source photogrammetry software such as VisualSFM, Meshroom, and MicMac, as well as commercial solutions like PhotoModeller, RealityCapture, and

Metashape, enable the generation of numerous photogrammetric outputs in digital format in a time and cost-effective manner.

2.5 Classification of Photogrammetry

Since its inception, photogrammetry has undergone various changes and developments, leading to its classification in different environments and under numerous classification categories. The utilization of photogrammetry in various scientific disciplines, differences in carrier platforms, techniques used, cameras employed, and evaluation methods have naturally increased the number of classification categories. In this study, we will classify photogrammetry based on significant classification categories widely accepted by the photogrammetry community. These categories include terrestrial, aerial, and close-range photogrammetry based on the photography position, as well as plane table, analog, analytical, and digital photogrammetry based on the photogrammetric evaluation method.

2.5.1 According to the Location of the Photograph Taken

2.5.1.1 Terrestrial Photogrammetry

Terrestrial photogrammetry is the class of photogrammetry that involves the use of photographs taken from the Earth's surface or a location close to the Earth's surface, typically with a camera mounted on a tripod. [37] It is commonly used in applications other than mapping: for the 3D modeling and documentation of buildings, in architecture, medicine, deformation analysis, and archaeological studies. **Figure 2.18** presents an example of photo acquisition from a camera located on tripod in order to survey and model of rock discontinuities. [38]

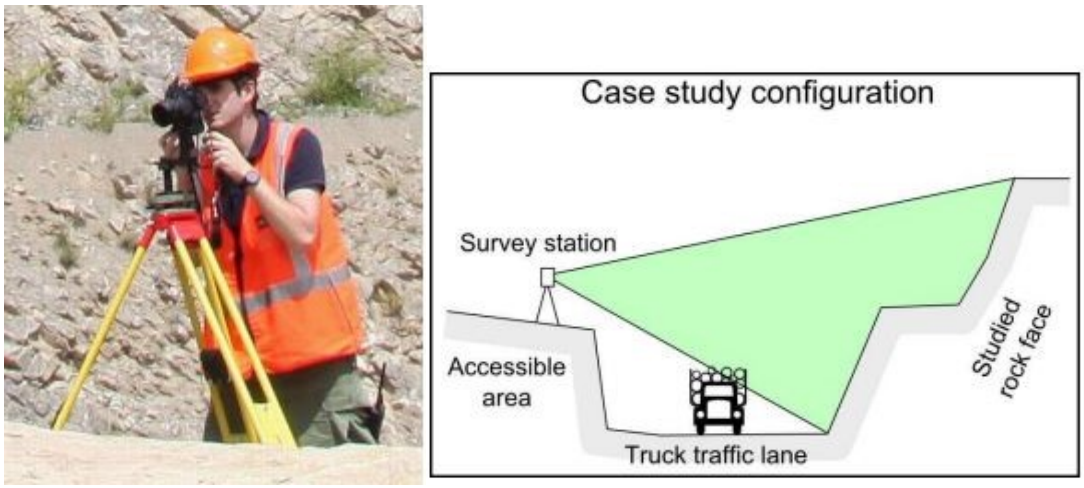

Figure 2.18: Example of photo acquisition from a camera located on tripod.

2.5.1.2 Close Range Photogrammetry

When the distance between the camera and the object is below 100 meters, terrestrial photogrammetry transforms into a new class called close-range photogrammetry. It typically involves capturing highly convergent photographs around a central object to obtain outputs such as a 3D point cloud and model. Thanks to advancements in computer and camera technologies, it has found applications in various fields such as biomechanics, architecture, archaeology, forensic analysis, historical documentation, and the automotive industry. [39] **Figure 2.19** illustrates data acquisition representation and output model of a wolf crania for zooarchaeology as an example of close range photogrammetry application.[40]

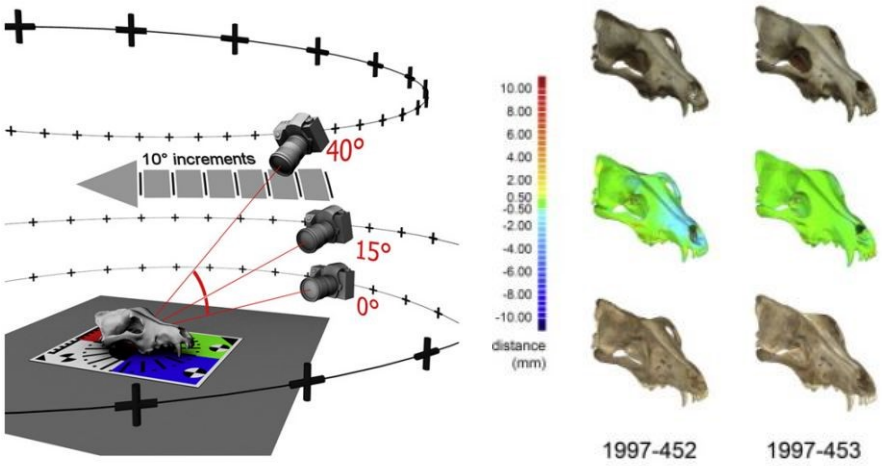

Figure 2.19: Data acquisition representation and output model of a wolf crania.

2.5.1.3 Aerial Photogrammetry

Aerial photogrammetry involves capturing photographs from an airborne platform such as a plane or UAV. High-quality digital cameras and GNSS receivers are typically used, following a flight plan, to capture overlapping images for creating outputs such as orthomosaics, topographic maps, elevation models, and contours. This technique is primarily used in areas such as surveying, urban planning, and GIS, among others. UAVs are increasingly popular due to their cost-effectiveness, flexibility, and time-saving advantages. **Figure 2.20** represents the data acquition of plane[41] and UAV[42] in aerial photogrammetry.

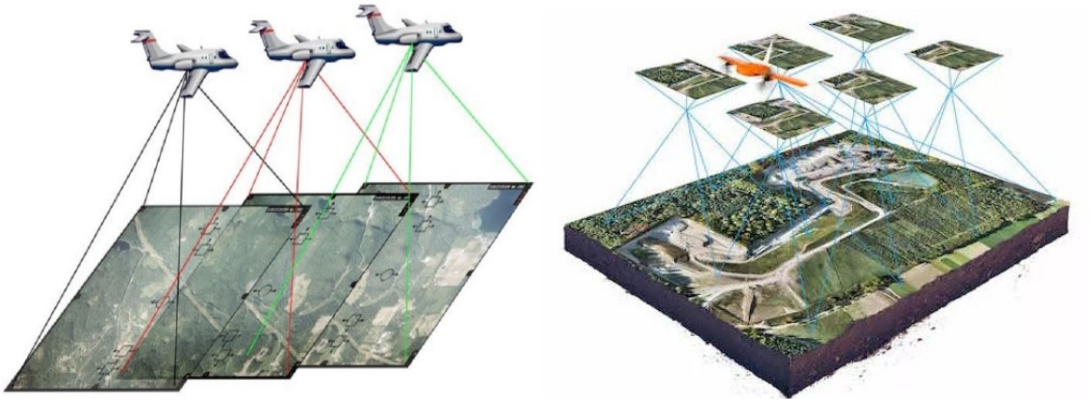

Figure 2.20: Represent the data acquition of plane (on the left) and UAV(on the right).

2.5.2 According to the Evaluation Method

2.5.2.1 Plane Table Photogrammetry

Plane table photogrammetry is a method of map production that involves using photographs and the concepts of perspective and projective geometry to measure directions and angles on a plane table. It was a technique used in the early days of photogrammetry but offered lower accuracy. The system consists of a carefully leveled and oriented plane table, a theodolite for measuring distances and angles, and a camera mounted on the theodolite. The process involves precisely processing the captured photograph and the angle and distance information obtained from the theodolite onto the plane table. However, this method has been replaced by more modern and efficient techniques in recent times.

2.5.2.2 Analog Photogrammetry

Analog photogrammetry is a type of photogrammetry that involves the use of specialized film-based cameras, as well as optical and mechanical devices, to obtain geometric or various qualitative information from physical objects. [43] This technique is generally based on stereometric vision. **Figure 2.21** illustrates the streographic vieweing.[44] It is a technique that involves the relative orientation of stereo photographs followed by the process of drawing, which includes the steps for creating 3D drawings. Film-based analog images are used as the image source, and optical and mechanical devices are utilized in the stereo viewing step. The output product consists of analog outputs generated after these photogrammetric processing steps.

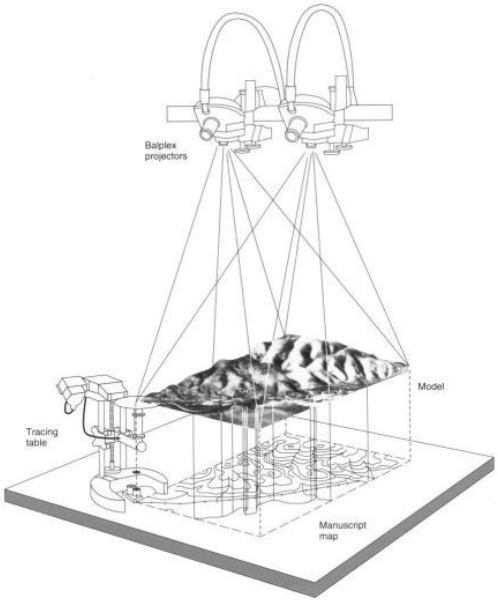

Figure 2.21: Stereographic vieweing

2.5.2.3 Analytical Photogrammetry

In analytical photogrammetry, similarly, analog film-based images obtained from specialized cameras are used. Due to the importance of the orientation angles and distances at the time of image capture, the camera setup is done meticulously. This method employs mathematical techniques, such as projective geometry, to extract geometrical and quantitative information from physical objects on the land surface. Unlike analog photogrammetry, in the stereo-viewing step, computers connected to a

stereoplotter are utilized. This technique provides more precise and reliable results compared to analog photogrammetry. [44] The output products are obtained digitally. **Figure 2.22** presents an example of analytical stereoplotter: BC3 Analytical Plotter. [44]

Figure 2.22: BC3 Analytical Plotter

2.5.2.4 Digital Photogrammetry

Digital photogrammetry is a technique that involves the processing of 2D digital images obtained from digital cameras on a computer using computer vision and photogrammetry algorithms, through various photogrammetric data processing software. It aims to extract 3D geometric and qualitative information from physical objects on the Earth's surface. [45] Due to the advantages it brings in terms of ease of use, cost, and accuracy, digital photogrammetry has replaced analog and analytical photogrammetry in modern times. The use of digital input and output data, along with the processing of photogrammetric steps on a computer and various automated processes, has made this technique a preferred choice. **Figure 2.23** shows a setup for digital photogrammetric stereoplotting.[46]

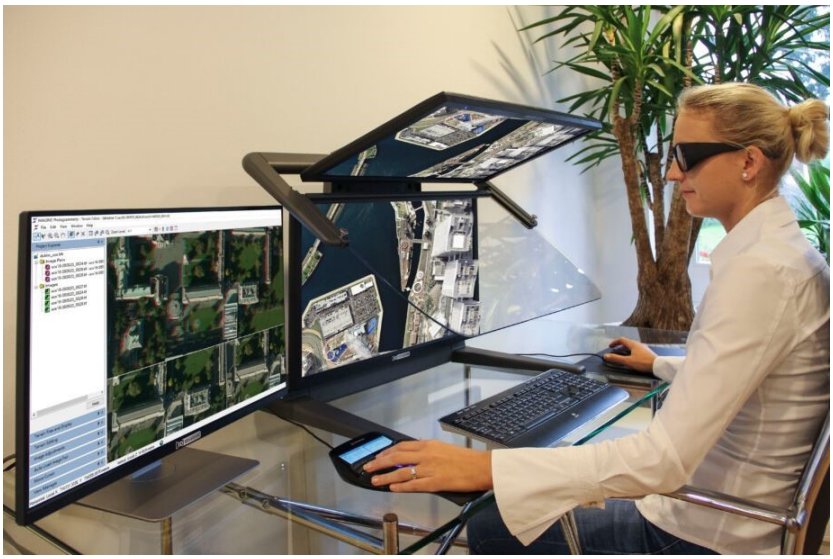

Figure 2.23: A setup for digital photogrammetric stereoplotting.

2.6 Camera Types used in Photogrammetry

Cameras can be categorized into various classes due to their different software and hardware features. They can be categorized based on the type of sensor used, such as Charge-Coupled Device (CCD) and Complementary Metal-Oxide Semiconductor (CMOS), or based on sensor size, such as medium format, full-frame, APS-C, etc. They can also be classified as DSLR (Digital Single-Lens Reflex) or mirrorless, depending on the presence or absence of a mirror in the lens-sensor plane. Furthermore, cameras can be categorized as metric or non-metric based on the availability of precise calibration and internal orientation parameters, and as analog or digital based on the method of image recording. The most general categorization among these classifications can be made between analog and digital cameras, as they can encompass the other categories simultaneously.

2.6.1 Analog Cameras

Analog cameras are devices that record and reproduce images by detecting changes in the frequency and amplitude of light entering the camera lens, based on the intensity and color characteristics of the light reflected from physical objects. In this type of camera, the light reflected from objects is recorded on light-sensitive photographic films through a chemical process. These films, which represent the physical form of the recorded light, undergo additional processes such as photo development to make

the images visible and, if needed, can be digitized for further processing. Analog cameras have been used for over a century and have played a significant role in the development of modern photography technology.

2.6.2 Digital Cameras

Digital cameras are electronic devices that record light reflected from physical objects onto photosensitive sensors, such as CCD and CMOS, in digital format. The image recording mechanism of digital cameras is closely associated with optics, electronics, and digital signal processing. The light rays that reach the sensors are first converted into electronic signals and then into digital signals before being recorded onto storage media, such as memory cards. Digital images consist of individual pixel values that vary in terms of color and brightness. These pixel values can be further utilized by various software applications for analysis, interpretation, and manipulation, depending on the intended use and purpose.

Digital cameras have replaced analog cameras in terms of ease of use, storage, image capture methods, and suitability for photogrammetry. They are widely used today. These cameras provide high-resolution images in terms of image quality, making them a popular choice in the field of photogrammetry.

2.7 Mathematical Background of Photogrammetry

To obtain photogrammetric products using overlapping photographs taken on the target object or the surface of the terrain, and to perform the necessary geometric and positional calculations, it is necessary to establish the mathematical relationship between the image and object coordinate systems by utilizing the principles of perspective geometry. [48] This mathematical relationship can generally be referred to as the transformation relationship between two coordinate systems. **Figure 2.24** respresents the relation between image and object coordinate systems.[47] The mathematical relationships established through projection equations are generally expressed as follows:

$$\begin{bmatrix} x - x_0 \\ y - y_0 \\ -c \end{bmatrix} = \frac{1}{s} . R. \begin{bmatrix} X - X_0 \\ Y - Y_0 \\ Z - Z_0 \end{bmatrix} \quad (2.1)$$

x,y : image coordinates,,
x_0, y_0 : image coordinates of the projection center,
c : focal length,
s : scale,
R : rotation matrix,
X,Y,Z: object coordinates,
X_0,Y_0, Z_0: object coordinates of the projection center.

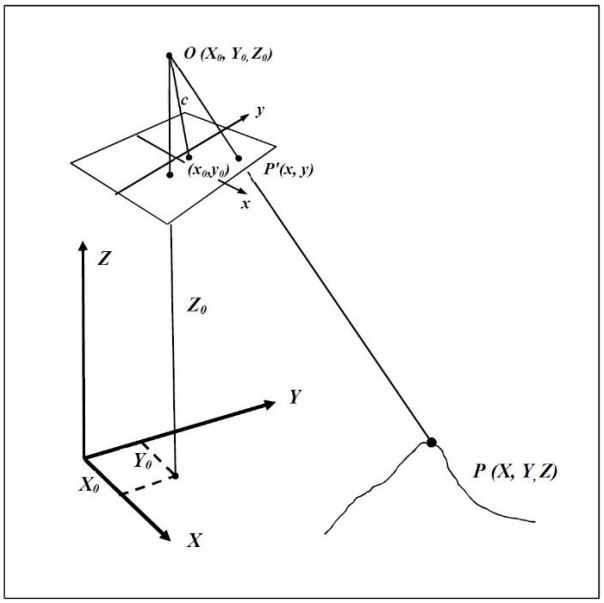

Figure 2.24: Relation between image and object coordinate systems

When x and y are left on the left side of the equations:

$$x = x_0 - c\frac{R_{11}(X-X_0)+R_{12}(Y-Y_0)+R_{13}(Z-Z_0)}{R_{31}(X-X_0)+R_{32}(Y-Y_0)+R_{33}(Z-Z_0)} \quad (2.2)$$

$$y = y_0 - c\frac{R_{21}(X-X_0)+R_{22}(Y-Y_0)+R_{23}(Z-Z_0)}{R_{31}(X-X_0)+R_{32}(Y-Y_0)+R_{33}(Z-Z_0)} \quad (2.3)$$

The terms (x_0, y_0) and c (focal length) in the equations represent the image coordinates of the camera's projection center and the focal length, respectively. These parameters are referred to as the internal orientation parameters. For precise photogrammetric cameras, the internal orientation parameters are obtained with accuracy either through camera calibration reports conducted by manufacturers in a laboratory environment or by satisfying the collinearity condition. [47]

The camera's projection center's object coordinates (X_0,Y_0, Z_0) and the rotation matrix (R) seen in the equations represent the external orientation parameters. The external orientation parameters are obtained by measuring them with the help of GNSS-IMU or through space resection method using GCPs.[47]

If the image coordinates given in equations (2.2) and (2.3) are written in terms of object coordinates:

$$X = X_0 + (Z - Z_0)\frac{R_{11}(x-x_0)+R_{21}(y-y_0)-R_{31}c}{R_{13}(x-x_0)+R_{23}(y-y_0)-R_{33}c} \tag{2.4}$$

$$Y = Y_0 + (Z - Z_0)\frac{R_{12}(x-x_0)+R_{22}(y-y_0)-R_{32}c}{R_{13}(x-x_0)+R_{23}(y-y_0)-R_{33}c} \tag{2.5}$$

equations can be written. As evident from the last equations, in order to obtain the object coordinates (X, Y, and Z) from image coordinates, it is necessary to have at least two photographs taken from different positions of the object. Thus, using the first image, we can write equations (2.6), and using the second image, we can write equations (2.7).

$$X = X_{01} + (Z - Z_{01})kx_1 \tag{2.6}$$
$$Y = Y_{01} + (Z - Z_{01})ky_1$$

$$X = X_{02} + (Z - Z_{02})kx_2 \tag{2.7}$$
$$Y = Y_{02} + (Z - Z_{02})ky_2$$

The Z value associated with the object can be obtained by substituting the X values obtained from equations (2.6) and (2.7) into equation (2.8).

$$Z = \frac{X_{02}-Z_{02}kx_2+Z_{01}kx_1-X_{01}}{kx_1-kx_2} \tag{2.8}$$

Chapter 3

Unmanned Aerial Vehicles

3.1 Definition of UAV

The term "Unmanned Aerial Vehicle" (UAV) refers to aircraft that can perform flight dynamics and are typically powered and controlled by an operator on the ground. The flight operator controls the UAV remotely through radio signals, allowing communication between the operator and the unmanned aircraft. These systems are widely used in robotics, computer science, and artificial intelligence, and have been extensively employed in the fields of photogrammetry and remote sensing since their inception. While terms such as "aerial robot" or commonly "drone" can be used to describe unmanned aerial vehicles, UAV is the most widely accepted term. The term UAV was first used in the 1970s and 1980s by the United States Department of Defense.[48]

The first aerial photograph was taken by Gaspard Tournachon using a manned balloon in 1858, and in the following years, it was replaced by manned balloons. [47] The experiment conducted by the Bavarian Pigeon Corps, in which they placed a camera on a pigeon's chest, is one of the remarkable examples of early developments. Various unmanned platforms such as kites and rockets were also used, but understanding the potential of unmanned aerial vehicles inevitably led to their strategic use in warfare. Examples of this include the unmanned aerial vehicles carrying explosive payloads during World War II, such as the 'unmanned V-1 and V-2,' and the use of the 'UAV Ryan 147' by the United States to gather information from the battlefield during the Vietnam War. [48]

One of the first experiments with fixed-wing unmanned aerial vehicles was conducted in 1979 by Przybilla and Wester-Ebbinghaus. In this experiment, a UAV with a 3m fuselage and a 2.6m wingspan, equipped with an optical camera, was used. The UAV was manufactured by Hegi company. **Figure 3.1** shows the model airplane developed by firma Hegi.[49] In 1980, the same team conducted a second test using a rotary-wing model helicopter carrying a medium-format Rolleiflex camera. Undoubtedly, such developments are pioneering steps in the field of unmanned aerial vehicles and represent significant milestones in the evolution of UAVs as we know them today. Like many other technologies, the development of unmanned aerial vehicles has gained momentum through military needs. When looking at statistical data, the United States is among the countries that invest the most in this field.

Figure 3.1: Model airplane developed by firma Hegi.

The advancement of technologies such as integrated circuitry, radio-controlled systems, GNSS and navigation systems, gimbal, and IMU, along with their integration into UAVs, has elevated the use of UAVs in photogrammetry and remote sensing to a gold standard position. The active utilization of these technologies in these systems allows for precise position and orientation measurements, enabling the acquisition of cm-level resolution and accurate products with low budget and minimal effort. UAVs offer advantages such as low cost, high accuracy, access to risky areas where manned aircraft cannot reach, and the ability to capture imagery at low altitudes in enclosed environments without being affected by cloud cover. Due to these advantages, UAVs have become an inevitable and sometimes necessary choice for photogrammetry and remote sensing applications.

3.2 Fundamental Compenents of UAV

UAVs, hardware and software components working in perfect harmony, are robotic systems that can operate either through remote control via radio communication or autonomously. Developments in electronics and software have had a significant impact on unmanned aerial vehicles, transforming them into complex mechanisms with a wide range of capabilities. The main components of UAVs can be divided into three categories: (i) aerial platform, (ii) ground control station, and (iii) communication system.[50] **Table 3.1** shows the main components of unmanned aerial vehicles.

Table 3.1: Main components of unmanned aerial vehicles.

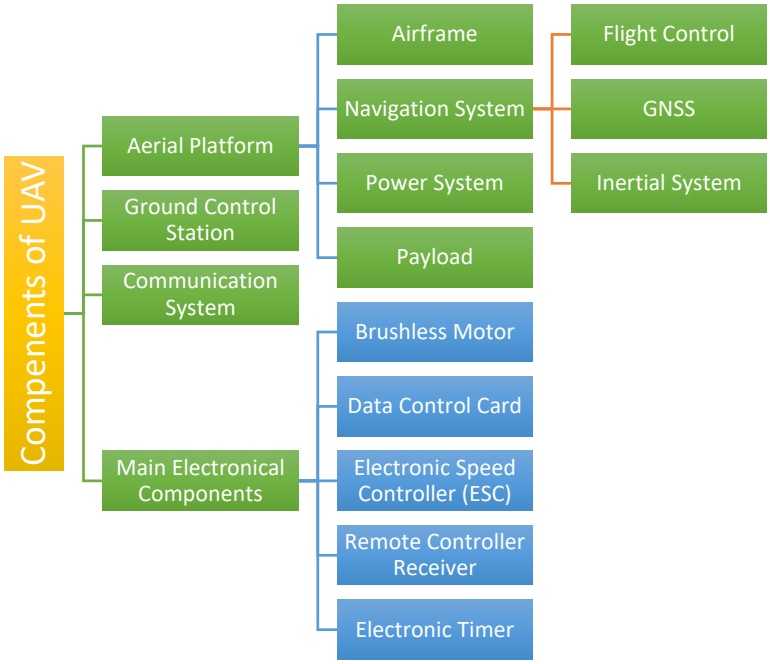

The airframe is the main component of an UAVs where all electronic components are mounted. It serves as the primary structure that protects the UAV against rain and potential physical contact to a certain extent. In fixed-wing systems, the thrust force acting on the wings affects this area of the UAV. Considering factors such as wind resistance, aerodynamics, and flight dynamics, the airframe should be made of lightweight and durable materials. Generally, polystyrene and plastic are preferred for fixed-wing systems, while aluminum and carbon fiber materials are commonly used in rotary-wing systems.

The navigation system is a crucial component for enabling autonomous or semi-autonomous flight UAVs. It consists of the flight control unit, GNSS (Global Navigation Satellite System), and the inertial system. The flight control unit is the most important element of the navigation system as it performs flight planning and enables the UAV to follow a predetermined trajectory. It can also interface with a storage unit to record data such as log files, telemetry, and images. On the other hand, GNSS plays a vital role in navigation. It allows for position measurement and navigation using single-frequency or dual-frequency, multi-constellation receivers such as GPS-GLONASS. [50] Real-Time Kinematic (RTK) modules allow for receiving real-time correction data, and raw data (pseudo-range and carrier phase) can be recorded for post-processing with techniques like Post Process Kinematic (PPK) to achieve high-precision positioning. It is an essential component for photogrammetric applications in UAVs. The final component of the navigation system is the inertial system, specifically the Inertial Measurement Unit (IMU). The IMU works in conjunction with the GNSS receiver in the UAV and is responsible for measuring the UAV's position and attitude angles in all three axes. **Figure 3.2** shows the definition of the UAVs attitude anglesfor fixed wing[51] and rotary wing[52] UAVs.

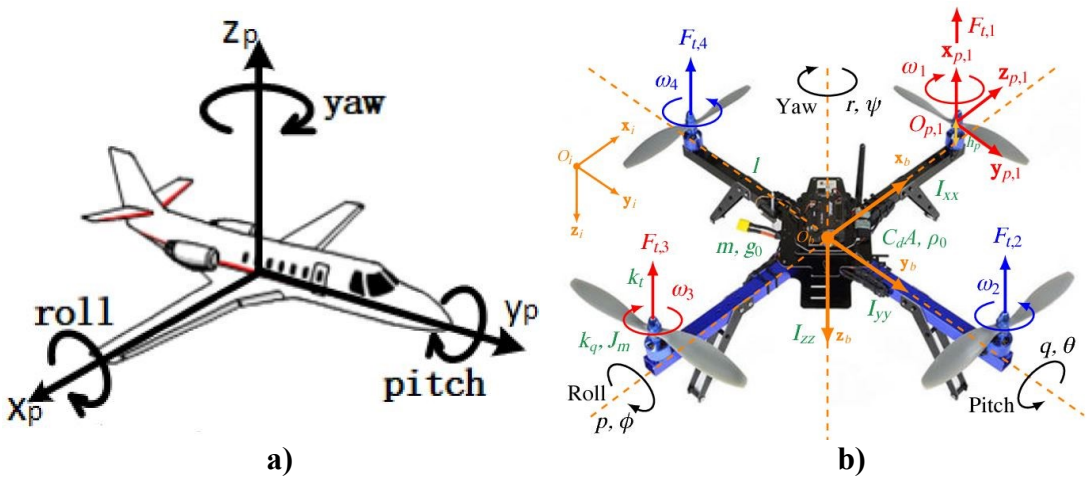

Figure 3.2: Definition of the UAVs attitude angles for fixed wing on the left (a) and rotary wing on the right (b)

Power systems are also vital components of UAVs. Different power systems such as fuel cells and electric solutions can be added to unmanned aerial vehicles. The most commonly used power source is lithium polymer (LiPo) batteries.

Depending on the intended use, various payloads can be added to unmanned aerial vehicles along with gimbals that provide stabilization in 1-3 axes of movement. The most commonly added payloads for surveying purposes are as follows: (i) digital cameras, (ii) thermal cameras, (iii) multispectral cameras, (iv) Light Detection and Ranging (LIDAR).

The ground control station is the structure that enables interactive communication between the UAV and the pilot. Communication and flight planning are typically done using Remote Controllers (RC) connected to touch screens or tablets. Flight planning involves defining photogrammetric flight parameters (e.g., side and front overlap, Ground Sampling Distance (GSD)), defining the flight area, setting camera parameters, and enabling autonomous flight.

Another component of UAV is the communication system. The connection and communication between the UAV and RC are established through radio connection. Radio Frequency (RF) is commonly used, typically within the range of 30 MHz to 3 GHz. [50]

Brushless motors are the most common type of direct current (DC) motors used in UAVs. [10] They are distinguished by their effective and consistent moment/speed relationship. On the other hand, the data control card is responsible for processing the information received from the RC and sensors in real-time. The Electronic Speed Controller (ESC) allows the control of motor speed based on the signals received from the flight control unit. Additionally, the electronic timer is an electronic UAV component that enables capturing photos at equal time intervals based on a predetermined or required time range. **Figure 3.3** presents a compenent of UAV over a custom build sample. [53]

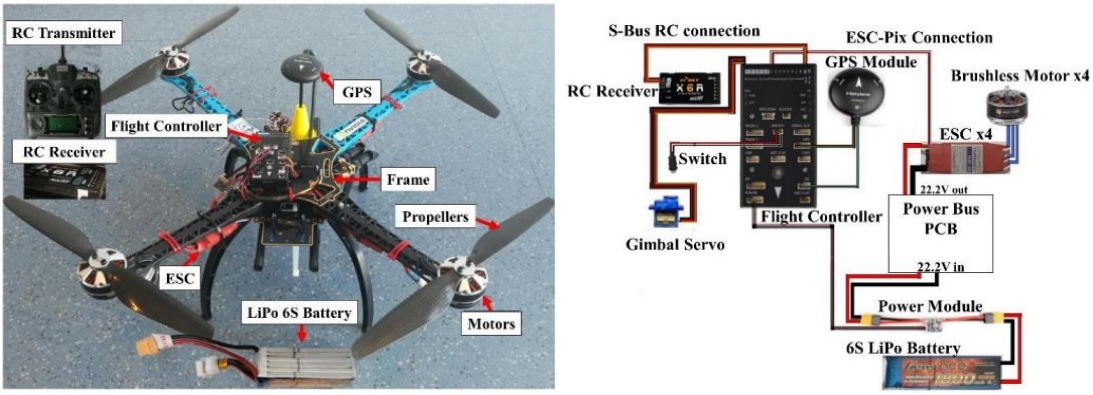

Figure 3.3: Compenents of UAV over a custom build sample.

3.3 Classification of UAVs

Due to the wide range of hardware components they possess, unmanned aerial vehicles (UAVs) can be classified into various categories by considering multiple criteria. Classes can be established based on features such as wing type, weight, power source, and intended use, among others. In his study, Eisenbeiß [49] classified unmanned aerial vehicles (UAVs) based on their characteristic features such as unpowered or powered, heavier than air or lighter than air, and flexible, fixed, or rotary wings. **Table 3.2** presents the classification of UAVs according to the classes lighter or heavier than air, powered and unpowered.[49] Another classification method for UAVs can be based on their characteristics such as size/weight, maximum flight height, flight duration, and endurance. This classification can include categories such as micro, mini, short-range, close-range, medium-range, long-range, and low, medium, and high altitude. [54] According to their usage, UAVs can be classified into categories such as commercial, military, and special purpose. While there are various classification methods for UAVs, in this study, we will examine them based on the most commonly used wing types for photogrammetric purposes, which are rotary-wing UAVs and fixed-wing UAVs.

Table 3.2: Present the classification of UAVs according to the classes lighter or heavier than air, powered and unpowered.

	Lighter than air	**Heavier than air**		
		Flexible wing	**Fixed wing**	**Rotary wing**
Unpowered	Balloon	Hang glider	Glider	Rotor-kite
		Paraglider		
		Kites		
Powered	Airship	Paraglider	Propeller	Sinle rotors
			Jet engines	Coaxial
				Quadrotors
				Multi-rotors

3.3.1 Rotary-Wing UAVs

Rotary-wing UAVs typically have rotating wings connected to brushless DC electric motors, and they take off and maneuver using the lift and thrust generated by these wings. This class can be further divided into subcategories based on the number of motors the unmanned aerial vehicle possesses, such as single-, double-, four-, and multi-rotary configurations. [49] Increasing the number of motors according to the intended use enhances the UAV's payload capacity, stability, and flight safety. Their small size and low weight allow them to perform flights even in confined spaces, and their ability to hover in the air enables them to fly in close proximity to target objects. **Figure 3.4** presents the DJI Matrice 30T as an example of rotary-wing UAV.[55] As a result, they have advantageous features such as the ability to perform circular oblique flights for reconnaissance, surveillance, and 3D modeling. Additionally, their Vertical Take-off and Landing (VTOL) capability allows them to take off and land from nearly any location, providing them with high maneuverability. However, these types of unmanned aerial vehicles have limitations in terms of wind resistance, flight duration, and range.

Figure 3.4: DJI Matrice 30T rotary-wing UAV.

3.3.2 Fixed-Wing UAVs

Fixed-wing UAVs, unlike rotary-wing UAVs with rotating wings, generate the necessary lift force by the upward force exerted on the wings of the UAV moving forward through the air. In this system, the motors enable forward motion to occur.

Fixed-wing UAVs can stay in the air for longer durations compared to rotary-wing UAVs, making them ideal for conducting photogrammetric flights over large areas. They also have higher wind resistance and can operate at higher altitudes. [49] Due to their flight dynamics, fixed-wing UAVs cannot hover in one position like rotary-wing UAVs, which can be a disadvantage in certain tasks such as getting close to target objects or conducting 3D modeling flights. Additionally, fixed-wing UAVs typically require a runway or a launching mechanism for takeoff and landing, necessitating an open and suitable area for these operations. Therefore, urban flights are not feasible with this type of UAV. Furthermore, some fixed-wing UAVs (e.g., SenseFly eBee X) have landing mechanisms that involve hitting the ground, which can potentially cause damage to both the UAV and the camera lens it carries over time.

Some fixed-wing UAVs used for surveying and mapping purposes, such as WingtraOne and Quantum Systems Trinity F90+, have the advantage of combining the benefits of fixed-wing design with the VTOL capability similar to rotary-wing UAVs. This means they are capable of vertical takeoff and landing, in addition to their fixed-wing flight capabilities. **Figure 3.5** shows the WingtraOne as an example of fixed-wing UAV. These types of UAVs perform vertical takeoff and landing and then transition to horizontal fixed-wing flight once they reach the designated altitude. This

allows them to reduce the required open space for takeoff and landing compared to other fixed-wing UAVs, eliminate the need for a launcher system, and avoid deformations encountered during landing.

Figure 3.5: WingtraOne as an example of fixed-wing UAV.

Some fixed-wing UAVs on the market (e.g., Alti Reach) address one of the most critical needs of all UAVs, which is extended flight duration and battery issues, by utilizing liquid-fueled engines. These types of UAVs, specifically designed for this purpose, are capable of conducting flights for over 10 hours. They combine the advantages of fixed-wing design with VTOL capabilities, offering an efficient and long-duration solution for various applications. **Figure 3.6** represents the Alti Reach fixed-wing UAV which has a liquid fuel engine and VTOL feature.[56]

Figure 3.6: Alti Reach fixed-wing UAV which has a liquid fuel engine and VTOL feature.

3.4 UAV for Photogrammetry

Unmanned aerial vehicles have been considered as suitable carrier platforms for photogrammetry since their early emergence, and they have been utilized for acquiring photogrammetric data. However, it is important to note that these mentioned unmanned aerial vehicles had very primitive and limited capabilities in terms of technology and variety compared to the systems used today. Following Nadar's capture of the first aerial photograph during his balloon flight in 1855, the use of unmanned balloons for capturing aerial photographs can be considered as the earliest form of unmanned aerial vehicles used for this purpose.

With the advancement of technology, unmanned aerial vehicles (UAVs) have evolved into much more suitable platforms for photogrammetric purposes. The improvement in sensor technology and resolution of photogrammetric cameras used as payload has played a significant role in capturing stable and high-quality photographs. The use of gimbals has become essential for precise and stabilized image acquisition. Additionally, the integration of Global Navigation Satellite System (GNSS) receivers and Inertial Measurement Units (IMUs) for accurate coordinate positioning, along with the incorporation of other auxiliary sensors such as compasses, gyroscopes, and accelerometers into UAV hardware, has made UAV-based photogrammetry an indispensable method in various fields today.

The advantages of using unmanned aerial vehicles (UAVs) for photogrammetric purposes compared to other systems can be summarized as follows:

- UAVs equipped with precision photogrammetric capabilities and automatic pilot software enable precise and accurate data acquisition through automated and systematic capture of photographs with specific front and side overlap. This simplifies the process of obtaining accurate coordinate measurements and facilitates the acquisition of precise and reliable data.

- UAVs allow for the completion of potentially less costly projects in a more cost-effective manner in terms of flight and data acquisition.

- UAVs are capable of flying at close distances to the desired objects for photography, providing an advantage in projects that require close-up shots. Additionally, the photo resolution increases in close-up photography.

- The maneuverability of rotary-wing UAVs, such as hovering and circular flight, provides an advantage in the use of UAVs for photogrammetric projects that involve 3D modeling.

- UAV systems are produced at a lower cost compared to other carrier systems such as airplanes, helicopters, and satellites, providing a cost advantage.

In addition to the advantages of unmanned aerial vehicles compared to other carrier systems, some of their shortcomings and disadvantages are as follows:

- UAVs have limitations in terms of flight duration and range compared to other carrier systems, which is why they have constraints in large-scale projects.
- Due to their lightweight structures, drones are less resistant and more sensitive to weather conditions such as wind and rain.
- The connection between UAVs and remote controllers (RC) provided by radio waves is limited, which imposes restrictions on the flight range of UAVs.
- UAVs have a low payload carrying capacity, which means they are unable to carry very heavy payloads.

Chapter 4

3D Models

4.1 3D Models as Output of Photogrammetry

One of the most important output data generated through modern photogrammetric studies is undoubtedly 3D models. 3D models can be defined as the extraction and reconstruction of the 3D geometry and appearance of a physical object or terrain surface through the use of 2D multiple overlapped photographs and algorithms. After the necessary processing, different types of 3D models (e.g., 3D mesh, 3D textured model, 3D tiled model) can be obtained, and it is possible to store these models in various file formats (e.g., ".dae," ".obj," and ".fbx" etc.).

In modern times, laser scanning and photogrammetric methods are commonly used to generate realistic 3D models of physical objects. Laser scanning method tends to provide more detailed models compared to the photogrammetric method. However, the texture quality of the model obtained through laser scanning is relatively weaker compared to models generated through photogrammetry. **Figure 4.1** represents the texture comparison of a Greek vase created by both laser scanning and photogrammetry method carrıed out by Polo M.-E et al.[57]. The photogrammetry method is preferred in many applications due to its ability to create optimal models with detailed geometry and high-quality textures.

Figure 4.1: Details from the texture of photogrammetric model (left) and the scanned model (right) of the replika Greek vase.

Before creating 3D models, the process of aerial triangulation or bundle block adjustment needs to be performed on the photographs to carry out relative orientation and absolute orientation operations. This way, the orientation of each photograph is determined, and the coordinates of objects in the photographs are calculated, forming "key points." By densifying these "key points," a "dense point cloud" is created. 3D mesh surfaces can be generated using either key points or dense point clouds. The 3D mesh surfaces, which are representations of 3D objects composed of interconnected triangles, can be textured using images obtained from the photographs to obtain 3D textured models. **Figure 4.2** illustrates an example of 3D mesh and 3D textured model.[58]

a) b)

Figure 4.2: An example of : (a)3D mesh and (b) 3D textured model.

Another type of model is the 3D tiled model. They are also created through similar photogrammetric processes. However, unlike standard single, large-sized models, this type of data is divided into small pieces called "tiles" and stored. With its hierarchical structure, the model loads and displays the tiles that are approached by the user during

the viewing stage. This approach and data type aim to make 3D models more manageable, efficient, and fast to display, especially in an online environment. It is particularly effective for 3D city planning projects where quick and efficient data handling is required.

4.2 Usage Area Analysis of 3D Models

Photogrammetric 3D models have a wide range of applications due to their visual quality, spatial accuracy, and cost-effective production. These chosen as a preferred method and tool by researchers in various academic disciplines and find extensive use in many industrial sectors. The usage of 3D models created through photogrammetric methods can be observed in fields such as surveying, GIS, urban planning, architecture, engineering, archaeology, geology, film, and game industry, among others. **Table 4.1** represents comprehensive examples of usage areas of photogrammetric 3D models.

Table 4.1: Comprehensive examples of usage areas of photogrammetric 3D models.

• 3d Urban Planning	• Historical Documentation
• Cultural Heritage Preservation	• Volume Calculation
• Restoration Works	• Industrial Applications
• Archeological Documentation	• Inspection
• 3D Surveying	• Renewable Energy Industry
• Real Estate Sector	• Real Estate Valuation
• Urban Renewal	• Disaster Management
• Inspection Works	• Building Roof Inspection
• Disaster Management	• Tourism Sector
• Virtual And Augmented Reality	• Geology
• Video Game Development	• Education and Training
• 3D Cadastre	• Infrastructre Planning

• Real Estate Insurance	• Management of Military and Security Operations
• Protection Of Critical Infrastructure Facilities	• Advertisement
• Academic Researchs	• Medical Research and Visualization
• Film And Animation	• Thermal Model Applications
• Forensic	• Crime Scene Investigation
• Compenet Endurance And Stabiliy Tests	• Feasibility Studies

While 3D models have various applications in many sectors, in this study, we will explain six of the most common usage areas. These six application areas are as follows: 3D Cadastre, Urban Planning, Cultural Heritage Documentation and Restoration, Virtual Reality, Video Game Development, and Renewable Energy Solutions.

4.2.1 3D Cadastre

Land and property have been important components of human life throughout history. In order to record, protect, and calculate taxes for the rights, restrictions, and responsibilities associated with this significant concept, countries have developed cadastre systems. However, the rapid population growth and urbanization, especially in terms of construction within cities, have led to the need for a cadastre system that can effectively protect the property and rights of citizens. In many countries, including our own, the existing cadastre system is two-dimensional. This two-dimensional structure often fails to resolve certain disputes due to a lack of information, highlighting the increasing need for a cadastre system with a 3D structure.

The application of 3D textured models, created from oblique photographs taken through the photogrammetry method, in the cadastre system would greatly facilitate the work of citizens and public institutions in protecting property rights and responsibilities. It would also establish a better relationship between property and its surroundings. In this regard, 3D models are highly beneficial tools for the cadastre system.

4.2.2 Urban Planning

City models integrate comprehensive strategies, spatial drawings, maps, and plans that encompass the management and development parameters of a region. Photogrammetric 3D models enhance the visual presentation and interpretation capabilities for the planning of a specific area, thereby increasing the effectiveness of the planning and plan presentation processes. For instance, these models enable urban planners to visualize city plans as more realistic 3D models, and their integration into GIS databases can serve as a foundation for various analyses and future planning initiatives.

On the other hand, applying a 3D city model created through architectural drawing methods onto a 3D surface model for areas where the planning has been done but the implementation is yet to take place can guide planners in analyzing the potential impacts or planning possible transportation routes before implementation. This type of 3D city model is exemplified in **Figure 4.3**. [59] The presentation to neighboring property owners using these models can provide preliminary information to the property owners regarding traffic, daylight, and the quantity of public spaces in the planned area.

Figure 4.3: An example of 3D city model

4.2.3 Cultural Heritage Documentation and Restoration

The documentation and preservation of cultural heritage are crucial for preserving our cultural identity and passing it on to future generations. For historical buildings,

sculptures, or any other type of artifact with a centuries-old history, recording them in a three-dimensional and realistic manner serves this purpose best. Close-range photogrammetry techniques, which are a subfield of photogrammetry, are used to create 3D textured models. These models can be securely stored using modern technology and presented to users on web 3D model presentation platforms like Sketchfab. Additionally, these models can serve as a valuable resource for restoration purposes in case any deformations occur in the structure. **Figure 4.4** presents photo acquisition of the real, 3D model and restored replika of Madonna of the Old Town Hall in Praque, located in the Praque City Museum.[60]

a) b) c)

Figure 4.4: Documentation of Madonna of the Old Town Hall in Praque: (a) data acquisition of the actual statue, (b) presentation of the actual statue and its interactive 3D model on tochscreen, (c) restored replika of the statue located on the Praque Atronomical Clock

4.2.4 Virtual Reality

The use of photogrammetric 3D models within the scope of Virtual Reality (VR) is becoming increasingly popular. Detailed and comprehensive 3D models immerse users in different virtual worlds and provide a sense of being present in the modeled environment. Nowadays, 3D models of buildings created using this method are presented on the internet for promotional purposes, allowing users to navigate through the modeled environment as if they were physically present, using VR equipment. They can explore the virtual space and view all the visual content required.

Another application is the creation of digital VR museums where cultural heritage is recorded in 3D. Users can explore the museum in a computer-generated environment, as if they were physically present, using 3D models created through photogrammetric methods and, if available, laser scans. They can access the necessary visual and written information during their virtual visit to the museum.

4.2.5 Video Game Development

Due to its advantages of precision, detail, and realistic 3D model output, photogrammetry is an ideal technique for producing 3D models needed in the video game industry. The 3D models created using this technique meet the industry's demand for realistic and detailed models in a cost-effective and efficient manner compared to traditional 3D model production methods. The models can be created to represent the desired game environment for a realistic and immersive gaming experience, and they can be integrated into the game interface. Additionally, character models can also be created using this method and incorporated into the game. Furthermore, this approach significantly reduces production costs by eliminating the need for a dedicated team of artists for traditional model production.

4.2.6 Renewable Energy Solutions

The use of photogrammetric 3D models is encountered in the renewable energy sector, especially in wind and solar energy applications. In these applications, 3D models are utilized for various purposes such as generating feasibility reports, determining installation locations, and conducting efficiency analyses before and after installation using the 3D models. For example, in wind energy, 3D models are employed to identify the installation point for wind turbines, perform wind flow analyses, and detect turbine deformations. [61]

Photogrammetric 3D models are also used in the solar energy sector for purposes such as panel layout and feasibility studies on the model, calculation of solar exposure and shading durations, and assessment of the efficiency and damage of installed panels.

Chapter 5

Materials and Methods

5.1 Study Area

Within the scope of the study, a business center building located in Dresden, the capital of the state of Saxony in eastern Germany, was selected as the study area. Dresden is the 12th largest city in Germany in terms of population and the 4th largest in terms of area. The city is also known as the "Florence of the Elbe" due to its historical background, vibrant cultural environment, and architectural structure. With these characteristics, Dresden is among the most visited cities in Germany by tourists. The study area`s center point is located approximately on the 51° 2' 55.90" North latitude and 13°42'34.57" East longitude. The area corresponds to an approximate area of 10,771 m^2. **Figure 5.1** presents the geographic location of the study area.[62]

Figure 5.1: Geographic location of the study area

5.2 Softwares and Equipments used in the Study

In the study, we used the popular 7 UAVs commonly found in the industry and the cameras mounted on these UAVs by most manufacturers for aerial photography. 7 different UAVs were used in the thesis to capture aerial photographs. **Table 5.1** presents the UAVs used in the study. Although DJI Mini 3 Pro does not include RTK and PPK modules that allow for precise positioning, we added it to the inventory. We wanted to investigate the accuracy of the model generated through photogrammetric processes and the GNSS receiver with meter-level accuracy for rough positioning, despite the absence of RTK and PPK modules. The results obtained from this will serve as a reference for studies that require a scaled model rather than absolute coordinates and are specifically focused on relative accuracy.

Table 5.1: UAVs used in the study.

UAV	Type of the UAV
DJI Mini 3 Pro	Rotary-wing
DJI Mavic 3E	Rotary-wing
DJI Mavic 3T	Rotary-wing
DJI Phantom 4 RTK	Rotary-wing
DJI Matrice 30T	Rotary-wing
DJI Matrice 300 RTK	Rotary-wing
WingtraOne Gen II	Fixed-wing

During the conducted flights, we utilized the DJI DRTK-2 Mobile Station GNSS receiver as a base station to obtain coordinate correction data, enabling us to acquire precise photo coordinates.

Unlike the other UAVs used, the WingtraOne Gen II has a PPK module, which requires an additional office-based PPK process to obtain accurate coordinates after obtaining the aerial photographs. For this purpose, we used the software called WingtraHub, developed by the manufacturer, to perform the PPK process.

To carry out the photogrammetric data processing steps and obtain the final output products, we used the Agisoft Metashape Pro software, which is widely used in the industry due to its advantages in output product quality and data processing speed.

5.2.1 DJI Mini 3 Pro

The DJI Mini 3 Pro model is one of the latest mini unmanned aerial vehicles released by DJI. It stands out for its small size, weighing less than 249 grams, and its successful camera performance considering its dimensions. **Figure 5.2** presents photograph of the DJI Mini 3 Pro. [63] The DJI Mini 3 Pro is favored by users for its low weight, as it falls below the legal restrictions imposed by many countries, allowing for flights without encountering legal limitations. This UAV features a 48MP effective pixel camera with a 1/1.3-inch CMOS sensor and a 24mm focal length, capable of recording 4K HDR/60 FPS videos. While it does not have an RTK or PPK receiver, it is equipped with a GNSS receiver that can connect to GPS, Galileo, and BeiDou satellites for rough coordinate measurements. The UAV is primarily designed for digital content creators for video and photo capture, as well as hobbyist use, and is not suitable for mapping purposes. We included it in this study because we wanted to investigate its performance in areas where absolute accuracy is not crucial, but relative accuracy in scaled models is required. **Table 5.2** shows the technical specifications of the DJI Mini 3 Pro. [63]

Table 5.2: Technical specifications of the DJI Mini 3 Pro.

Aircraft	Takeoff Weight	<249 g
	Max Flight Time	34 min (with Intelligent Flight Battery) 47 min (with Intelligent Flight Battery plus)
	Max Wind Speed Resistance	10.7 m/s
	Operatin Temperature	-10° to 40° C
	GNSS	GPS+Galileo+BeiDou
	Operating Frequency	2.400-2.4835 GHz 5.725-5.850 GHz
	Hovering Accuracy Range	Vertical: ±0.5 m (with GNSS positioning) Horizontal: ±0.5 m (with high-precision positioning system)
Gimbal	Stabilization	3-axis mechanical gimbal
Camera	Sensor	1/1.3-inch CMOS Effective Pixels: 48 MP
	Lens	FOV: 82.1° Focal Lenght: 24 mm Aperture: f/1.7 Focus Range: 1 m to ∞
	ISO Range	Video: 100-6400

Camera		Photo: 100-6400
	Shutter Speed	Electronic Shutter: 2-1/8000 s
	Max Image Size	8064 x 6048
	Video Resolution	4K: 3840×2160@24/25/30/48/50/60fps FHD: 1920×1080@24/25/30/48/50/60fps
	Zoom Range	4K: 2x FHD: 4x
Battery	Capacity	2453 mAh (Intelligent Flight Battery) 3850 mAh (Intelligent Flight Battery Plus)

Figure 5.2: DJI Mini 3 Pro.

5.2.2 DJI Mavic 3E

The DJI Mavic 3E is an unmanned aerial vehicle that features a 4/3-inch CMOS Wide camera, 56x hybrid zoom capability, a maximum flight time of 45 minutes, and a compact design, making it stand out in the market. **Figure 5.3** presents photograph of the DJI Mavic 3E. With the option to mount an RTK module, the DJI Mavic 3E is capable of achieving survey-grade positioning with horizontal accuracy of 1cm and vertical accuracy of 1.5cm. This feature enhances its capabilities as a high-precision UAV for surveying applications. [64] The DJI Phantom 4 RTK, which has been a gold standard in the industry for a long time, has been replaced by the DJI Mavic 3E survey-grade UAV with relatively better features, thanks to its small and compact design and an additional zoom (tele) camera. This UAV will continue to maintain its popularity in the industry for a long time. **Table 5.3** shows the technical specifications of the the DJI Mavic 3E. [65]

Figure 5.3: DJI Mavic 3 E.

Table 5.3: Technical specifications of the DJI Mavic 3E.

Aircraft	Takeoff Weight	915 g
	Max Flight Time	45 min
	Max Wind Speed Resistance	12 m/s
	Operatin Temperature	-10° to 40° C
	GNSS	GPS+Galileo+BeiDou+ GLONASS
	Operating Frequency	2.400-2.4835 GHz 5.725-5.850 GHz
	Hovering Accuracy	Vertical: ±0.1 m Horizontal: ±0.1m
Gimbal	Stabilization	3-axis mechanical gimbal
Camera	Sensor	4/3-inch CMOS (Wide Camera) 1/2-inch CMOS (Tele Camera) Effective Pixels: 20 MP (Wide Camera) Effective Pixels: 12 MP (Tele Camera)
	Lens	FOV: 84° (Wide Camera) Focal Lenght: 24 mm (Wide Camera) Aperture: f/2.8-f/11 (Wide Camera) Focus Range: 1 m to ∞ (Wide Camera) FOV: 15° (Tele Camera) Focal Lenght: 162 mm (Tele Camera) Aperture: f/4.4 (Tele Camera) Focus Range:3 m to ∞ (Tele Camera)
	ISO Range	100-6400 (Wide and Tele Camera)
	Shutter Speed	Electronic Shutter: 8-1/8000 s (Wide and Tele Camera) Mechanical Shutter: 8-1/2000s (Wide Camera)
	Max Image Size	5280 x 3956 (Wide Camera)

Camera		4000x3000 (Tele Camera)
	Video Resolution	4K: 3840×2160@30/fps FHD: 1920×1080@30fps
	Digital Zoom	8x (56x zoom)
Battery	Capacity	5000 mAh
RTK Module	RTK Positioning Accuracy	Horizontal : 1 cm + 1 ppm Vertical : 1.5 cm + 1 ppm

5.2.3 DJI Mavic 3T

Although the DJI Mavic 3T shares similar features with the DJI Mavic 3E, they differ from each other in some important aspects. Firstly, the Mavic 3T has three cameras, including wide-angle, tele (zoom), and thermal cameras. **Figure 5.4** presents photograph of the DJI Mavic 3T. [66] The tele camera in the Mavic 3T is the same as in the Mavic 3E. However, the wide-angle camera in the Mavic 3T differs from the one in the Mavic 3E. It has a smaller sensor size and lacks the mechanical shutter feature, which puts it at a disadvantage compared to the Mavic 3E. Additionally, the Mavic 3T does not have the TimeSync and level arm correction features, and it cannot record GNSS raw data for PPK processing. Due to these disadvantages, the Mavic 3T is not as suitable for mapping purposes compared to the Mavic 3E. It is primarily designed for applications such as inspection, firefighting, and research and rescue, even though it can achieve relatively accurate positioning with the RTK module. **Table 5.4** shows the technical specifications of the the DJI Mavic 3T. [65]

Figure 5.4: DJI Mavic 3 T.

Table 5.4: Technical specifications of the DJI Mavic 3T.

Aircraft	Takeoff Weight	920 g
	Max Flight Time	45 min
	Max Wind Speed Resistance	12 m/s
	Operatin Temperature	-10° to 40° C
	GNSS	GPS+Galileo+BeiDou+ GLONASS
	Operating Frequency	2.400-2.4835 GHz 5.725-5.850 GHz
	Hovering Accuracy	Vertical: ±0.1 m, Horizontal: ±0.1m
Gimbal	Stabilization	3-axis mechanical gimbal
Camera	Sensor	1/2-inch CMOS (Wide Camera) 1/2-inch CMOS (Tele Camera) Uncooled VOx Microbolometer (Thermal Camera) Effective Pixels: 48 MP (Wide Camera) Effective Pixels: 12 MP (Tele Camera) 640x512 Pixels (Thermal Camera)
	Lens	FOV: 84° (Wide Camera) Focal Lenght: 24 mm (Wide Camera) Aperture: f/2.8 (Wide Camera) Focus Range: 1 m to ∞ (Wide Camera) FOV: 15° (Tele Camera) Focal Lenght: 162 mm (Tele Camera) Aperture: f/4.4 (Tele Camera) Focus Range:3 m to ∞ (Tele Camera) DFOV: 61° (Thermal Camera) Focal Lenght: 40 mm(Thermal Camera) Aperture: f/1.0 (Thermal Camera) Focus Range:5 m to (Thermal Camera)
	ISO Range	100-25600(Wide and Tele Camera)
	Shutter Speed	Electronic Shutter: 8-1/8000 s (Wide and Tele Camera)
	Max Image Size	8000 x 6000(Wide Camera) 4000x3000 (Tele Camera)
	Video Resolution	4K: 3840×2160@30/fps FHD: 1920×1080@30fps 640x512@30fps (Thermal Camera)
	Digital Zoom	8x (56x zoom)
	Temperature Accuracy	±2°C
	Temperature Measurement Range	-20° to 150°C (High Gain Mode) 0° to 500°C (Low Gain Mode)
Battery	Capacity	5000 mAh
RTK Module	RTK Positioning Accuracy	Horizontal : 1 cm + 1 ppm Vertical : 1.5 cm + 1 ppm

5.2.4 DJI Phantom 4 RTK

The DJI Phantom 4 RTK is an unmanned aerial vehicle specifically developed and produced by DJI for surveying and mapping purposes. It stands out with its 1-inch CMOS sensor camera, TimeSync technology, OcuSync system, and compatibility with the D-RTK 2 Mobile Station. **Figure 5.5** shows the photograph of the DJI Phantom 4 RTK. [67] The Phantom 4 RTK features the TimeSync technology, which plays a crucial role in obtaining precise coordinates and orientation parameters. It accurately processes the metadata information of captured images and integrates it into the image EXIF file, enabling the acquisition of high-quality data for accurate mapping and modeling. Additionally, the OcuSync feature allows for HD video and image transmission of up to 7 km, making it suitable for large-scale projects. The DJI D-RTK 2 Mobile Station, specifically designed for use with the Phantom 4 RTK, ensures seamless compatibility and facilitates easy and precise RTK operations. While the D-RTK 2 Mobile Station can be used with other DJI drones, when using it as a GNSS receiver in rover mode, only the remote controller of the Phantom 4 RTK can serve as the data collector. Overall, the Phantom 4 RTK is widely recognized and utilized in the mapping industry for its mapping capabilities. **Table 5.5** shows the technical specifications of the the DJI Phantom 4 RTK. [68]

Table 5.5: Technical specifications of the DJI Phantom 4 RTK.

Aircraft	Takeoff Weight	1391 g
	Max Flight Time	30 min
	Max Wind Speed Resistance	10 m/s
	Operatin Temperature	0° to 40° C
	GNSS	GPS+Galileo+BeiDou+ GLONASS
	Operating Frequency	2.400-2.4835 GHz 5.725-5.850 GHz
	Hovering Accuracy	Vertical: ±0.1 m, Horizontal: ±0.1m
Gimbal	Stabilization	3-axis mechanical gimbal
Camera	Sensor	1-inch CMOS Effective Pixels: 20 MP
	Lens	FOV: 84° Focal Lenght: 24 mm Aperture: f/2.8.f/11 Focus Range: 1 m to ∞
	ISO Range	100-3200 (Auto) 100-12800(Auto)

Camera	Shutter Speed	Mechanıcal Shutter : 8-1/8000 s Electronic Shutter: 8-1/8000 s
	Max Image Size	4864 x 3648 (4:3) 5472 x 3648 (3:2)
	Video Resolution	4K: 3840×2160@30/fps
Battery	Capacity	5870 mAh
RTK Module	RTK Positioning Accuracy	Horizontal : 1 cm + 1 ppm (RMS) Vertical : 1.5 cm + 1 ppm (RMS)

Figure 5.5: DJI Phantom 4 RTK

5.2.5 DJI Matrice 30T

The DJI Matrice 30T is a highly popular next-generation unmanned aerial vehicle in the search and rescue, firefighting, and inspection domains. It is equipped with three cameras, namely wide, zoom, and thermal cameras, as well as a laser rangefinder. These features make it suitable for search and rescue, firefighting, inspection, and even photogrammetry purposes. The UAV is capable of performing rgb and thermal applications with ease, thanks to its well-equipped detection systems. The wide camera has a 1/2-inch CMOS sensor with 12 MP resolution, while the zoom camera features a 1/2-inch CMOS sensor with 48 MP resolution. This hardware combination allows for versatile and high-quality imaging capabilities.[69] The zoom camera is equipped with a 200x hybrid zoom feature, allowing you to capture imagery of objects located kilometers away. **Figure 5.6** shows the photograph of the DJI Matrice 30 Thermal. [69] This UAV is designed to be highly durable against challenging conditions. It has an IP55 certification, making it resistant to water and dust, and it can operate in temperatures ranging from -20°C to 50°C. With its high wind resistance capability (maximum 15 m/s), this UAV is suitable for advanced low-light First Person View (FPV) flights, ensuring safe operations and clear imaging. Additionally, it is equipped

with a hardware-based RTK antenna that provides horizontal accuracy of 1 cm and vertical accuracy of 1.5 cm, enabling precise coordinate measurements. The thermal camera allows for temperature sensing and the acquisition of colorized thermal images. **Table 5.6** shows the technical specifications of the DJI Matrice 30T. [70]

The DJI Matrice 30T stands out with its redundant hardware components, which allow it to continue its mission with confidence in the event of any failure during flight. It is equipped with duplicated hardware components, such as IMU, barometer, RTK+GNSS antennas, compass, visual sensors, transmission antennas, and batteries. These duplicated components provide backup functionality to ensure the UAV's continued operation in case of any component failure. Additionally, the UAV is designed with the capability to perform a safe landing with three motors in the event of a failure in one of the four motors.

Figure 5.6: DJI Matrice 30 T.

Table 5.6: Technical specifications of the DJI Matrice 30T.

Aircraft	Takeoff Weight	3770 g
	Max Flight Time	41 min
	Max Wind Speed Resistance	15 m/s
	Operatin Temperature	-20° to 50° C
	GNSS	GPS+Galileo+BeiDou+ GLONASS
	Operating Frequency	2.400-2.4835 GHz 5.725-5.850 GHz
	Hovering Accuracy	Vertical: ±0.1 m, Horizontal: ±0.1m
Gimbal	Stabilization	3-axis mechanical gimbal

Camera	Sensor	1/2-inch CMOS, Effective Pixels: 12 MP (Wide Camera) 1/2-inch CMOS, Effective Pixels: 48 MP (Zoom Camera) Uncooled VOx microbolometer, Effective Pixels: 12 MP (Thermal Camera)
	Lens	**Wide Camera:** FOV: 84° Focal Lenght: 4.5 mm (equivalent:24mm) Aperture: f/2.8 Focus Range: 1 m to ∞ **Zoom Camera:** Focal Lenght: 21-75 mm (equivalent:113-405mm) Aperture: f/2.8-f/4.2 Focus Range: 5 m to ∞ **Thermal Camera:** FOV: 61° Focal Lenght: 9.1 mm (equivalent: 40mm) Aperture: f/1.0 Focus Range: 5 m to ∞
	ISO Range	100-25600(Wide and Zoom Camera)
	Shutter Speed	Electronic Shutter: 8-1/8000s - 1/2 s (Wide and Zoom Camera)
	Max Image Size	4000 x 3000(Wide Camera) 4000x6000 (Zoom Camera) 1280x1024, 640x512 (Thermal Camera)
	Video Resolution	3840x2160 (Wide and Zoom Camera) 1280x1024, 640x512 (Thermal Camera)
	Digital Zoom	5x-16x Optical Zoom 200x Max Hbrid Zoom
	Temperature Accuracy	±2°C
	Temperature Measurement Range	-20° to 150°C (High Gain Mode) 0° to 500°C (Low Gain Mode)
Laser Module	Measurement Range	3-1,200 m
	Measurement Accuracy	± (0.2m + Dx0.15 %) D: Distance to vertical surface
Battery	Capacity	5880 mAh
RTK Module	RTK Positioning Accuracy	Horizontal : 1 cm + 1 ppm Vertical : 1.5 cm + 1 ppm

This UAV, which has a portable and lightweight structure, has the capability to be used with a DJI Dock Station specifically designed for challenging areas with no human settlements, such as volcano craters, dense forests, and hazardous terrains. It is water-resistant and can withstand temperatures ranging from -35°C to 50°C, with a range of 7 km. With this station, it can perform automated takeoff, landing, and flight, allowing the UAV to continue its mission seamlessly with a quick 25-minute recharge. Real-time mission data, video footage, and flight parameters can be instantly shared and collaboratively worked on through cloud-based streaming, facilitating effective teamwork. **Figure 5.7** shows the photograph of the DJI Matrice 30T landed on the DJI Dock Station. [69]

Figure 5.7: DJI Matrice 30 T landed on the DJI Dock Station.

This advanced UAV, which offers many advantages, does not have the TimeSync and level arm correction features as its main purpose of production is not mapping. This detailed information is not widely known to many people as it is not provided in the technical specifications provided by the manufacturer. However, we obtained this information from our own tests and conversations with DJI officials. Due to this disadvantage, this UAV may not provide excellent accuracy results for mapping purposes in RTK positioning. Nevertheless, precise and accurate mapping can still be achieved with proper distribution of ground control points.

5.2.6 DJI Matrice 300 RTK

DJI, with its latest release, the DJI Matrice 300 RTK, has set new standards for commercial UAV usage. This UAV stands out among unmanned aerial vehicles with its advanced capabilities, including artificial intelligence technologies, and the ability to carry various payloads, making it highly versatile in fields such as surveying and mapping, inspection, search and rescue, and security. **Figure 5.8** shows the photograph of the DJI Matrice 300 RTK and Zenmuse P1 camera.[71]

The DJI Matrice 300 RTK has the same features as the DJI Matrice 30T, along with additional advantages, making it a preferred choice in many fields. This UAV offers impressive features such as a maximum flight time of 55 minutes, a transmission range of 15 km, cm-level dual RTK antennas, and the ability to operate in temperatures ranging from -20°C to 50°C. **Table 5.7** shows the technical specifications of the DJI Matrice 300 RTK. [72]

Figure 5.8: DJI Matrice 300 RTK and Zenmuse P1.

Table 5.7: Technical specifications of the DJI Matrice 300 RTK.

Aircraft	Max Takeoff Weight	9kg
	Max Flight Time	55 min
	Max Wind Speed Resistance	15 m/s
	Operatin Temperature	-20° to 50° C
	GNSS	GPS+Galileo+BeiDou+ GLONASS
	Operating Frequency	2.400-2.4835 GHz 5.725-5.850 GHz
	Hovering Accuracy	Vertical: ±0.1 m Horizontal: ±0.1m

Gimbal	Stabilization	3-axis mechanical gimbal
Zenmuse P1 (Camera as seperate Payload)	Sensor	35.9 x 24 mm (Full frame) Effective Pixels :45 MP
	Lens	DJI DL 35 mm F2.8, FOV: 63.5° Aperature Range: f/2.8- f/16
	ISO Range	100- 25600
	Shutter Speed	Mechanical Shutter: 1/2000-1s Electronic Shutter: 1/8000-1s
	Max Image Size	3:2 (8192x5460)
	Video Resolution	16:9 (1920x1080) 16:9 (3840x2160)-Only with 35mm lens
	Supported DJI Gimbals	Zenmuse XT2/XT S/Z30/H20/H20T/DJI P1/DJI L1
Battery	Capacity	5000 mAh
RTK Module	RTK Positioning Accuracy	Horizontal : 1 cm + 1 ppm Vertical : 1.5 cm + 1 ppm

The DJI Matrice 300 RTK has a wind resistance of 15 m/s, IP45-rated protection against water and dust, and a maximum service ceiling of 7000m, making it resilient against challenging flight scenarios. It provides advanced flight information and navigation system parameters on the flight control unit, ensuring enhanced flight awareness. Additionally, it features the Advanced Dual Control capability, which allows flight and payload control to be performed using two separate remote controllers, providing advantages in various applications. [71] For instance, during a oblique flight mission for 3D modeling, one pilot can handle the flight control while the other pilot can control the payload camera, enabling safe flight operations and obtaining high-quality data. Additionally, the unmanned aerial vehicle provides advantageous modes such as "Smart Track" and "Pinpoint Mode" that are particularly beneficial for inspection and security purposes. These modes enable intelligent object tracking and real-time object coordinate measurements.

The DJI M300 RTK, similar to the DJI Matrice 30 series drones, is equipped with redundant hardware components for security purposes. These components include IMU, barometer, RTK+GNSS antennas, compass, visual sensors, transmission antennas, and batteries.

The DJI M300 RTK supports the simultaneous connection of three payloads, allowing for flexible payload configuration based on the intended use case. The commonly used payloads for this unmanned aerial vehicle are the Zenmuse P1 (full-frame

photogrammetric camera), Zenmuse L1 (lidar sensor), and Zenmuse H20T (wide camera, radiometric thermal camera, zoom camera, and laser range finder combination). **Figure 5.9** shows payloads for DJI Matrice 300. [73] In this thesis, we utilized the Zenmuse P1 camera as a payload in conjunction with the DJI M300 RTK. The DJI M300 RTK features the "Smart Oblique Capture" mode specifically designed for the Zenmuse P1 camera. In this mode, the gimbal automatically moves to different angles while capturing photos along the flight path. This functionality not only reduces the mission time for 3D modeling tasks but also improves the quality of the model by capturing oblique photos. Additionally, the DJI M300 RTK, with its TimeSync 2.0 and level arm correction features, allows for the acquisition of precise coordinate outputs in the image metadata, which is crucial for surveying and mapping applications.[73]

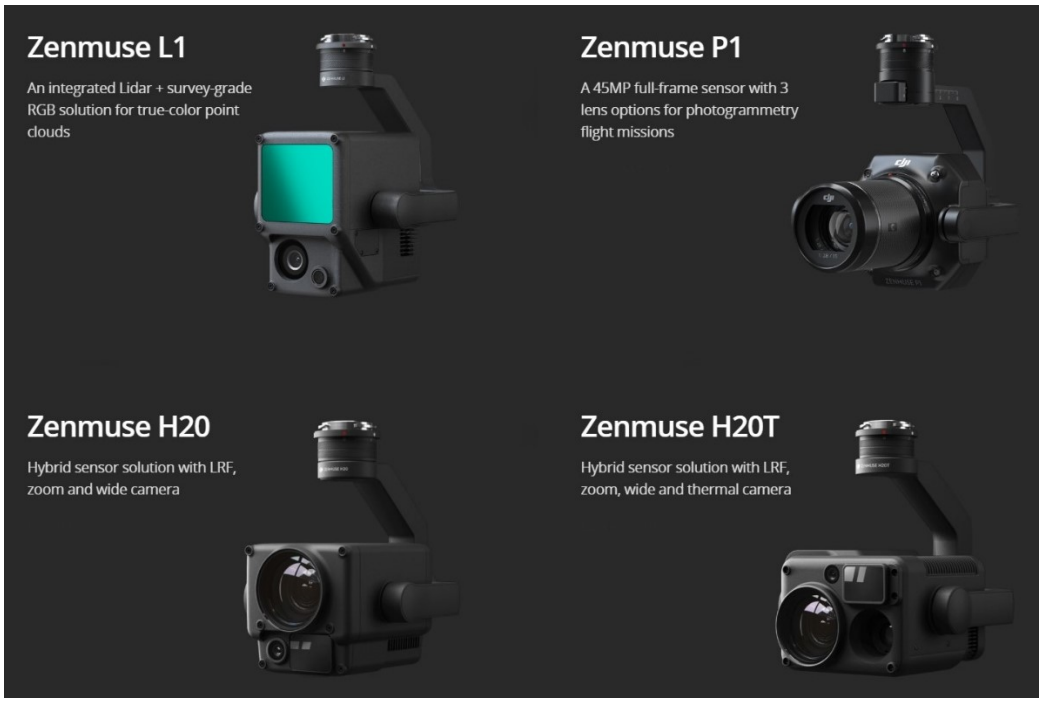

Figure 5.9: Payloads for DJI M300 RTK

5.2.7 WingtraOne Gen II

WingtraOne Gen II, a fixed-wing unmanned aerial vehicle (UAV) manufactured by the Swiss company Wingtra, stands out among UAVs designed for surveying and mapping purposes due to its superior performance. It combines the advantage of long flight endurance typically found in fixed-wing UAVs with the flexibility and vertical takeoff and landing (VTOL) capability, eliminating the need for a runway like rotary-

wing UAVs. With its VTOL capability, the WingtraOne Gen II can take off and land vertically, allowing for flight missions to be conducted in various locations, similar to rotary-wing UAVs. **Figure 5.10** shows the photograph of the WingtraOne.

The WingtraOne Gen II has different camera configurations. Among them, the RGB cameras are Sony RX1R II and Sony a6100, the oblique camera is the Oblique Sony a6100, and the multispectral camera is the MicaSense RedEdge-P. However, for this thesis, we used the most common camera configuration, which is the Sony RX1R II. This camera is highly successful for surveying and mapping purposes due to its full-frame sensor size, 42 MP resolution, and mechanical shutter. In fact, it can achieve a Ground Sample Distance (GSD) of 1.2 cm/px with a flight altitude of 93m. **Table 5.8** shows the technical specifications of the WingtraOne Gen II.[74]

Figure 5.10: WingtraOne fixed wing, VTOL UAV

Table 5.8: Technical specifications of the WingtraOne Gen II.

Aircraft	Drone Type	Tailsitter vertical take-off and landing (VTOL)
	Max Takeoff Weight	4.5 kg
	Wingspan	125 cm
	Max Flight Time	59 min
	Max Wind Speed Resistance	12 m/s
	Operatin Temperature	-10° to 40° C
	GNSS	GPS+Galileo+BeiDou+ GLONASS
	Radio Link	Bi-directional 10 km in direct line of sight, obstacles reduce the range

Aircraft		2.4016-2.4776 GHZ
	Operational cruise speed	16 m/s
	Auto-landing accuracy	< 2m
Sony RX1R II (Camera as Payload)	Sensor	35.9 x 24 mm (Full frame) Effective Pixels :42.4 MP
	Lens	FOV: 63° Focal length: 35mm Aperture: F2-22 Focus range: 24cm to ∞
	ISO Range	100- 25600
	Shutter Speed	Mechanical Shutter: Program Auto (30" – 1/4000 sec)
	Max Image Size	8000X5320
	Lowest possible GSD	0.7 cm /px (55 m flıght altitude and 90 ha coverage)
Battery	Capacity	Two 99 Wh batteries
RTK Module	RTK Positioning Accuracy	Horizontal: 1 cm + 1 ppm Vertical: 3 cm + 1 ppm

With its fixed-wing design and a maximum flight time of 59 minutes, the WingtraOne Gen II can cover a much larger area in a single flight, allowing for the completion of large projects in a short amount of time. This not only saves time but also reduces measurement costs. For instance, in a project where a flight data with a GSD value of 1.2 cm/px is required, the DJI Phantom 4 RTK can cover an area of 8 hectares from an altitude of 44 meters in a single flight. In comparison, the WingtraOne Gen II with VTOL capabilities can cover an area of 110 hectares at an altitude of 93 meters. Similarly, other VTOL unmanned aerial vehicles such as the Ebee X and Aeria/Delair UX11 can cover an area of 70 hectares from an altitude of 57 meters. [75] These data demonstrate that the WingtraOne Gen II possesses distinct advantages over both rotary-wing unmanned aerial vehicles (UAVs) and many other fixed-wing UAVs. **Figure 5.11** shows maximum coverage of drones with one flight against WingtraOne configured with RX1R II camera. [75]

Figure 5.11: Maximum coverage of several drones with one flight against WingtraOne configured with RX1R II camera

The UAV is equipped with a multi-frequency (including L1 and L2) PPK GNSS receiver, providing a horizontal positioning accuracy of 1cm and a vertical positioning accuracy of 3cm. Having a PPK receiver eliminates the need for continuous connectivity between the base GNSS receiver, remote controller, and the UAV, which is typically required in RTK receivers. This mitigates the risk of errors that could arise from potential connection disruptions between these systems. The raw GNSS observations collected by the PPK receiver can be easily processed in an office environment using the WingtraHub software, along with additional observation data obtained from the user's own base GNSS receiver or Continuously Operating Reference System (CORS) receivers, enabling convenient geotagging procedures.

WingtraOne Gen II unmanned aerial vehicle (UAV) is a preferred choice for users who require high-quality data, particularly in large projects. However, it does have some disadvantages compared to other systems. One drawback is its higher cost compared to other UAVs. Although it has VTOL capabilities, its circular trajectory during the transition from vertical to horizontal flight may pose safety concerns for takeoff and landing in urban areas. Additionally, it cannot be used for tasks that require manual flight control.

5.2.8 DJI DRTK-2 Mobile Station

DJI D-RTK 2 is a high-precision GNSS receiver developed by DJI. It supports GPS, GLONASS, Beidou, and GALILEO satellite signals, providing cm-level positioning accuracy by transferring real-time differential correction data. Thanks to its built-in high-gain antenna, it has the ability to capture more satellite signals even in the presence of obstacles. **Figure 5.12** shows the DJI D-RTK 2 Mobile Station. [76] The D-RTK 2 Mobile Station offers various communication and data transfer options such as 4G, OcuSync, LAN, and Wi-Fi. Additionally, it can connect to a maximum of 5 different remote controllers simultaneously, allowing for the simultaneous transmission of verification data to 5 different unmanned aerial vehicles in coordinated flight missions. It features a durable carbon fiber body and has an IP65 protection rating, providing robustness and protection against environmental factors. **Table 5.9** shows the technical specifications of the DJI D-RTK 2 Mobile Station. [77] The disadvantage of this GNSS receiver is that it requires the use of the remote controller specifically designed for the Phantom 4 RTK as a data collector.

Figure 5.12: DJI D-RTK 2 Mobile Station.

Table 5.9: Technical specifications of the DJI D-RTK 2 Mobile Station.

GNSS Recevier	GNSS Frequency	Simultaneously receive: GPS: L1 C/A, L2, L5 BEIDOU: B1,B2,B3 GLONASS: F1,F2 Galileo: E1,E5A,E5B
	Positioning Accuracy	Single Point: Horizontal: 1.5 m (RMS) Vertical: 3.0 m (RMS) RTK: Horizontal: 1cm+ 1ppm (RMS) Vertical: 2cm +1ppm (RMS)
	Positioning Update Rate:	1 Hz, 2Hz, 5Hz, 10 Hz, and 20Hz
IMU	Features	6-axis accelerometer Movement monioring Slope measurements Electronic Bubble level
Communication and Data Storage	Data Link	OcuSync, Wi-Fi, LAN, 4G
	Operating Frequency	2.4 GHz to 2.483 GHz 5.725 GHz to 5.850 GHz

5.2.9 Agisoft Metashape Professional

Agisoft Metashape Pro is an intelligent and cutting-edge software developed by Agisoft, based in St. Petersburg, Russia. It specializes in generating advanced photogrammetry solutions. The software stands out for its fast, reliable, and high-precision photogrammetric outputs, capable of producing results with up to 3cm accuracy for aerial photogrammetry and up to 1mm accuracy for close-range photogrammetry. [78]. It produces successful solutions in fast data processing with its automatic, intuitive, and GPU acceleration features.

Agisoft Metashape Pro has the capability to process over 50,000 photos in a single project. Additionally, the software offers Agisoft Cloud, a cloud-based version that allows for data processing, measurements, and presentation. With the open-source photogrammetric output viewer, Agisoft Viewer, it provides the ability to view various file formats widely used in the industry and perform calculations such as length, area, and volume measurements.

Agisoft Metashape Pro is capable of processing rgb, multispectral, and thermal images, and it can generate various photogrammetric output products such as dense point clouds, textured models, georeferenced true orthomosaics, and DSM/DTM. Agisoft also provides a software called "Texture De-Lighter" that removes shadows from textured 3D models. Additionally, with Agisoft Metashape Pro, vegetation indices can be calculated, and base data can be generated for applications such as smart agriculture and land use and land cover analysis.

5.2.10 WingtraHub

WingtraHub is a software developed by Wingtra for processing flight photos and PPK raw data obtained from the WingtraOne UAV and for flight planning. With WingtraHub, PPK processing can be performed to obtain precise coordinates for geotagging, which involves accurately tagging the captured photos with their corresponding geographic coordinates. Additionally, WingtraHub provides a user-friendly interface for flight planning, allowing users to create flight plans. The created flight plan can be transferred first to the UAV remote controller and then to the UAV itself to execute the intended flight mission.

5.2.11 Thermo Converter

Thermal cameras are sensor systems that detect the radiant energy emitted by objects and create images based on this detection. The detected energy corresponds to thermal wavelengths that are not visible to the human eye within the electromagnetic spectrum. These cameras typically record absolute or relative temperature information in the image metadata and often save the images in ratiometric JPEG or TIFF formats. Photogrammetric data processing software also includes algorithms for processing thermal imagery. By loading thermal images into the software and making necessary adjustments, the software can read the metadata of thermal photos to extract radiometric temperature data. It can then generate a thermal reflection map and apply a specific color palette for visual interpretation. However, some thermal cameras have complex metadata structures that photogrammetric software cannot read. If the software cannot recognize the metadata of images taken with such cameras, it cannot

read the radiometric data, treating the images as regular RGB images. As a result, temperature data cannot be interpreted on the orthomosaic output.

The Thermal Converter is a tool that converts ratiometric JPEG images obtained from cameras such as Mavic 3T and Matrice 30T into the TIFF format. This conversion allows the images to be in a format that photogrammetric software can read the radiometric data from the metadata. As a result, during data processing, the radiometric data can be read, and temperature information can be extracted at any point on the output orthomosaic.

5.3 Method

As part of this thesis, we have organized our project implementation method into four main sections: planning, data acquisition, data processing, and comparison. In the planning phase, we conducted activities such as planning the study area, creating flight plans, and designing the ground control point (GCP) network. Moving on to the data acquisition phase, we performed tasks such as establishing and measuring the coordinates of GCPs in the field, conducting photogrammetric oblique flights, and reviewing and eliminating excess or faulty aerial photographs. Next, we proceeded to the data processing stage, where we evaluated and processed the acquired data. In this step, we first imported our flight photographs into Agisoft software. Since the temperature data in the metadata of the ratiometric thermal photographs obtained from the Mavic 3T and Matrice 30T drones were not directly readable by the Agisoft software, we used a software called "Thermal Converter" to convert the thermal photographs from these UAVs into TIFF images with updated metadata in a readable format for the software. Following this step, we performed processes such as photo alignment, introducing ground control points to the software, and generating point clouds, meshes, textures, and orthomosaics. In the final stage of comparison, we compared the quality and accuracy of the models created using different UAVs. **Table 5.10** presents the whole project workflow and processing stages.

Table 5.10: Project workflow diagram.

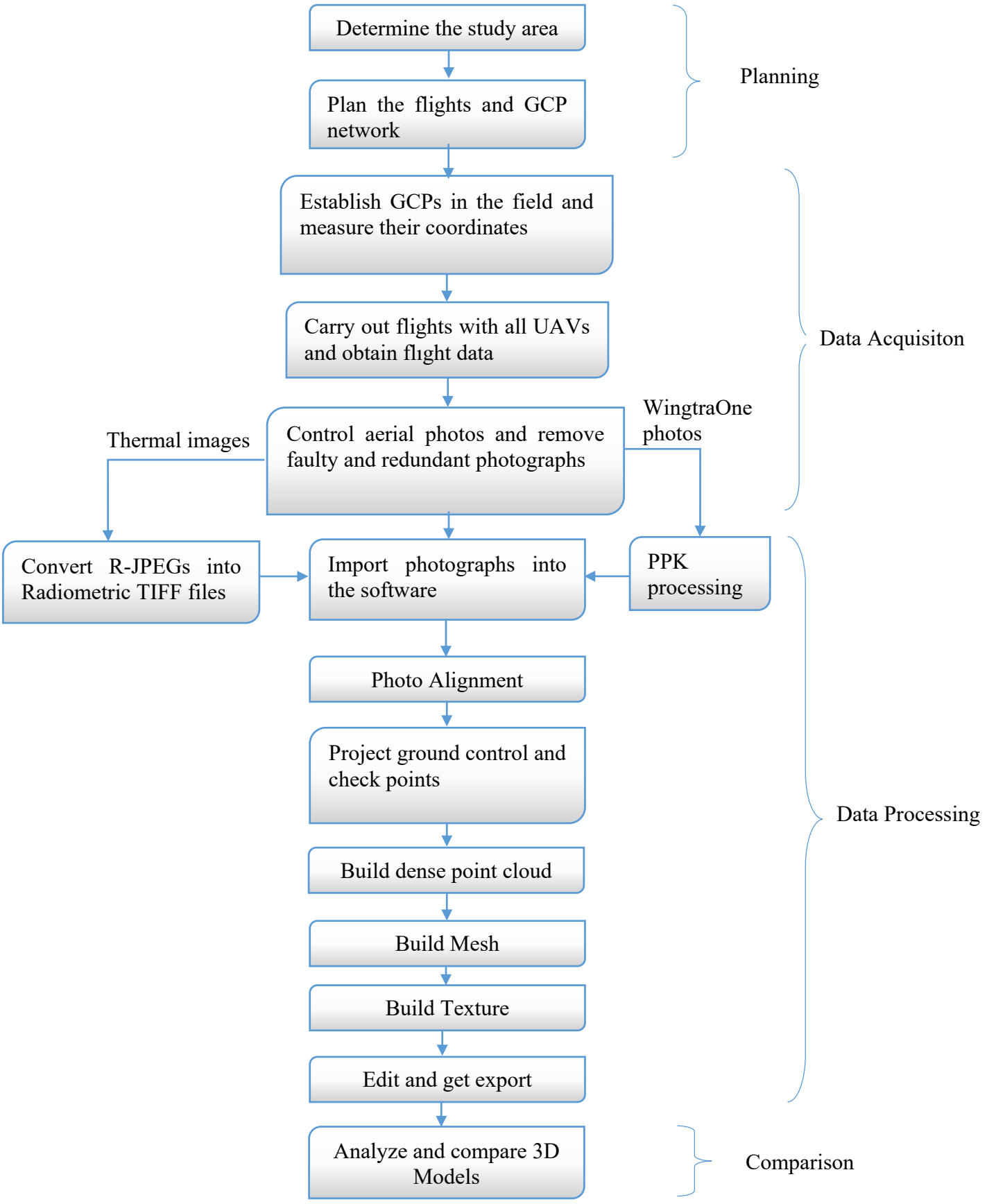

5.3.1 Planning

Within the scope of the project, the planning phase started with the determination of the area where the work would be carried out. In this regard, a business center located in Dresden, Altstadt, as detailed in section 5.1, was chosen as the preferred location.

After determining the study area, the Ground Control Point (GCP) network to be established in the study area was planned using Google Earth Pro software. During the planning of the GCP network, care was taken to distribute the points in a suitable and well-distributed manner within the study area. **Figure 5.13** shows the GCP network of the study area on Google Earth Pro software.

Figure 5.13: GCP network of the study area

5.3.2 Data Acquisition

5.3.2.1 Establishment and Measurement of GCPs

In the data acquisition phase carried out within the project scope, the first step was to establish the GCP network in the study area according to the planned locations in the

office environment. For this purpose, 5 GCPs and 1 check point were established in the project area using GCP markers, and the coordinates of the GCPs were measured with DJI D-RTK 2 Mobile Station. **Figure 5.14** presents a photograh from the GCP coordinate measurement stage. The coordinate measurements were obtained using the RTK method and the WGS-84 coordinate system, utilizing positional verification data obtained through the internet protocol from the German satellite positioning service "Der Satellitenpositionierungsdienst der Deutschen Landesvermessung" (SAPOS). SAPOS is a government service similar to the "Turkey National Permanent GNSS Network Active" (TUSAGA-Aktif) in Turkey, providing verification data and other positional services through continuously observing GNSS stations nationwide. After the point measurement with DJI D-RTK 2 Mobile Station, since the instrument does not automatically record the ellipsoidal height, the fixed instrument height of 1.8011 m was subtracted from all GCP height values within the project scope to use the GCP ellipsoidal heights. **Table 5.11** shows the coordinates of the GCPs and the check point in WGS-84 coordinate system.

Figure 5.14: Photograph from the GCP coordinate measurement stage.

Table 5.11: Shows the coordinates of the GCPs and check point in WGS84 coordinate system.

ID	Latitude	Longitude	Altitude	stdLat	stdLng	stdAlt
P.1	51.04877443	13.71040068	161.727867	0.028233	0.009247	0.043288
P.2	51.04885701	13.70979946	161.836012	0.021424	0.008545	0.025941
P.3	51.04881137	13.70949412	162.154201	0.011631	0.007792	0.018184
P.4	51.04877111	13.70961086	161.913237	0.014424	0.011244	0.02109
P.5	51.04867527	13.70908748	163.414169	0.019314	0.007274	0.021475
Check point	51.04899222	13.70918916	162.231667	0.021121	0.00699	0.019326

5.3.2.2 Obtaining Aerial Photos via UAV

Within the project scope, flight plans were prepared based on the oblique flight modes and capabilities of the 7 different UAVs included in the project, in order to carry out the necessary photogrammetric flights for 3D model generation. In the resulting textured 3D models, special attention was given to improving the mesh and texture quality of building facades. For this purpose, manual flights were conducted with UAVs whenever possible, taking into account flight safety and UAV capacity, to capture detailed photographs of the building facades. Depending on the UAV model, various flight modes such as circular Point of Interest (POI), oblique, manual, and standard flights were used for oblique flights. In cases where environmental safety and UAV capability permitted, multiple flight modes were employed to enhance the model quality through photogrammetric flights. **Table 5.12** shows flight planning modes used for fotogrammetric oblique flight with different UAVs.

Table 5.12: Flight planning modes used for fotogrammetric oblique flights.

UAV	Used Flight Modes
Mini 3 Pro	POI, Manual
Mavic 3 Enterprise	Oblique, Manual
Mavic 3 Thermal	Oblique, Manual
Phantom 4 RTK	3D Photogrammetry, Manual
Matrice 30 Thermal	Oblique
Matrice 300 RTK	Oblique
WingtraOne Gen II	Standtard

During the flights, great attention was paid to capturing all the details of the building, and the necessary flight parameters were entered into the flight planning software to

achieve this goal. **Table 5.13** shows flight setting adjusted for oblique flights. During the flights conducted with Mavic 3E, Mavic 3T, Phantom 4 RTK, Matrice 30T, and Matrice 300 RTK unmanned aerial vehicles (UAVs), RTK positioning was performed using DJI D-RTK 2 Mobile Station as the base GNSS receiver. In the case of WingtraOne Gen II, which has a built-in PPK module, PPK (Post-Processed Kinematics) method was used for positioning. Furthermore, for the WingtraOne Gen II flight, Receiver Independent Exchange Format (RINEX) observation data obtained from the SAPOS service was used for PPK processing.

Table 5.13: Flight setting adjusted for oblique flights.

Flight altitude	50m
Side overlap	70%
Front overlap	80%
Oblique side overlap	60%
Oblique front overlap	70%
Gimbal pitch angle	45°
RTK type	Mobile Station (base GNSS station)
Number of photographs	Mini 3 Pro: 847 Mavic 3E: 244 Mavic 3T: 819 (rgb), 828 (thermal) Phantom 4 RTK: 236 Matrice 30T: 389 (rgb), 372 (thermal) Matrice 300 RTK: 436 Wingtraone Gen II: 350
Estimated GSD (cm/px)	Mini 3 Pro: 1.79 Mavic 3E: 0.68 (at 50m altitude) Mavic 3T: 1.81 (at 50m altitude, rgb wide camera) Phantom 4 RTK: 1.37 (at 50m altitude) Matrice 30T: 1.81 Matrice 300 RTK: 0.63 (at 50m altitude) Wingtraone Gen II: 3.23 (at 250m altitude)

Since the DJI Mavic Mini 3 Pro unmanned aerial vehicle (UAV) does not have an RTK or PPK module, no specific steps for positioning could be taken prior to the flight. Therefore, the flight images obtained from this UAV have the coordinates recorded in

the EXIF files based on the rough GNSS solution from the GNSS receiver available on the UAV hardware.

During our flights in a densely populated urban area, we encountered some challenges with the DJI Matrice 30T, DJI M300 RTK, and WingtraOne Gen II unmanned aerial vehicles (UAVs) due to their larger and heavier size compared to other UAVs. For safety reasons, it was not possible to conduct low-altitude manual flights and capture photos around buildings during Matrice 30T and Matrice 300 RTK flights. Instead, an automatic oblique flight plan was executed at an altitude of only 50 meters for photo acquisition. Although the WingtraOne Gen II UAV has vertical takeoff and landing (VTOL) capability, its maneuver of gaining a circular altitude after vertical takeoff posed a risk to flight safety. Moreover, the UAV's predominantly autonomous flight characteristic limited effective and swift intervention in case of sudden risks during such low-altitude oblique missions. Consequently, we were unable to conduct flights with the WingtraOne Gen II in the main flight area. **Figure 5.15** shows how WingtraOne Gen II passes to the fixed wing hovering flight after vertical take off. [79] Instead, flights were conducted at an altitude of 120 meters in Bahretal, a region located in the Saxony state, away from urban areas. Using the WingtraOne Gen II, aerial photographs were obtained from this location.

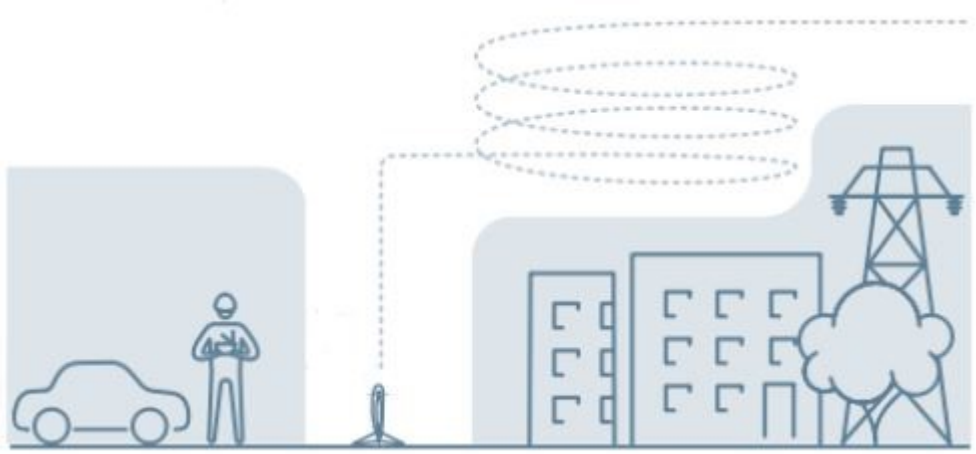

Figure 5.15: The way how WingtraOne Gen II passes to the fixed wing hovering flight after vertical take off.

After the fieldwork, which involved obtaining flight data and GCP coordinates, the data was transferred to the appropriate file locations, ensuring organized file arrangements to prevent confusion. The flight photographs were reviewed, and any

faulty, redundant, or photos with focus or exposure issues were removed, preparing the data for further processing.

5.3.3 Data Processing

After obtaining aerial photographs through UAV and collecting coordinate and observation data using a GNSS receiver, a series of photogrammetric data processing steps were conducted in the office environment. In addition to other photo data, a metadata and file format conversion was performed for thermal photographs, and a PPK (Post-Processed Kinematics) process was applied to WingtraOne Gen II photographs. Subsequently, the obtained accurately georeferenced photographs and GCP coordinates were imported into Agisoft Metashape Pro software to perform photo alignment, dense cloud creation, mesh and texture creation, as well as edit and analyze steps.

5.3.3.1 Pre-Processing of Photographs

Before transferring the radiometric thermal images in JPEG format obtained from DJI Mavic 3T and DJI Matrice 30T unmanned aerial vehicles (UAVs) to Agisoft Metashape Pro software, a metadata conversion was applied using the "ThermoConverter" software. The main purpose of this conversion is to transform the photos from the different metadata structure of Mavic 3T and Matrice 30T UAVs into the ".geoTIFF" format, which allows temperature values to be read by the Agisoft software. DJI also provides a software called "DJI Thermal Analysis Tool 3.0" specifically designed for UAVs equipped with thermal cameras, which enables image palette adjustment and point-based temperature reading. However, this software only allows analysis on a single-photo basis and does not perform any metadata or output format conversion. Therefore, it is necessary to perform this step on the thermal images obtained from these UAVs in order to proceed with further processing steps. **Figure 5.16** shows a thermal image viewed on the DJI Thermal Analysis Tool 3.0. The raw thermal images were transferred to the "ThermoConverter" software for conversion, and the desired output parameters were entered into the program. The thermal images were then transformed and obtained as output in the ".geoTIFF" format. **Figure 5.17** presents the export settings of the TermoConverter.

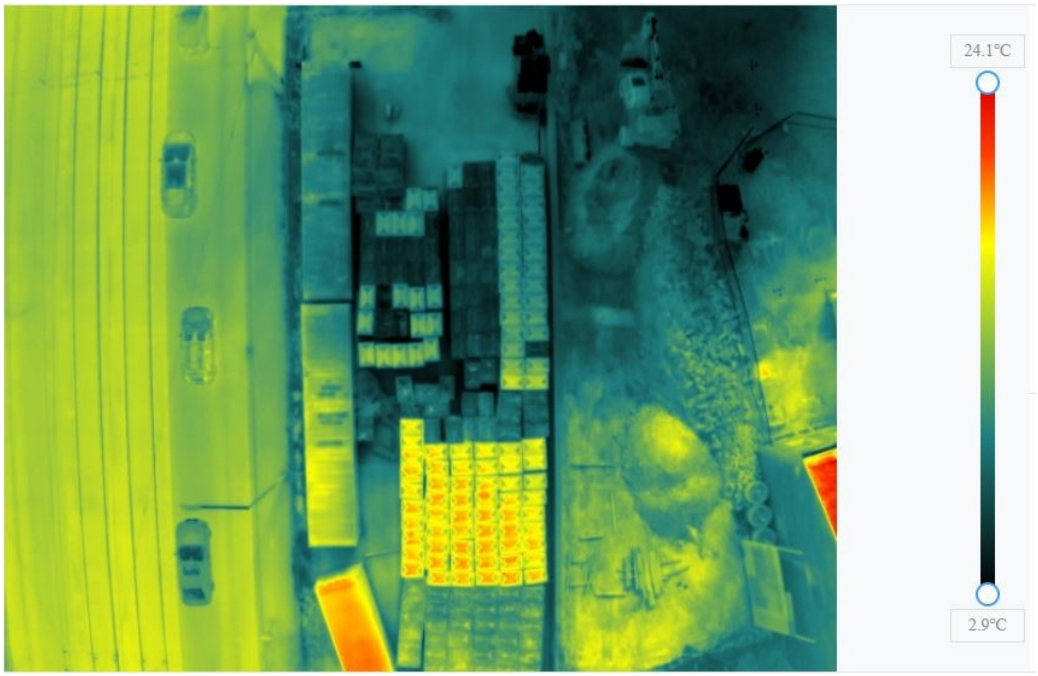

Figure 5.16: A thermal image viewed on the DJI Thermal Analysis Tool 3.0.

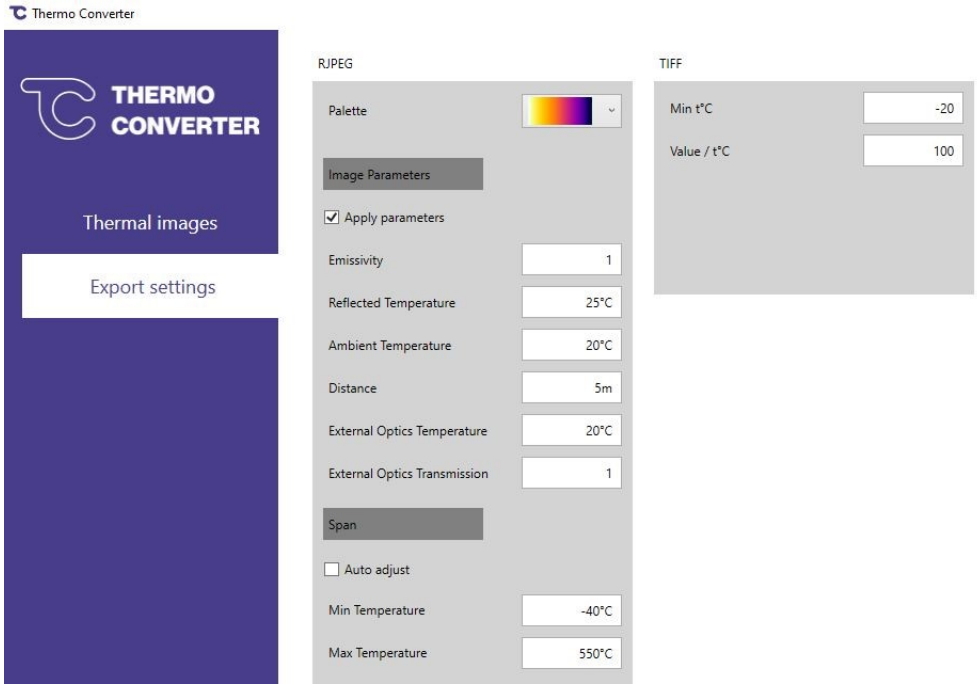

Figure 5.17: Export settings of the TermoConverter.

The photos obtained from the WingtraOne Gen II unmanned aerial vehicle and the raw GNSS observation data underwent PPK (Post-Processing Kinematic) processing to obtain accurate photo coordinates. For this process, the raw UAV GNSS data, photos, RINEX observation file from a continuously observing station closest to the flight area, and receiver coordinates were used. These data were transferred to the "WingtraHub" software to perform the PPK processing, and the coordinates of the

precise photo capture points were obtained and saved in ".csv" format. **Figure 5.18** shows the PPK processing interface of the WingtraHub software.

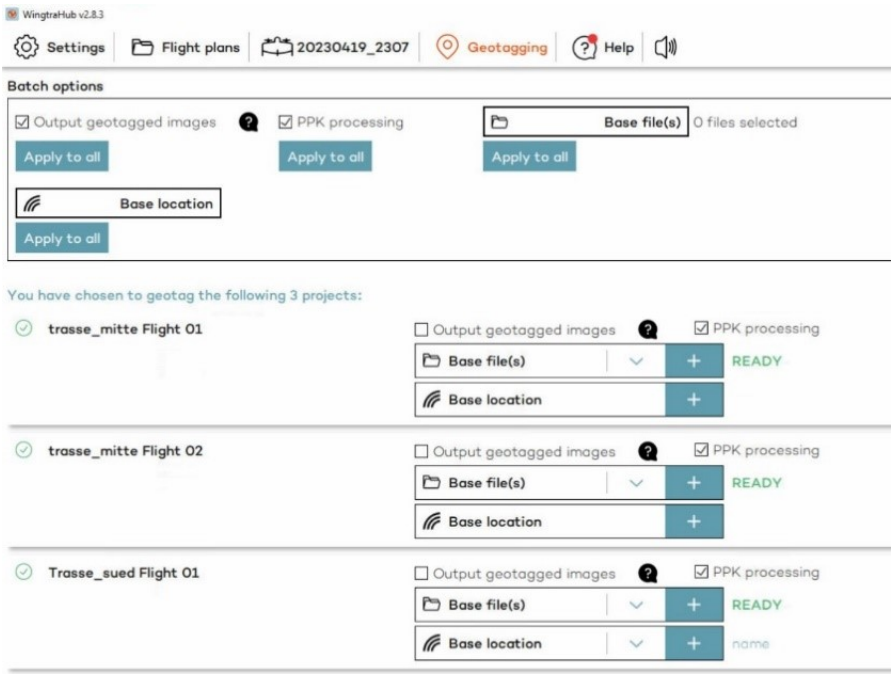

Figure 5.18: PPK processing interface of the WingtraHub software.

After the aerial photographs obtained from all unmanned aerial vehicles were prepared for photogrammetric processing, a total of 7 different project files were created in Agisoft Metashape Pro software for each UAV. The output and photo coordinate system for the projects were selected as "WGS-84 (EPSG:4326)", and the aerial photographs were imported into Agisoft Metashape Pro software.

5.3.3.2 Photo Alignment

The photo alignment step is the photogrammetric process where aerial triangulation and bundle block adjustment take place. In this step, Agisoft Metashape Pro utilizes the overlapping photographs, photo coordinates, orientation information, and camera calibration data provided to identify and match common features as "tie points" along the photos. Additionally, the position of each photo capture point is computed, and the camera calibration parameters, such as interior orientation (IO) and exterior orientation (EO), are updated with corrections. [80] Camera IO parameters are defined as the camera's focal length, coordinates of principal points, and lens distortion coefficients.

Camera EO parameters, on the other hand, are defined as the camera's position (e.g., projection center coordinates (X0, Y0, Z0)) and orientation parameters (e.g., rotation around the three axes (omega, phi, and kappa)) in the object coordinate system. [81]

To perform the photo alignment step, after the necessary pre-processing of the data obtained from each UAV, they were transferred to separate folders, and different Agisoft Metashape Pro project files were created for each. Within the software, the project and camera coordinate system were set as WGS 84 (EPSG: 4326), and the respective UAV photos were imported into each project. Then, the "Align Photos" tool was executed. The accuracy option was set to "High", the key point limit was set to "40,000", and the tie point limit was set to "20,000" before starting the process. **Figure 5.19** shows the selected setting for the photo alignment stage on the Agisoft Metashape Pro. As a result of this process, tie points (e.g., sparse point cloud) were obtained, and camera positions were determined. **Figure 5.20** presents the output tie point formed by the data captured with DJI Mavic 3E.

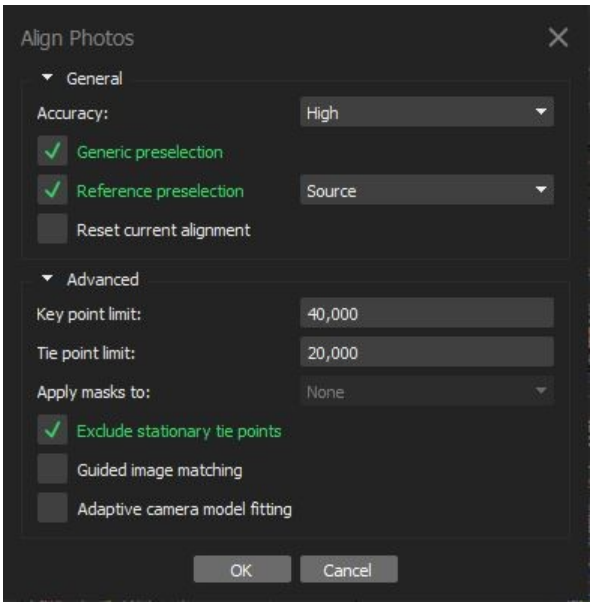

Figure 5.19: Settings for the photo alignment stage on the Agisoft Metashape Pro.

Figure 5.20: Present the output tie point formed by the data captured with DJI Mavic 3E.

After the generation of tie points, ground control points (GCPs) and a check point were introduced to the software through the "reference" section. The GCP coordinate system (WGS84 (EPSG:4326)), as well as the row, column, and delimiter information of the data in the file, were selected, and the GCPs were imported into the software. Each GCP was shifted to its correct position in the photos where it should be visible. In this process, it is necessary to have a minimum of 2 different photo identifications for each GCP, and blurry, low-contrast, and points near the edges of the photos should be avoided. To increase accuracy, care was taken to introduce as many GCPs as possible that adhere to these rules. **Figure 5.21** shows GCP import settings, and a GCP view from an aerial photograph.

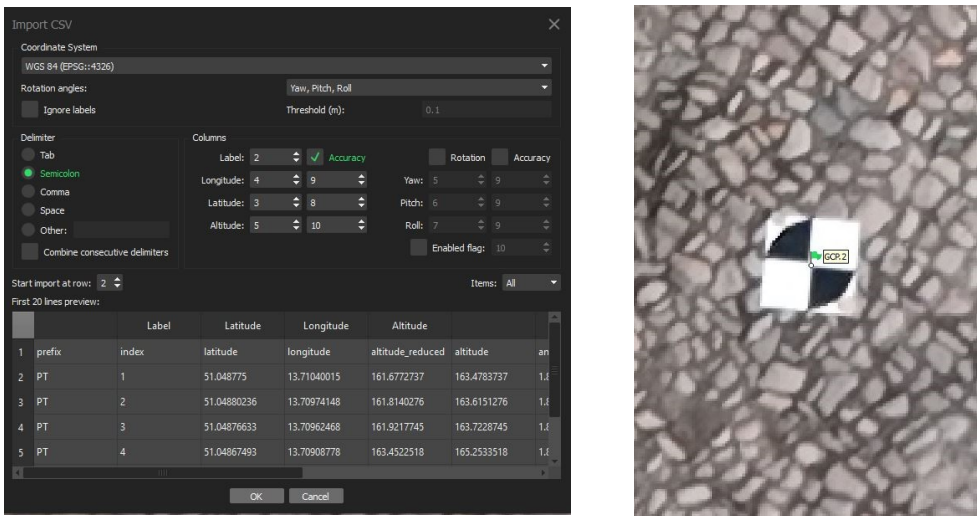

a) b)

Figure 5.21: a) GCP import settings, and b) GCP view from an aerial photograph.

After the introduction of GCPs, the "Optimize Cameras" tool in the "Reference" section was executed to update the camera's interior and exterior orientation as well as the tie point outputs based on the precise GCP coordinates provided to the software. **Figure 5.22** presents the camera alignment optimization settings.

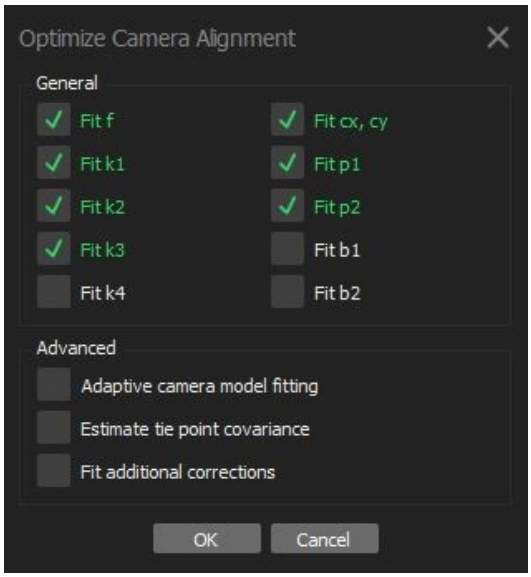

Figure 5.22: Camera alignment optimization settings.

5.3.3.3 Build Dense Point Cloud

After the GCP definition and optimization of camera orientations, the process moved on to the dense point cloud generation stage. In this step, the software utilizes the depth maps produced based on the camera's interior and exterior orientation parameters determined during the bundle adjustment phase. The depth maps are created using the relative camera interior and exterior orientation parameters of the overlapping image pairs. During the formation of the dense point cloud, the depth maps generated separately for each camera are merged, and errors in the overlapping regions are resolved. The combined depth maps are then transformed into a point cloud, incorporating color information from the photographs, in separate parts. In the final stage, these parts are merged together to form a single, seamless dense point cloud. [82]

In Agisoft Metashape Pro, to perform this process, we first defined the desired working area using a "bounding box" to prevent unnecessary data generation and reduce processing time. This step excludes the areas outside the bounding box from the data

processing, eliminating unnecessary data processing and saving time. Then, we utilized the "Build Point Cloud" tool found in the Workflow section. The source data was set as "Depth Maps", with a quality setting of "Medium" and mild depth filtering. Additionally, the "Calculate point colors" option was enabled to incorporate colors into the dense point cloud. This resulted in the generation of the dense point cloud. **Figure 5.23** shows dense point cloud which include about 10 million point and created by using the data captured by the DJI Phantom 4 RTK.

Figure 5.23: Dense point cloud created by using the data captured by the DJI Phantom 4 RTK.

5.3.3.4 Build Mesh and Texture

After the point cloud production, we need to create the mesh surface, which will be the digital representative of the 3D model we will produce. The software we use at this stage creates a triangular face by connecting the neighboring points in the selected source data (e.g., sparse point cloud, dens point cloud, and depth map) to each other as seamlessly and continuously as possible. Thus, this continuous triangular face forms the mesh surface of our 3D model.[83]

To generate the mesh, the "Build Mesh" tool in the "Workflow" tab was used. The surface type was set to "Arbitrary (3D)", the quality was set to "High", and the face count was adjusted to "Medium". The "Calculate vertex colors" option was selected to include vertex colors in the mesh. As for the source data, two separate processes were performed for each project using "Point cloud" and "Depth map" to test which data would result in a higher quality mesh surface. **Figure 5.24** presents the settings used

for the creation of mesh: a) with “depth map” as source data, and b) with “point cloud” as source data in Agisoft Metashape Pro. Afterwards, the undesired, unnecessary, or flawed parts of the output mesh surface were removed by cutting, resulting in a refined mesh surface. **Figure 5.25** shows the output mesh a)created from the data captured by the rgb camera of DJI M30T , and b) created from the data captured by the thermal camera of DJI M30T.

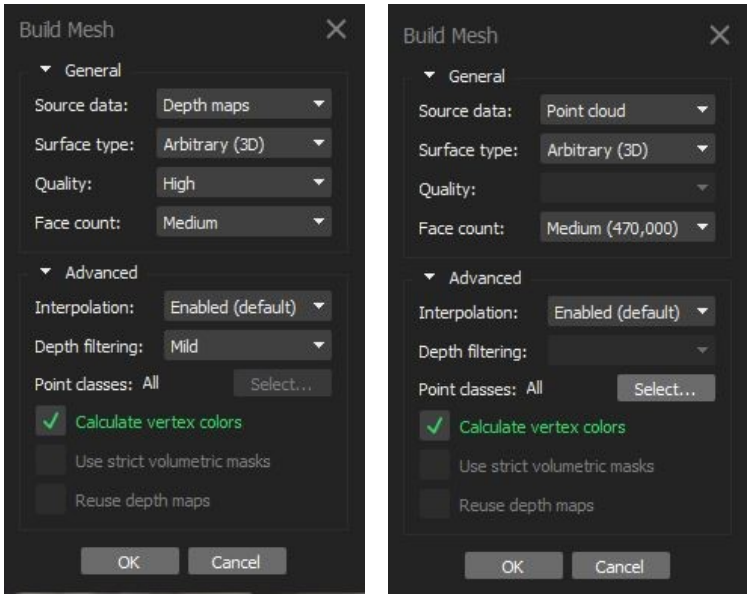

a) b)

Figure 5.24: Settings used for the creation of mesh: a) with “depth map” as source data, and b) with “point cloud” as source data

a)

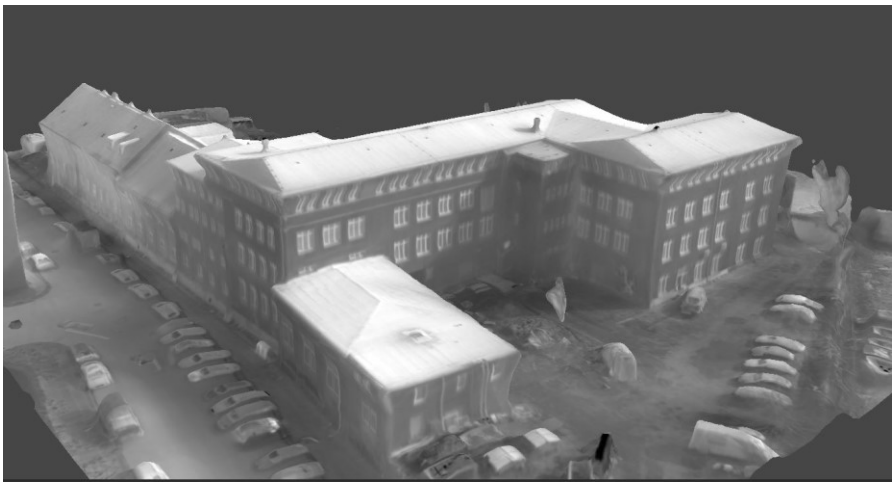

b)

Figure 5.25: Output mesh a) created from the data captured by the rgb camera of DJI M30T, and b) created from the data captured by the thermal camera of DJI M30T.

After creating the mesh, the texture building process is performed to enhance the model quality and achieve a more realistic visual representation. In this process, the original aerial photographs taken are stitched together by the software to create a texture map. By wrapping this texture map onto the mesh, a photo-realistic, textured 3D model is obtained.

To perform the texture building process and apply texture to the mesh surface, the "Build Texture" tool in the "Workflow" tab was utilized. The settings chosen for this process include the texture type as "Diffuse map," source data as "Images," mapping mode as "Generic," blending mode as "Mosaic," and a texture size/count of "4036 x 30." With these configurations, the texture was successfully applied to the mesh surface. **Figure 5.26** shows setting used for building texture over the mesh.

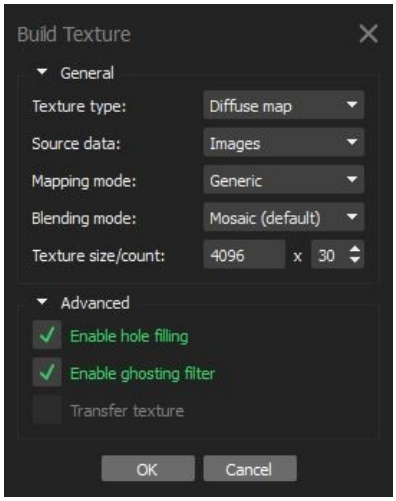

Figure 5.26: Settings used for building texture

The models generated by wrapping photographs onto mesh surfaces result in realistic textured 3D models. **Figure 5.27** presents the output textured mesh created from the data captured by the rgb camera of DJI M30T.

Figure 5.27: Output textured mesh created from the data captured by the rgb camera of DJI M30T.

In order to display the temperature information from the image metadata as an index in Celsius (°C) on the mesh surfaces created through texture building using thermal photographs captured by DJI Mavic 3T and DJI Matrice 30T drones, a raster transformation process is required. At the beginning of the data processing stage for thermal images, we used the "ThermoConverter" software to perform the R-JPEG to GeoTIFF conversion, resulting in single-band thermal images. To convert the pixel values of these images to temperature information, Equation (5.1) needs to be applied.

$$0.01 * B1 - 20 \tag{5.1}$$

The coefficient '0.01' in the equation is the default value recommended by the software. The value '-20' in the equation corresponds to the minimum temperature value (-20°C) of the selected image recording mode (-20°C–150°C) on the UAV remote controller. When this process is applied to the textured model using the 'Raster calculator' tool in Agisoft Metashape Pro software, the resulting product will allow temperature information to be read as an index at each point on the orthomosaic.". **Figure 5.28** shows the implementation the Equation (5.1) for the thermal band by using the “raster calculator” tool in Agisoft Metashape Pro.

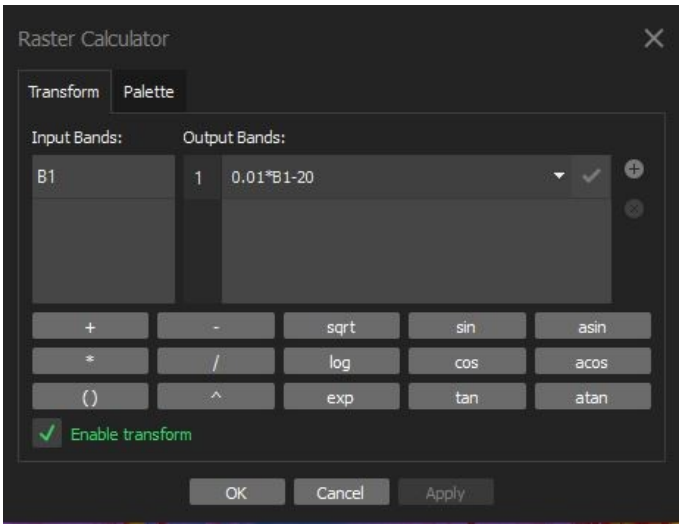

Figure 5.28: Implementation the Equation (5.1) for the thermal band

Another process is to configure a "Palette" in order to provide pseudocolor visualization and better interpretation of the thermal model. To perform this task, the "Raster calculator" tool in the "Tools" section was used. In the "Palette" tab of the Raster calculator, the "custom" option was selected, and 11 colors with corresponding value ranges were manually chosen. During the color assignment, an attempt was made to manually adjust the pseudocolor configuration to the commonly used "Iron Red" in thermal applications. The start and end values of the histogram table in the interface were adjusted to make the model coloring meaningful and interpretable. Once this was done, the "Palette" operation was applied. **Figure 5.29** and **Figure 5.30** show the histogram graph and palette configuration, and output pseudocolor textured mesh created from the data captured by the thermal camera of DJI M30T respectively.

Figure 5.29: Histogram graph and palette configuration of the data captured by DJI Matrice 30T.

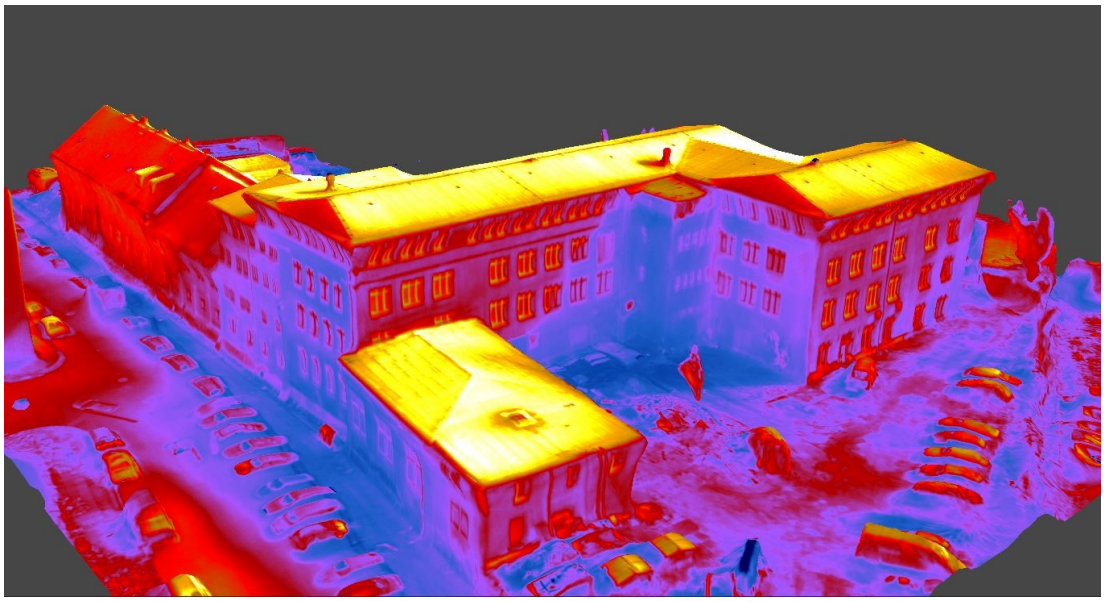

Figure 5.30: Output pseudocolor textured mesh created from the data captured by the thermal camera of DJI M30T.

From the "Build Orthomosaic" tool in the "Workflow" tab, an orthomosaic can be generated, and temperature information can be extracted from each point on the orthomosaic as an index in the software interface. **Figure 5.31** presents the pseudocolor thermal orthomosaic and the temperature information for a point in celcius (°C) unit as index.

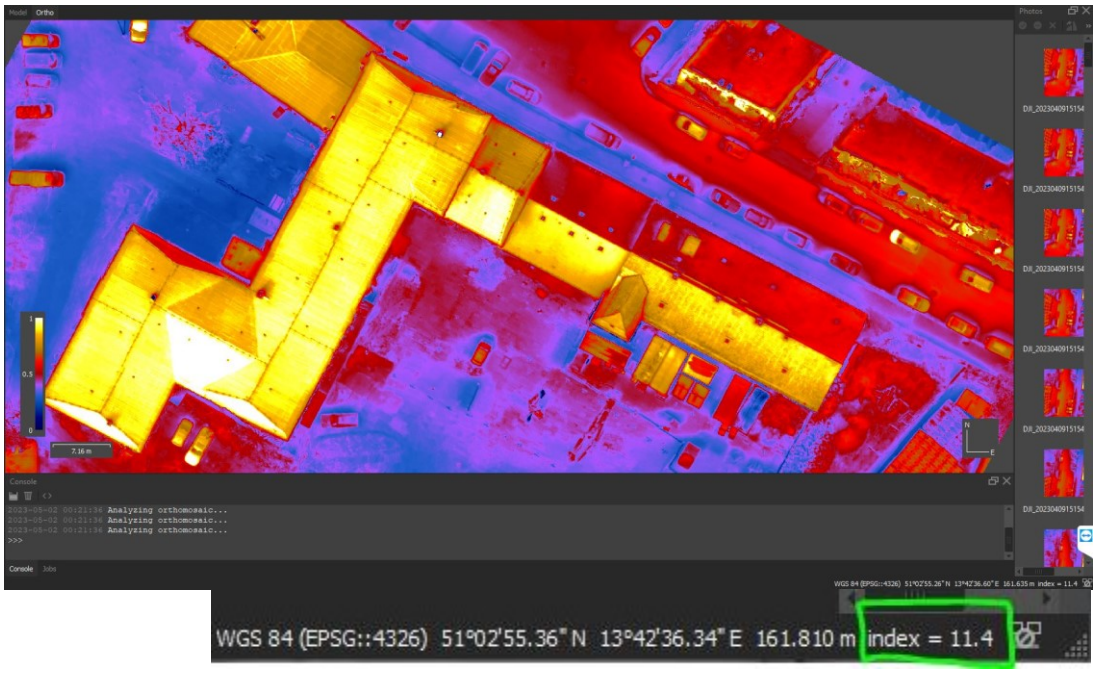

Figure 5.31: The pseudocolor thermal orthomosaic and the temperature value as index.

Another method for temperature reading and pseudocolor interpretation is the use of software called "DJI Thermal Analysis 3.0". These software tools are developed by DJI and are designed to visualize photos captured using unmanned aerial vehicles equipped with thermal cameras. In this software, the photos can be viewed with different palette options, temperature information can be read from individual points, and the minimum-maximum temperature values can be obtained within areas defined by shapes such as lines, rectangles, and circles. However, it's important to note that all these operations can be performed on a single photo at a time. **Figure 5.32** shows a thermal image captured by the thermal camera of the DJI Matrice 30 Thermal on DJI Thermal Analysis Tool 3.0.

Figure 5.32: A thermal image captured by the thermal camera of the DJI Matrice 30T on DJI Thermal Analysis Tool 3.0.

5.3.3.5 Edit and Analyze

After each step of the photogrammetric process (e.g., tie point generation, dense point cloud creation, mesh processing, etc.), editing can be performed. Furthermore, after the formation of the tie point cloud, the area of interest can be defined to ensure that it remains within the three-dimensional workspace, providing advantages in terms of output data size and processing time. Additionally, before exporting each output product outside the software, manual editing operations such as cropping, deleting,

color calibration, point cloud classification, point cloud decimation, and mesh face count reduction can be performed to achieve the desired quality. Once the output product reaches the desired quality, it can be exported.

After all the data processing and editing steps carried out within the scope of the thesis, RGB and pseudocolor 3D textured models, as well as thermal orthomosaics, were obtained. Additionally, in order to gain an understanding of the accuracy of the output data for all project data except thermal photographs, the Root-Mean-Square-Error (RMSE) values of the control points applied were obtained. **Table 5.14** shows RMSE values of GCPs for 7 different UAV processes.

Table 5.14: Total RMSE values of GCPs and check point for 7 different UAV processes.

Drone Model	Latitude error	Longitude error	Altitude error	Total Error (GCP)	Error (Check point)	Pixel error (cm/px)
Phantom 4 RTK	0.020442	0.016144	0.013262	0.029229	0.034331	0.503
Mavic 3E	0.018500	0.015834	0.024291	0.034395	0.083944	1.028
Matrice 300	0.021941	0.057895	0.034238	0.070749	0.037273	0.688
WingtraOne	0.031888	0.062037	0.020340	0.072658	0.214163	2.445
Mavic 3T	0.044501	0.015485	0.102156	0.112498	0.098517	1.446
Matrice 30T	0.278220	0.095899	0.199906	0.355760	0.285443	3.439
Mini 3 Pro	0.290440	0.152344	0.884780	0.943610	3.919671	0.812

After the final editing and cropping steps, the obtained models were saved in various formats for future output needs. **Figure 6.1**, **Figure 6.2** and **Figure 6.3** show 3D models created from photographs captured by DJI Mini 3 Pro, DJI Mavic 3E and Mavic 3T respectively**.** **Figure 6.4** presents 3D models created from thermal photographs captured by DJI Mavic 3T. **Figure 6.5** and **Figure 6.6** show 3D models created from photographs captured by DJI Phantom 4 RTK, and DJI Matrice 30T respectively**.** **Figure 6.7** presents 3D models created from thermal photographs captured by DJI Matrice 30T. **Figure 6.8** and **Figure 6.9** show 3D models created from photographs captured by DJI Matrice 300 RTK, and WingtraOne Gen II respectively.

Figure 6.1: 3D model created from photographs captured by DJI Mini 3 Pro.

Figure 6.2: 3D model created from photographs captured by DJI Mavic 3E.

Figure 6.3: 3D model created from rgb photographs captured by DJI Mavic 3T.

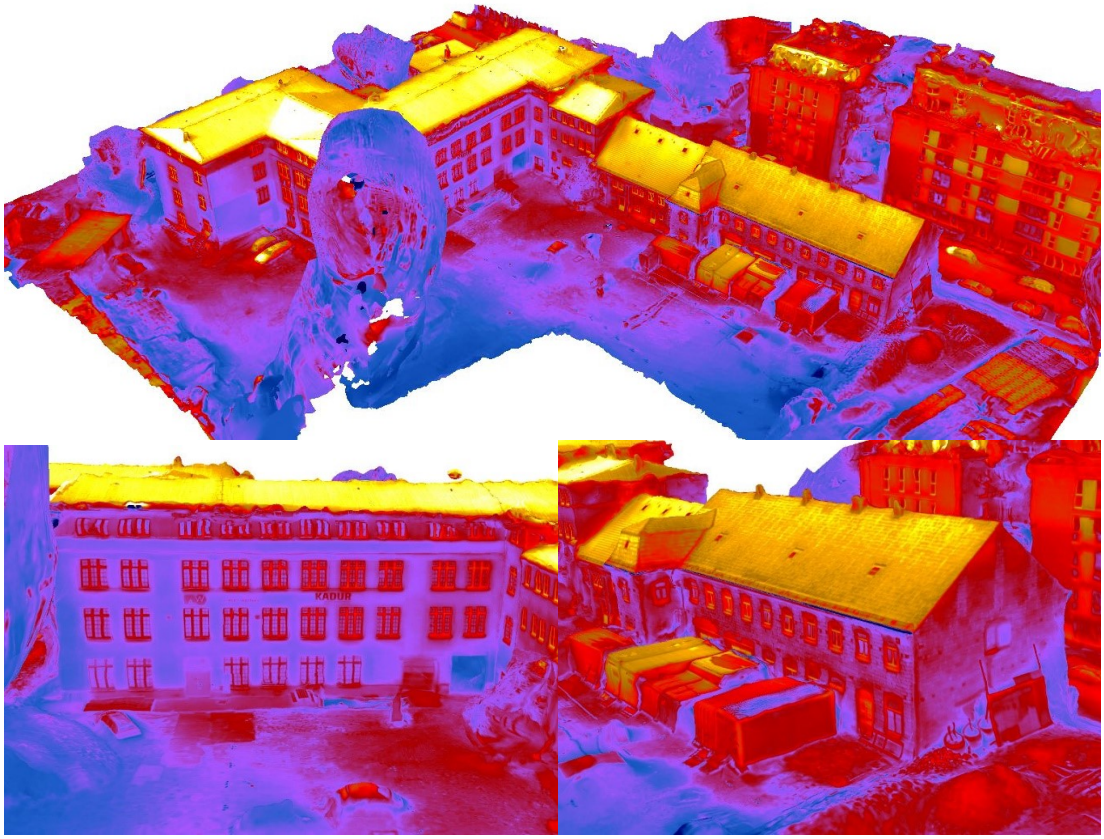

Figure 6.4: 3D model created from thermal photographs captured by DJI Mavic 3T.

Figure 6.5: 3D model created from photographs captured by DJI Phantom 4 RTK.

Figure 6.6: 3D model created from rgb photographs captured by DJI Matrice 30T.

Figure 6.7: 3D model created from thermal photographs captured by DJI Matrice 30T.

Figure 6.8: 3D model created from photographs captured by DJI Matrice 300RTK.

Figure 6.9: 3D model created from photographs captured by WingtraOne Gen II.

Chapter 6

Results and Discussions

Within the scope of our thesis, a commercial building located in Dresden with an area of 10,771 $m^2$was selected as the study area, and nadir and oblique flights were conducted using seven popular unmanned aerial vehicles (e.g., DJI Mini 3 Pro, DJI Mavic 3E, DJI Mavic 3T, Phantom 4RTK, DJI Matrice 30T, DJI Matrice 300RTK, and WingtraOne Gen II) commonly used in the surveying and mapping industry. The flights with unmanned aerial vehicles were performed using both automatic and manual flight modes to capture overlapping RGB and thermal aerial photographs that encompassed all facades of the modeled building. For detailed facade imagery around the building, low-altitude manual flights were conducted using DJI Mini Pro, DJI Mavic 3E, DJI Mavic 3T, and DJI Phantom 4RTK within the study area. However, due to safety concerns, low-altitude manual flights could not be performed using DJI Matrice 30T, DJI Matrice 300RTK, and WingtraOne Gen II. Additionally, due to safety risks associated with the VTOL and fixed-wing structure of WingtraOne Gen II, flights within the urban area of the study site could not be conducted. Instead, flights conducted in Bahretal, a rural area in the Saxony state, were used to analyze the 3D model generation performance of WingtraOne Gen II.

The data obtained within the study area was processed using photogrammetry software called Agisoft Metashape Pro. Additionally, software tools such as “Thermo Converter”, “WingtraHub”, and “DJI Thermal Analysis Tool 3.0” were utilized. During the data processing, 5 Ground Control Points (GCPs) and a check point were used for WingtraOne Gen II, and 5 GCPs were used for other DJI unmanned aerial vehicles to enhance positional accuracy. ThermoConverter software was employed to convert the image metadata of the images captured by DJI Mavic 3T and DJI Matrice

30T into a readable format, allowing us to generate index maps that contain temperature values.

DJI Mini 3 Pro has a GNSS receiver that can provide rough positioning for navigation purposes only. Therefore, without the use of Ground Control Points (GCPs), its positional accuracy is significantly lower. However, for projects that only require relative accuracy, such as creating scaled 3D models for solar panel installations, it can still deliver satisfactory results. On the other hand, DJI Mavic 3E, DJI Mavic 3T, Phantom 4 RTK, DJI Matrice 30T, and DJI Matrice 300 RTK unmanned aerial vehicles are equipped with RTK modules, while WingtraOne Gen II has a PPK module. WingtraOne Gen II can achieve precise photo capture coordinates only through post-processing kinematics (PPK) solution performed in the office environment. Additionally, DJI Mavic 3E, Phantom 4 RTK, and DJI Matrice 300 RTK can record raw GNSS data as extra flight data, which can be used along with various PPK software for additional PPK solutions. This feature is advantageous in resolving positioning issues caused by connection problems during the flight, as accurate photo capture coordinates can be obtained by performing PPK solution using raw data in the office environment.

DJI Mavic 3T and DJI Matrice 30T do not have the capability to record raw GNSS data, and therefore, PPK method cannot be applied. Moreover, since these unmanned aerial vehicles are not specifically designed for surveying and mapping purposes, they lack features like "TimeSync" that helps in synchronizing the RC, camera, and flight controller for precise positioning, as well as "level arm correction" that defines the relationship between the GNSS receiver and the camera's perspective center. As a result, DJI Mavic 3T and DJI Matrice 30T have lower positional accuracy. Furthermore, the disadvantage of DJI Mavic 3T and DJI Matrice 30T is that their thermal cameras do not process temperature data directly, requiring additional preprocessing using software like ThermoConverter.

In our study, we found that DJI Phantom 4 RTK, which has been a workhorse unmanned aerial vehicle for surveying and mapping purposes for many years, lags behind other DJI drones we examined in terms of both software and hardware aspects. Although it provides successful results in terms of positional accuracy, when compared to DJI Mavic 3E, which can be considered in the same class, Mavic 3E outperforms

Phantom 4 RTK in terms of camera quality, user-friendly remote controller, compact design, long battery life, and intelligent software features. Therefore, Mavic 3E is a more advantageous UAV for surveying and 3D modeling purposes compared to Phantom 4 RTK.

The DJI Mavic 3T and DJI Matrice 30T unmanned aerial vehicles (UAVs) used in the study stand out for their superior performance in areas such as research and rescue, inspection, and firefighting. Both drones are equipped with various cameras including zoom, wide-angle, and thermal cameras. The DJI Matrice 30T additionally features a laser range finder sensor. Having thermal cameras enables the creation of temperature index maps and thermal 3D models. The Matrice 30T is also compatible with the DJI Dock station and has cloud-based intelligent systems and intelligent software features that facilitate teamwork. Therefore, the DJI Matrice 30T is in a much more advanced position compared to the DJI Mavic 3T.

When examining the visual quality of the 3D textured models obtained from the unmanned aerial vehicles used in the study, it is observed that the highest visual model quality is achieved with the full-frame Zenmuse P1 camera mounted on the DJI Matrice 300 RTK. The second-best visual quality is obtained with the DJI Mavic 3E. The images obtained from the DJI Phantom 4 RTK have lower brightness levels compared to other models due to the smaller camera sensor size (1-inch CMOS), which puts them at a disadvantage in low-light scenarios. The models obtained through DJI Mavic 3T and DJI Matrice 30T also exhibit satisfactory and moderate visual quality. Additionally, although the output model from the DJI Mini 3 Pro has blurry texture structures in some parts, it still maintains an acceptable level of quality. On the other hand, the model obtained through WingtraOne Gen II, which involves flights conducted at a much higher altitude (i.e., 250m) for safety purposes and with a camera gimbal angle of 90° (i.e., nadir), is lower in quality compared to the other models as expected. However, considering its ability to provide quick solutions for large-scale projects, it still exhibits a reasonable visual quality. In this study, we used the Sony RX1R II nadir camera for WingtraOne Gen II flights. However, for future work, we recommend using the Sony a6100 camera, which can be mounted on the unmanned aerial vehicle at an oblique angle, to enable oblique flights and create higher-quality models. In our study, we used the DJI Mavic 3T and DJI Matrice 30T unmanned aerial

vehicles with additional thermal cameras. When examining the 3D pseudocolor thermal models created using the thermal photos from these drones, it was determined that, although the camera specifications are similar, the model generated from the data collected by the DJI Matrice 30T exhibits better visual quality.

When examining the RMSE values of the ground control points of the 3D models generated from the data obtained from UAVs used in the study, it was observed that the most successful UAV in terms of positional accuracy was the Phantom 4 RTK with a horizontal RMSE of 1.83 cm and a vertical RMSE of 1.33 cm. The DJI Mavic 3E, on the other hand, was observed to have the second most accurate positional accuracy with horizontal RMSE of 1.72 cm and vertical RMSE of 2.43 cm. As shown in **Table 6.1**, the ranking continues as follows: DJI Matrice 300 RTK, WingtraOne Gen II, DJI Mavic 3T, DJI Matrice 30T, and DJI Mini 3 Pro. Despite having RTK modules in terms of hardware, DJI Mavic 3T and DJI Matrice 30T exhibited lower positional accuracy performance than expected due to the lack of 'TimeSync' and 'lever-arm correction' features required for survey-grade precise positioning. The total GCP RMSE value for DJI Mavic 3T was observed to be 11 cm, while it was 35.6 cm for DJI Matrice 30T. The UAV model with the poorest positional accuracy was found to be DJI Mini 3 Pro, with a total GCP RMSE value of 94 cm. This is attributed to the absence of RTK and PPK modules in terms of hardware. However, it was noted that the model still produced successful scaled models in terms of relative accuracy and could be used by users seeking cost-effective solutions for projects that only require scaling and do not demand precise positional accuracy.

Based on the analysis considering criteria such as positional accuracy, model quality, and cost, the recommended unmanned aerial vehicle model for 3D modeling purposes is the DJI Mavic 3E with a horizontal root-mean-square error of 1.72 cm and a vertical root-mean-square error of 2.43 cm. Furthermore, the DJI Matrice 30T is recommended for thermal applications and modeling, while the WingtraOne Gen II model is recommended for large-scale city modeling projects.

In our study, we examined the output 3D models generated by the data sperately captured by 7 different popular unmanned aerial vehicles (UAVs) commonly used in various fields such as engineering, archaeology, 3D city planning, historical documentation, and frequently employed in the surveying and mapping sector. We

thoroughly examined the applications of 3D models and conducted 3D model production using the 7 different UAVs. The output models were then analyzed in terms of their visual and positional performance. This study aims to serve as a guide and provide assistance to users who face indecision when selecting from numerous unmanned aerial systems available in the industry for 3D model production, helping them find the most suitable UAV in terms of desired quality and positional accuracy. The tests, comments, and analyses conducted in this study can assist readers in choosing the appropriate UAV for their specific purposes and serve as a valuable resource for UAV selection.

Chapter 7

Conclusions

Realistic 3D textured models are widely used in various sectors such as archaeology, architecture, historical documentation, and virtual reality. Additionally, pseudocolor 3D models created from thermal camera images offer a useful tool for exploratory applications. The most suitable technique for creating realistic 3D models is photogrammetry. By processing oblique aerial photographs captured by unmanned aerial vehicles through necessary preprocessing stages and using photogrammetry software such as Agisoft Metashape Pro, 3D textured models can be generated. These models have a wide range of applications in many sectors. The increasing use of unmanned aerial vehicles in photogrammetry has facilitated the acquisition of high-quality, fast, cost-effective, and efficient data for the necessary photogrammetric processes in 3D model production.

In the expanding sector of unmanned aerial vehicles, with increasing usage and production, the availability of options with various hardware and software features can lead to confusion and indecisiveness among users who intend to use UAVs for 3D model production. Therefore, within the scope of this thesis, analyses were conducted on the 3D model production and application areas of 7 popular UAVs used in the surveying and mapping industry (e.g., DJI Mini 3 Pro, DJI Mavic 3E, DJI Mavic 3T, Phantom 4 RTK, DJI Matrice 30T, DJI Matrice 300 RTK, and WingtraOne Gen II). The usage areas of 3D models in various sectors were analyzed. Subsequently, a commercial office building covering an area of 10,771m^2 in Dresden was selected as the study area, and thermal and RGB aerial photographs were captured from an altitude of approximately 50 meters in both nadir and oblique modes. Additionally, 5 ground control points and a check point were established in the study area, and their coordinates were measured and included in the photogrammetric processes to enhance

positional accuracy. Due to flight and environmental safety concerns in the city center study area, flights could not be conducted using the WingtraOne Gen II UAV. Instead, flights conducted in the Bahretal region, located in the Saxony state away from the city center, were utilized. In this region, 5 ground control points and a check point were also used, and flights were conducted at an altitude of 250 meters.

Each unmanned aerial vehicle (UAV) and the data obtained from GNSS receivers were analyzed and compared with the processed data in various software. As a result of these analyses, taking into account criteria such as positional accuracy, model quality, and cost, it is recommended that the DJI Mavic 3E UAV, with a root-mean-square error of 1.72 cm horizontally and 2.43 cm vertically, is the optimal model for 3D modeling purposes. Furthermore, the DJI Matrice 30T is recommended for thermal applications and modeling, while the WingtraOne Gen II model is recommended for large-scale city modeling projects.

It is advised that DJI Matrice 30T, DJI Matrice 300 RTK, and WingtraOne Gen II, which are heavier and larger compared to other UAVs used in the study, are not suitable for UAV takeoff and landing in urban areas due to safety reasons. Particularly, it is suggested that DJI Matrice 300 RTK and WingtraOne Gen II are more suitable for the production of large-scale 3D city models when taking off from a suitable location away from the city center. Additionally, for the WingtraOne Gen II, it is recommended to use the oblique Sony a1600 camera, which can be mounted at an angle, instead of the Sony RX1RII camera used as a payload in the study, as it provides a better option for 3D model production.

This study aims to guide users who are experiencing uncertainty in 3D model generation and are seeking the most suitable unmanned aerial vehicle (UAV) for their required workspace. The conducted tests, reviews, and analyses can be evaluated to assist readers in selecting a UAV for different purposes. This study provides users with a guide to choose the most suitable unmanned aerial vehicle in terms of the requested quality and positional accuracy.

References

[1] Nikolakopoulos KG, Soura K, Koukouvelas IK, Argyropoulos NG. UAV vs classical aerial photogrammetry for archaeological studies. *J Archaeol Sci Reports*. 2016; 14(2017): 758–73.

[2] Lambert JM, Jacob Skousen B. A critical review of UAS-based aerial photography and photogrammetry of Cahokia's Grand Plaza. *J Archaeol Sci Reports* [Internet]. 2022; 47(November 2022): 103789. Available from: https://doi.org/10.1016/j.jasrep.2022.103789

[3] Duerer A. Early developments 1. The center of photogrammetric training. 1977.

[4] Konecny G. The International Society for Photogrammetry and Remote Sensing-75 Years Old, or 75 Years Young. *Photogramm Eng Remote Sensing*. 1985; 51(7): 919–33.

[5] Suveg I, Vosselman G. Reconstruction of 3D building models from aerial images and maps. *ISPRS J Photogramm Remote Sens*. 2004; 58(2004): 202–24.

[6] Using AI to Generate 3D Models! | by Andrew Blance | Towards Data Science [Internet]. Using AI to Generate 3d Models, Fast. Available from: https://towardsdatascience.com/using-ai-to-generate-3d-models-2634398c0799

[7] Li M, Nan L. Feature-preserving 3D mesh simplification for urban buildings. *ISPRS J Photogramm Remote Sens* [Internet]. 2021; 173(January 2021): 135–50. Available from: https://doi.org/10.1016/j.isprsjprs.2021.01.006

[8] Matys M, Krajcovic M, Gabajova G. Creating 3D models of transportation vehicles using photogrammetry. *Transp Res Procedia*. 2021 Jan 1; 55(2021): 584–91.

[9] Gomez C, Kennedy B. Capturing volcanic plumes in 3D with UAV-based photogrammetry at Yasur Volcano – Vanuatu. *J Volcanol Geotherm Res*. 2018 Jan 15; 350(2018): 84–8.

[10] Karakiş S, Sefercik UG, Bilir T, Atalay C. Precise monitoring of temporal topographic change detection via unmanned air vehicle. *Bull Miner Res Explor* [Internet]. 2020 Apr 15 [cited 2023 Feb 20]; 161(161): 151–6. Available from: https://dergipark.org.tr/en/pub/bulletinofmre/issue/42676/524179

[11] Jeong GY, Nguyen TN, Tran DK, Hoang TBH. Applying unmanned aerial vehicle photogrammetry for measuring dimension of structural elements in traditional timber building. *Measurement*. 2020 Mar 1; 153(1 March): 107386.

[12] Forlani G, Roncella R, Nardinocchi C. Where is photogrammetry heading to? State of the art and trends. *Rend Lincei*. 2015; 26: 85–96.

[13] Mikrut S. Classical photogrammetry and UAV - Selected ascpects. *Int Arch Photogramm Remote Sens Spat Inf Sci - ISPRS Arch*. 2016; 2016-Janua(July): 947–52.

[14] Houser KW. Light, Light, Light. *http://dx.doi.org/101080/15502724201110732153* [Internet]. 2013 [cited 2023 Feb 25]; 8(1): 5–7. Available from: https://www.tandfonline.com/doi/abs/10.1080/15502724.2011.10732153

[15] Bhatt R. Remote Sensing [Internet]. [cited 2023 Feb 25]. Available from: https://ruchi-nagar.medium.com/remote-sensing-3a614255808

[16] Cox MJ. Optics of the Human Eye</br>D.A. Atchison, G. Smith; Butterworth-Heinemann, Oxford, 2000, 269 pages, ISBN 0-7506-3775-7, £27.50. *Ophthalmic Physiol Opt* [Internet]. 2001 Sep 1 [cited 2023 Feb 25]; 21(5): 426–426. Available from: https://onlinelibrary.wiley.com/doi/full/10.1046/j.1475-1313.2001.00577.x

[17] Peres MR. The Focal Encyclopedia of Photography. 13 April 2. Vol. 4th Editio, The Focal Encyclopedia of Photography. Routledge; 2007. 563–572 p.

[18] Best photogrammetry software for drone mapping | Wingtra [Internet]. [cited 2023 Feb 25]. Available from: https://wingtra.com/best-photogrammetry-software/

[19] Scaggion C, Castelli S, Usai D, Artioli G. 3D digital dental models' accuracy for anthropological study: Comparing close-range photogrammetry to μ-CT scanning. *Digit Appl Archaeol Cult Herit*. 2022 Dec 1; 27(December 2022): 245.

[20] Westoby MJ, Brasington J, Glasser NF, Hambrey MJ, Reynolds JM. "Structure-from-Motion" photogrammetry: A low-cost, effective tool for geoscience applications. *Geomorphology* [Internet]. 2012; 179(2012): 300–14. Available from: http://dx.doi.org/10.1016/j.geomorph.2012.08.021

[21] Aber JS, Marzolff I, Ries JB, Aber SEW. Principles of Photogrammetry. *Small-Format Aer Photogr UAS Imag*. 2019; 19–38.

[22] A wide range of maps with the same drone | Wingtra [Internet]. [cited 2023 Feb 27]. Available from: https://wingtra.com/mapping-drone-wingtraone/aerial-map-types/#orthomosaic-maps

[23] What is photogrammetry? [Internet]. GeoNadir. 2022 [cited 2023 Feb 27]. Available from: https://geonadir.com/what-is-photogrammetry/

[24] Habib M. Evaluation of DEM interpolation techniques for characterizing terrain roughness. *CATENA*. 2021 Mar 1; 198(March 2021): 105072.

[25] Zheng X, Xiong H, Gong J, Yue L. A morphologically preserved multi-resolution TIN surface modeling and visualization method for virtual globes. *ISPRS J Photogramm Remote Sens*. 2017 Jul 1; 129(July 2017): 41–54.

[26] Doyle FJ. The Historical Development of Analytical Photogrammetry [Internet]. Semi-Annual Meeting, Wellesley Island, N. Y. 1963 [cited 2023 Mar 3]. p. 259–65. Available from: https://www.asprs.org/wp-content/uploads/pers/1964journal/mar/1964_mar_259-265.pdf

[27] Hauck HG. Datei:Hauck Neue Constructionen der Perspective und

Photogrametrie.png – Wikipedia [Internet]. Journal of Pure and Applied Mathematics. 1845 [cited 2023 Mar 3]. Available from: https://de.wikipedia.org/wiki/Datei:Hauck_Neue_Constructionen_der_Perspective_und_Photogrametrie.png

[28] Konecny G. Keynote Address :75 Years Old, or 75 Years Young. In: The International Society for Photogrammetry and Remote Sensing. Hannover, Germany; 1985.

[29] Granshaw SI. First World War aerial photography: 1918. *Photogramm Rec* [Internet]. 2018 Dec 1 [cited 2023 Mar 4]; 33(164): 396–405. Available from: https://onlinelibrary.wiley.com/doi/full/10.1111/phor.12260

[30] 1940: Coast Guard Provides Aircraft and Crews for the US Coast and Geodetic Survey | Coast Guard Aviation History [Internet]. [cited 2023 Mar 4]. Available from: https://cgaviationhistory.org/1940-coast-guard-and-geodetic-survey/

[31] Bean RK. Development Of The Er-55 Projector*. *Sect oj Phologrammelry, Topogr Div U S Geol Surv*. 1953; 71–84.

[32] Brown DG. New Developments in Photogeodesy. *Photogramm Eng Remote Sens*. 1994; 60(7): 877–94.

[33] Hughes D, Fricker P, Chapuis A, Traversari E, Schreiber P, Schapira F. Development of Photogrammetry in Switzerland [Internet]. Virtual Archive of Wild Heerbrugg. [cited 2023 Mar 7]. Available from: https://wild-heerbrugg.ch/en/produkte/photogrammetrie-photogrammetry

[34] Williams DR. Explorer 6 [Internet]. Nata Space Science Data Coordinated Archieve. 2022 [cited 2023 Mar 7]. Available from: https://www.google.com/search?q=EXPLORER+6&oq=EXPLORER+6&aqs=chrome..69i57j0i512l5j46i175i199i512j0i512j46i175i199i512j0i512.2828j0j7&sourceid=chrome&ie=UTF-8

[35] Roberts LG. Machine Perception of Three-Dimensional Solids [Internet]. [Massachusetts]: Massachusetts Institute of Technology; 1963 [cited 2023 Mar 6]. Available from: https://dspace.mit.edu/bitstream/handle/1721.1/11589/33959125-MIT.pdf?sequence=2

[36] History of Photogrammetry [Internet]. Open Educational Resources for the Digital Arts & Humanities. [cited 2023 Mar 6]. Available from: https://teach.dariah.eu/mod/hvp/view.php?id=860

[37] Stojakovic V. Terrestrial photogrammetry and application to modeling architectural objects. *Facta Univ - Ser Archit Civ Eng*. 2008; 6(1): 113–25.

[38] Assali P, Grussenmeyer P, Villemin T, Pollet N, Viguier F. Surveying and modeling of rock discontinuities by terrestrial laser scanning and photogrammetry: Semi-automatic approaches for linear outcrop inspection. *J Struct Geol*. 2014 Sep 1; 66(September 2014): 102–14.

[39] Jiang R, Ja´uregui D V., White KR. Close-range photogrammetry applications in bridge measurement: Literature review. *Measurement* [Internet]. 2008 [cited 2023 Mar 7]; 41(2008): 823–34. Available from: https://pdf.sciencedirectassets.com/271454/1-s2.0-S0263224108X00077/1-s2.0-S0263224108000031/main.pdf?X-Amz-Security-Token=IQoJb3JpZ2luX2VjEH0aCXVzLWVhc3QtMSJIMEYCIQDPVkO7XLGlobcxHhJssEfQlFFJJ6jNfcoU9weendMAEgIhAOZWvYDWkuZV9rXF%2BcFh6HO2P%2BWgNtXs5uS5ZiN7

[40] Evin A, Souter T, Hulme-Beaman A, Ameen C, Allen R, Viacava P, et al. The use of close-range photogrammetry in zooarchaeology: Creating accurate 3D models of wolf crania to study dog domestication. *J Archaeol Sci Reports*. 2016 Oct 1; 9(October 2016): 87–93.

[41] Concepts of Photogrammetry [Internet]. Satpalda. [cited 2023 Mar 19]. Available from: https://www.satpalda.com/blogs/concepts-of-photogrammetry

[42] Torres G. Photogrammetry vs. LIDAR: what sensor to choose for a given application | Wingtra [Internet]. Wingtra: Drone know-how. 2023 [cited 2023 Mar 19]. Available from: https://wingtra.com/drone-photogrammetry-vs-lidar/

[43] Leberl FW. Digital Photogrammteric Plotting Techniques [Internet]. [cited 2023 Mar 19]. p. 2–13. Available from: https://online.tugraz.at/tug_online/voe_main2.getvolltext?pCurrPk=73480

[44] Habib AF. Digital Photogrammetric Systems Chapters 1-5 [Internet]. [cited 2023 Mar 19]. p. 1–139. Available from: https://engineering.purdue.edu/CE/Academics/Groups/Geomatics/DPRG/Courses_Materials/Photogrammetry_2019Fall/AKAM_CE59700_CH6_AKAM

[45] Dering GM, Micklethwaite S, Thiele ST, Vollgger SA, Cruden AR. Review of drones, photogrammetry and emerging sensor technology for the study of dykes: Best practises and future potential. *J Volcanol Geotherm Res* [Internet]. 2019 [cited 2023 Mar 19]; 373(2019): 148–66. Available from: https://doi.org/10.1016/j.jvolgeores.2019.01.018

[46] 3D-Stereo-Visualisierung von Geodaten: Verbesserter Workflow in der Photogrammetrie [Internet]. Virtual Reality Magazin. 2022 [cited 2023 Mar 19]. Available from: https://www.virtual-reality-magazin.de/3d-stereo-visualisierung-von-geodaten-verbesserter-workflow-in-der-photogrammetrie/

[47] Karakış S. Küçük Alanlarda Model Uçaklarla Haritalama Amaçli Veri Üretim Olanaklarının Araştırılması. Zonguldak Karaelmas University; 2011.

[48] Colomina I, Molina P. Unmanned aerial systems for photogrammetry and remote sensing: A review. *ISPRS J Photogramm Remote Sens*. 2014; 92(2014): 79–97.

[49] Eisenbeiß H. UAV Photogrammetry. ETH Zürich; 2009.

[50] Giordan D, Adams MS, Aicardi I, Alicandro M, Allasia P, Baldo M, et al. The use of unmanned aerial vehicles (UAVs) for engineering geology applications. *Bull Eng Geol Environ*. 2020; 79(7): 3437–81.

[51] Zhang J, Liu Z, Zhang G, Zhang J;, Liu Z;, Zhang G. Pose Measurement for Unmanned Aerial Vehicle Based on Rigid Skeleton. *Appl Sci* [Internet]. 2021 Feb 3 [cited 2023 Mar 23]; 11(4): 1373. Available from: https://www.mdpi.com/2076-3417/11/4/1373/htm

[52] Masse C, Gougeon O, Nguyen DT, Saussie D. Modeling and Control of a Quadcopter Flying in a Wind Field: A Comparison between LQR and Structured ∞ Control Techniques. In: 2018 International Conference on Unmanned Aircraft Systems, ICUAS 2018. Institute of Electrical and Electronics Engineers Inc.; 2018. p. 1408–17.

[53] She XTP, Lang H, Lin X. A Data-Driven Power Consumption Model for Electric UAVs. In: 2020 American Control Conference Denver [Internet]. Denver / USA; 2020 [cited 2023 Mar 24]. p. 4957–62. Available from: https://sci-hub.ru/https://ieeexplore.ieee.org/document/9147622

[54] van Blyenburgh P. UAVs: an overview. *Air Sp Eur*. 1999 Sep 1; 1(5–6): 43–7.

[55] DJI Matrice 30 Serie [Internet]. Kompaktes professionelles Kraftpaket - DJI. [cited 2023 Mar 25]. Available from: https://www.dji.com/de/matrice-30

[56] Industry Leader in VTOL Technology [Internet]. ALTI UAS-Vertical Reliability Horizontal Performance. [cited 2023 Mar 25]. Available from: https://www.altiuas.com/

[57] Polo ME, Felicísimo AM, Durán-Domínguez G. Accurate 3D models in both geometry and texture: An archaeological application. 2022 [cited 2023 Feb 18]; 2022: 2212–0548. Available from: https://doi.org/10.1016/j.daach.2022.e00248

[58] Tsilimantou E, Delegou ET, Nikitakos IA, Ioannidis C, Moropoulou A. GIS and BIM as Integrated Digital Environments for Modeling and Monitoring of Historic Buildings. *Appl Sci 2020, Vol 10, Page 1078* [Internet]. 2020 Feb 6 [cited 2023 Mar 25]; 10(3): 1078. Available from: https://www.mdpi.com/2076-3417/10/3/1078/htm

[59] wm (@wolski.m.85) - Sketchfab [Internet]. Płock - MPZP “Stare Miasto” cz I (wyłożenie 2). 2021 [cited 2023 Mar 26]. Available from: https://sketchfab.com/wolski.m.85

[60] Ubik S, Kubišta J, Dvořák T. Interactive 3D models: Documenting and presenting restoration and use of heritage objects. *Digit Appl Archaeol Cult Herit*. 2022; 27(August 2020).

[61] Pierce SG, Burnham K, McDonald L, MacLeod C harle. N, Dobie G, Summan R, et al. Quantitative inspection of wind turbine blades using UAV deployed photogrammetry. *e-Journal Nondestruct Test* [Internet]. 2018 Nov 1 [cited 2023 Mar 30]; 23(11). Available from: https://www.ndt.net/search/docs.php3?id=23360

[62] Verwaltungskarte 1:2 500 000 - Länder (VK2500-L) [Internet]. Bundesamt für Kartographie und Geodäsie. [cited 2023 Apr 10]. Available from: https://gdz.bkg.bund.de/index.php/default/open-data/verwaltungskarte-1-2-500-000-laender-vk2500-l.html

[63] DJI Mini 3 Pro - Fly Mini, Create Big [Internet]. DJI. [cited 2023 Apr 3]. Available from: https://www.dji.com/nz/mini-3-pro

[64] DJI Mavic 3 Enterprise [Internet]. Globe Flıght. [cited 2023 Apr 3]. Available from: https://www.globe-flight.de/DJI-Mavic-3-Enterprise-DE-Shop

[65] DJI Mavic 3 Enterprise Series - Specs [Internet]. DJI. [cited 2023 Apr 3]. Available from: https://www.dji.com/nz/mavic-3-enterprise/specs

[66] DJI Mavic 3 Thermal [Internet]. DJI. [cited 2023 Apr 4]. Available from: https://www.globe-flight.de/DJI-Mavic-3-Thermal-DE-Shop

[67] Phantom 4 RTK - DJI [Internet]. DJI. [cited 2023 Apr 5]. Available from: https://www.dji.com/nz/phantom-4-rtk?site=brandsite&from=insite_search

[68] Phantom 4 RTK - Product Information [Internet]. DJI. [cited 2023 Apr 5]. Available from: https://www.dji.com/nz/phantom-4-rtk/info#specs

[69] Matrice 30 Series - Power in Portability [Internet]. DJI. [cited 2023 Apr 7]. Available from: https://www.dji.com/nz/matrice-30

[70] Matrice 30 Series - Specs [Internet]. DJI. [cited 2023 Apr 7]. Available from: https://www.dji.com/nz/matrice-30/specs

[71] Matrice 300 RTK – Built Tough. Works Smart. [Internet]. DJI. [cited 2023 Apr 7]. Available from: https://www.dji.com/nz/matrice-300

[72] MATRICE 300 RTK - Specifications [Internet]. DJI. [cited 2023 Apr 7]. Available from: https://www.dji.com/nz/matrice-300/specs

[73] Zenmuse P1 - Full-frame Aerial Surveying [Internet]. DJI. [cited 2023 Apr 7]. Available from: https://www.dji.com/nz/zenmuse-p1

[74] WingtraOne Technical specifications [Internet]. Wingtra. [cited 2023 Apr 8]. Available from: https://wingtra.com/mapping-drone-wingtraone/technical-specifications/

[75] Mapping drone for fast and accurate survey data every time [Internet]. Wingtra. [cited 2023 Apr 8]. Available from: https://wingtra.com/

[76] D-RTK 2 Mobile Station [Internet]. DJI. [cited 2023 Apr 8]. Available from: https://www.dji.com/nz/d-rtk-2

[77] D-RTK 2 - Product Information [Internet]. DJI. [cited 2023 Apr 8]. Available from: https://www.dji.com/nz/d-rtk-2/info#specs

[78] Intelligent photogrammetry Agisoft [Internet]. Agisoft Metashape. [cited 2023 Apr 10]. Available from: https://www.agisoft.com/pdf/metashape_presentation.pdf

[79] Prepare for take-off [Internet]. Wingtra Knowledgebase. [cited 2023 Apr 16]. Available from: https://knowledge.wingtra.com/en/4.-prepare-for-take-off

[80] Agisoft Metashape User Manual [Internet]. Professional Edition, Version 2.0. 2023 [cited 2023 May 1]. p. 1–222. Available from: https://www.agisoft.com/pdf/metashape-pro_2_0_en.pdf

[81] Jacobsen K. Exterior Orientation Parameters [Internet]. 2001 [cited 2023 May 1]. p. 1321–32. Available from: https://www.ipi.uni-hannover.de/fileadmin/ipi/publications/jac_ExterOr.pdf

[82] Bergsjö J. Photogrammetric point cloud generation and surface interpolation for change detection. [Stocholm / Sweden]: Royal Institute of Technology(KTH); 2016.

[83] Mason A. Making 3D Models with Photogrammetry [Internet]. Getting Started with Agisoft PhotoScan. [cited 2023 May 1]. Available from: https://thehaskinssociety.wildapricot.org/resources/Documents/Tutorials/PhotogrammetrywithPhotoScanTutorial.pdf

Appendices

Appendix A

UAVs used in the thesis

Figure A.1: DJI Mini 3 Pro.

Figure A.2: DJI Mavic 3E.

Figure A.3: DJI Mavic 3T.

Figure A.4: DJI Phantom 4 RTK.

Figure A.5: DJI Matrice 30T.

Figure A.6: DJI Matrice 300 RTK.

Figure A.7: WingtraOne Gen II.

Appendix B

Samples of aerial photographs

Figure B.1: Sample (1) of photograph captured by DJI Mini 3 Pro on 09.04.2023.

Figure B.2: Sample (2) of photograph captured by DJI Mini 3 Pro on 09.04.2023.

Figure B.3: Sample (1) of photograph captured by DJI Mavic 3E on 09.04.2023.

Figure B.4: Sample (2) of photograph captured by DJI Mavic 3E on 09.04.2023.

Figure B.5: Sample (1) of photograph captured by DJI Mavic 3T on 09.04.2023.

Figure B.6: Sample (2) of thermal photograph captured by DJI Mavic 3T on 09.04.2023.

Figure B.7: Sample (1) of photograph captured by DJI Phantom 4 RTK on 09.04.2023.

Figure B.8: Sample (2) of photograph captured by DJI Phantom 4 RTK on 09.04.2023.

Figure B.9: Sample (1) of photograph captured by DJI Matrice 30T on 13.04.2023.

Figure B.10: Sample (2) of thermal photograph captured by DJI Matrice 30T on 13.04.2023.

Figure B.11: Sample (1) of photograph captured by DJI Matrice 300 RTK on 13.04.2023.

Figure B.12: Sample (2) of photograph captured by DJI Matrice 300 RTK on 13.04.2023.

Figure B.13: Sample (1) of photograph captured by WingtraOne Gen II on 10.02.2022

Figure B.14: Sample (2) of photograph captured by WingtraOne Gen II on 10.02.2022

Appendix C

Aerial photograph locations and orientations

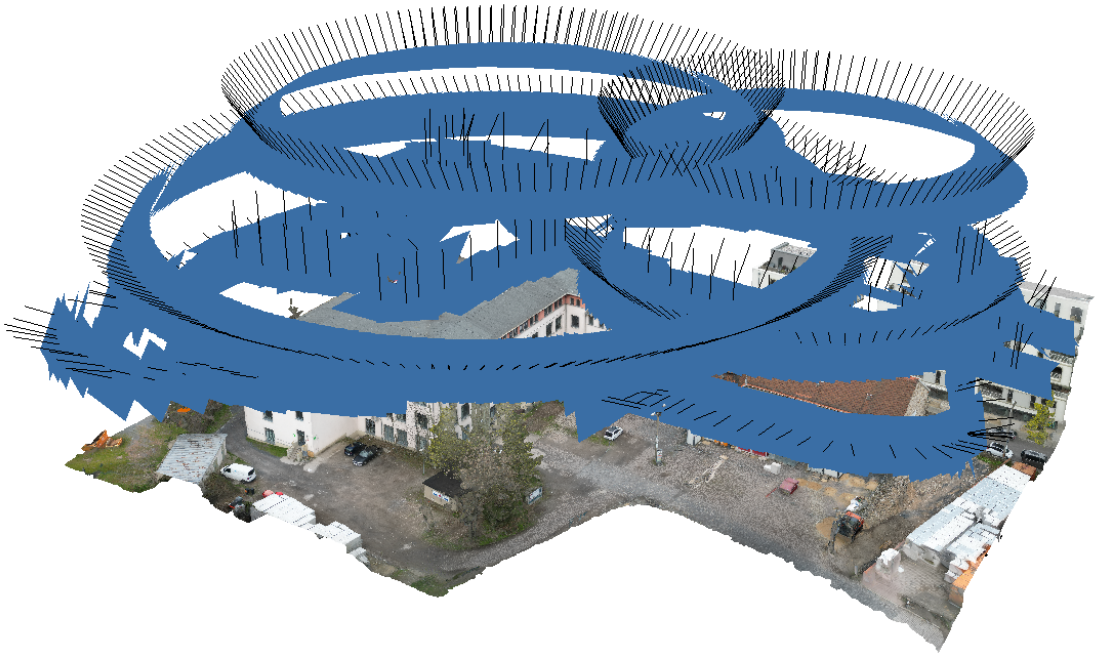

Figure C.1: Aerial photograph locations and orientations of DJI Mini 3 Pro.

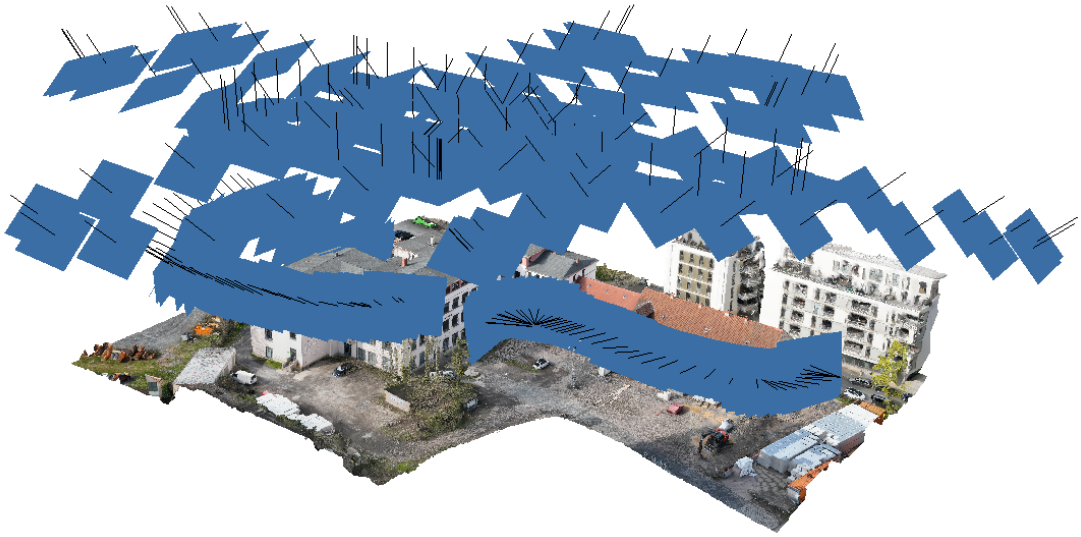

Figure C.2: Aerial photograph locations and orientations of DJI Mavic 3E.

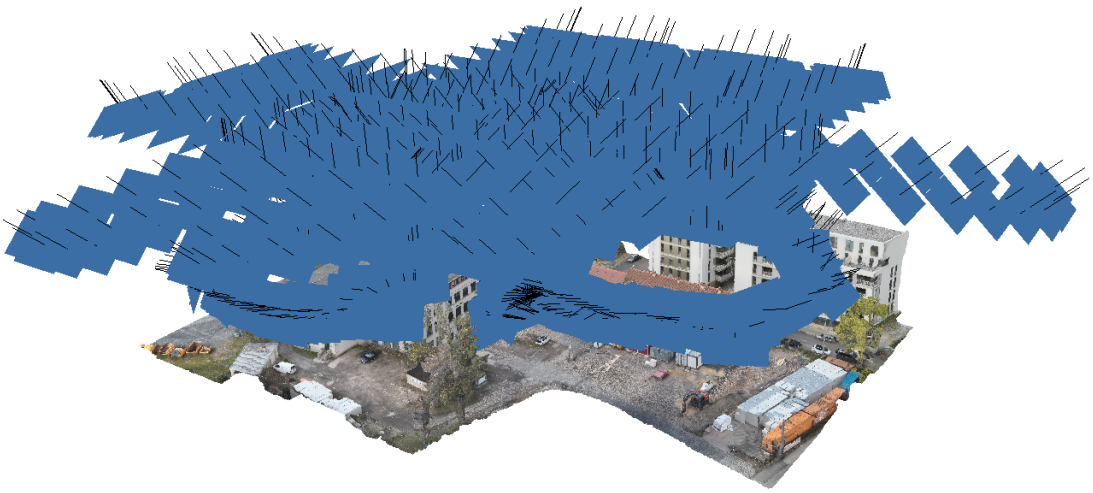

Figure C.3: Aerial photograph locations and orientations of DJI Mavic 3T.

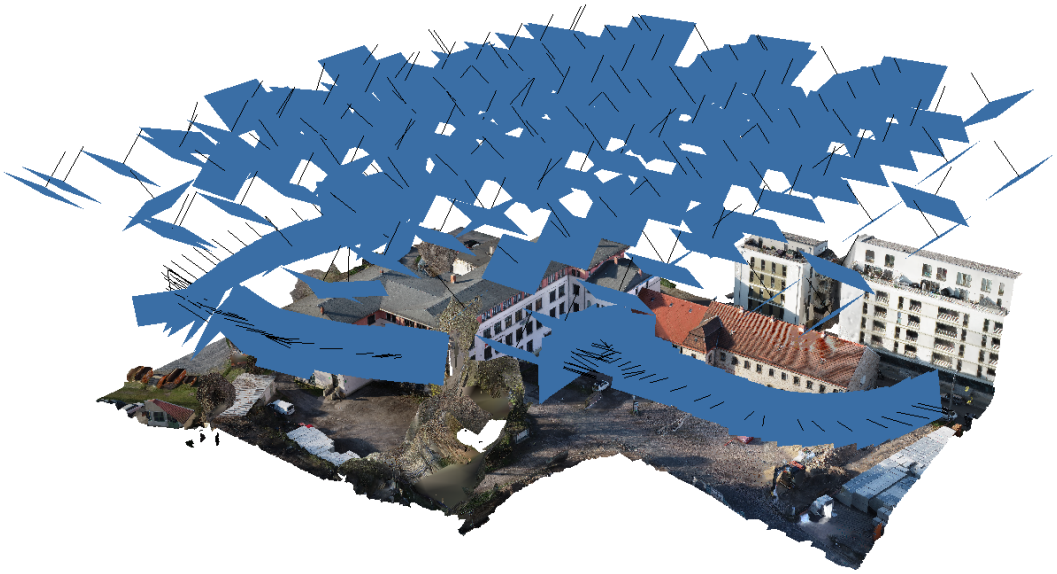

Figure C.4: Aerial photograph locations and orientations of DJI Phantom 4 RTK.

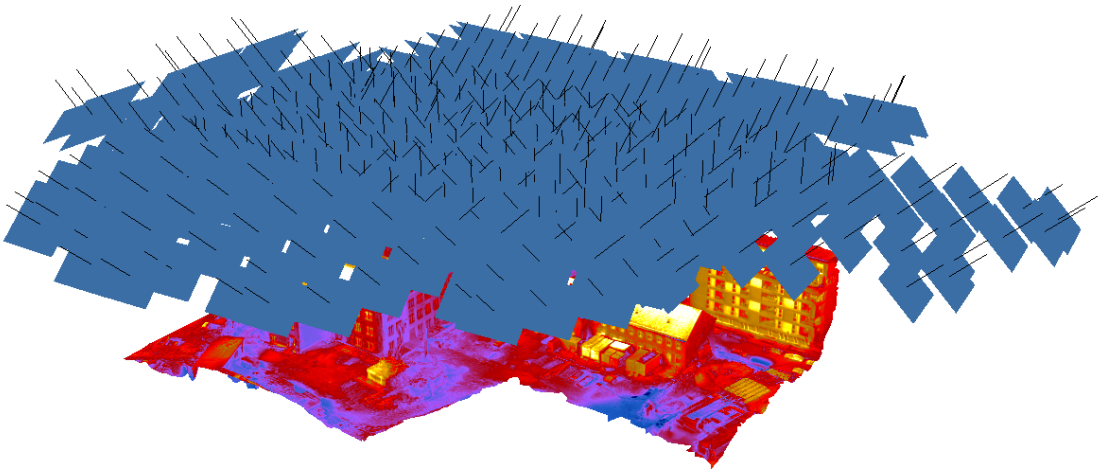

Figure C.5: Aerial photograph locations and orientations of DJI Matrice 30T.

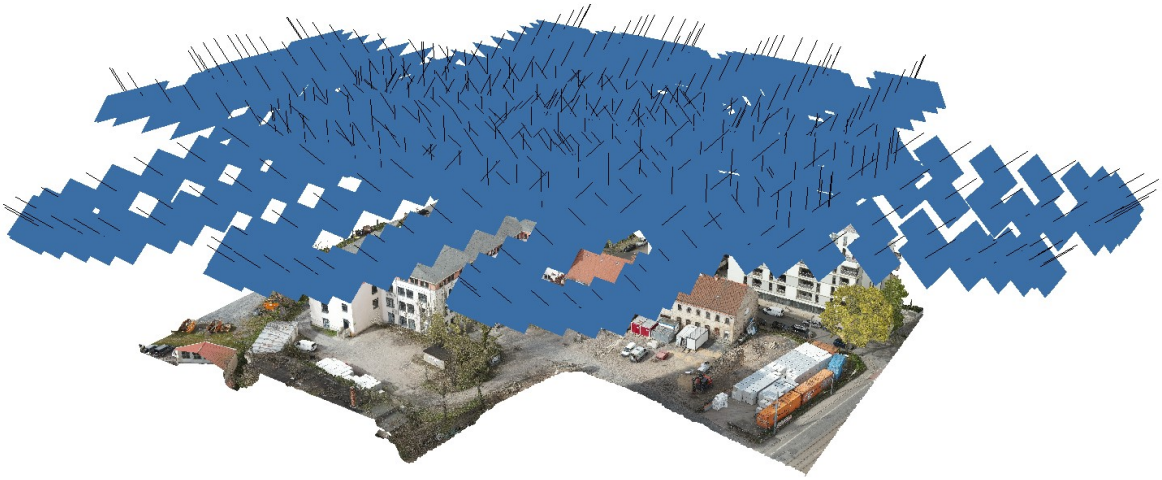

Figure C.6: Aerial photograph locations and orientations of DJI Matrice 300 RTK.

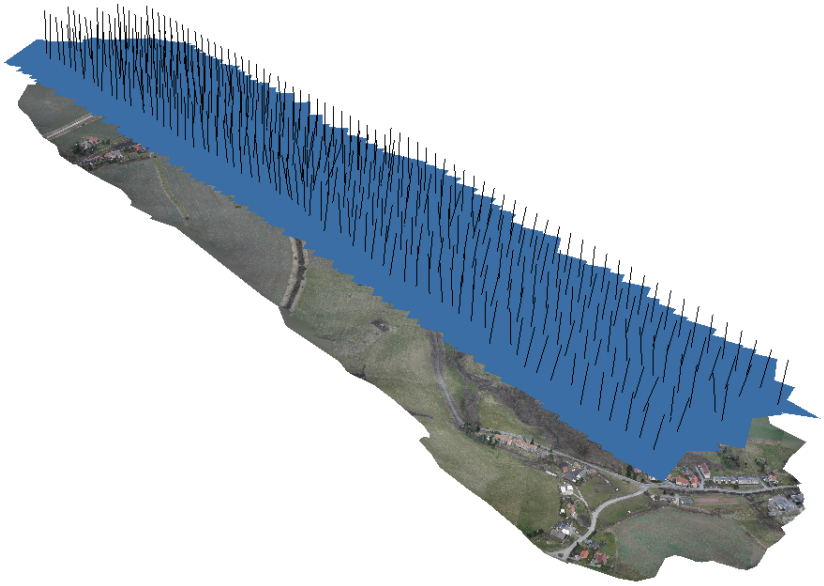

Figure C.7: Aerial photograph locations and orientations of WingtraOne Gen II.

Appendix D

Publications from the Thesis

Conference Paper

1. Maral M, Karakış S. 3D Modelling Performance and Usage Area Analysis of Popular Unmanned Aerial Vehicles in the Surveying and Mapping Industry. 9th International Congress on Engineering and Technology Management. 2023 April-May 29-30-01; Istanbul, Türkiye. 912.

Curriculum Vitae

Name Surname : Metehan MARAL

Education:

2020–2023	İzmir Kâtip Çelebi University, Dept. of Geomatics Eng. (M.Sc.)
02-07/2019	University of Warmia and Mazury in Olsztyn, Dept. of Geodesy and Cartography (Erasmus+ Edecation Program)
2015–2020	İzmir Kâtip Çelebi University, Dept. of Geomatics Eng. (B.Sc.)

Work Experience:

2022- Present	Airclip Service GmbH-(Dresden)
2020 – 2021	Sahara Engineering -(Ankara)

Publications:

1. Maral M, Karakış S. 3D Modelling Performance and Usage Area Analysis of Popular Unmanned Aerial Vehicles in the Surveying and Mapping Industry. 9th International Congress on Engineering and Technology Management. 2023 April-May 29-30-01; Istanbul, Türkiye. 912.